PLASMA SURFACE MODIFICATIONS FOR BIOMEDICAL AND ELECTRICAL APPLICATIONS

by

DHIMAN BHATTACHARYYA

Presented to the Faculty of the Graduate School of

The University of Texas at Arlington in Partial Fulfillment

of the Requirements

for the Degree of

DOCTOR OF PHILOSOPHY

THE UNIVERSITY OF TEXAS AT ARLINGTON

December 2008

DEDICATION

I want to dedicate this dissertation to my parents, Mr. Dilip K. Bhattacharyya and Mrs. Protima Bhattacharyya. They are always there with all kinds of support, for which I will be eternally grateful.

ACKNOWLEDGEMENTS

You see things; and you say, 'Why?' But I dream things that never were; and I say, "Why not?" Imagination is the beginning of creation. You imagine what you desire, you will what you imagine and at last you create what you will.

- George Bernard Shaw

This is a wonderful opportunity for me to identify those persons who have contributed significantly to my academic career.

Ms. Bithika Mukherjee, my first private tutor in school days, is the first person who inspired me and taught me to see myself as a scientist. My brother, Dr. Partha Bhattacharyya, is my second teacher and idol. I will never forget his contributions and sacrifices he has made for my career. I would like to name Professors Haraprasad Chatterjee, Satyendranath Gupta, Priyabrata Sarkar, Krishnan Rajeshwar, Liping Tang, Zoltan A. Schelly, Kytai T. Nguyen and Subhransu S. Mandal. I was lucky to have them as my mentors in building my personal and career life.

The person without whom this journey would have never been completed is Professor Richard B. Timmons. I was fortunate enough to find him as my research supervisor. He never acted like a “Boss”. He always supported and encouraged me whatever ideas (crazy!) I wanted to discuss with him. Without his encouragement, it would have been difficult for me to explore my ideas and implement them into reality.

I would also like to thank my family, relatives and friends. Especially, I would mention two names, Shaon and Smaranjit, who unquestionably helped me to survive in tough times.

The last couple of years have changed my living style, my look, my ambitions and made me a complete man. All credits go to my beautiful, charming, loving friend and wife Jhimly. I believe in God. This is my wish; He/She will keep protecting and directing us in our future to work for mankind.

November 5, 2008

ABSTRACT

PLASMA SURFACE MODIFICATIONS FOR BIOMEDICAL AND ELECTRICAL APPLICATIONS

Dhiman Bhattacharyya, PhD.

The University of Texas at Arlington, 2008

Supervising Professor: Prof. Richard B. Timmons

The focus of this work centers on molecular structuring of surfaces. The surface modifications were achieved using plasma polymerization technology, specifically variable duty cycle pulsed plasmas. The results obtained demonstrate that both exacting film chemistry and film thickness control were achieved during deposition of thin polymeric films on selected substrates. The following achievements are detailed in this thesis:

- Identification of a new class of volatile monomers which can be successfully used to synthesize thermoresponsive hydrogel films. A unique aspect of this work is that the lower critical solution temperatures of these gels can be

controllably varied by simple adjustment of the plasma polymerization deposition conditions.

- Successful covalent attachment of proteins and anti-bodies to plasma modified surfaces, including ultrafine particles as small as nanoparticles. In particular, the use of spacer molecules was shown to be effective in tethering the biomolecules to particle surfaces, without compromise of the biological function of the attached biomolecules.
- Surfaces were successfully constructed for tissue culture applications, as illustrated with fibroblast and endothelial cells. Significant enhancement in both initial cell surface attachment and subsequent growth were obtained for both cell lines, as achieved by control of surface chemistry and film thickness of the plasma deposited polymers. This is the first study to document the efficacy of combining surface tailoring and film thickness to improve tissue culture growth.
- A novel plasma polymerization process was developed to produce layered structures of bipolar films, as achieved by depositing alternate layers of –COOH and $–NH_2$ functionalized films. Polar entities were created by spontaneous proton transfer from –COOH groups to $–NH_2$ functionalities, as documented by detailed spectroscopic characterization of these films. The dielectric constants (κ) of these multilayered structures were found to be in excess of 6, an extremely large value for an all-organic film.

A number of potential future applications are briefly identified for the technology developed in this work. Among these future applications are drug delivery, tissue culture, and flexible dielectric films for electronic applications.

TABLE OF CONTENTS

LIST OF ILLUSTRATIONS

LIST OF TABLES

CHAPTER 1

INTRODUCTION

1.1 Surface Modification of Materials

Controlled modification of surfaces represents an extremely active area of materials science research at the present time. Interest in this area simply reflects the fact that although bulk properties are important in establishing many physical properties of materials, it is surface chemistry which frequently dictates the overall efficacy of many devices. For example, numerous advances in fields such as biomedical materials, microelectronics, separation sciences, sensors, etc. can be attributed to gains achieved in surface science. The following represent but a few examples of the recent work in the area of surface modifications to enhance device performance: improving the biocompatibility of materials,[1-5] tailoring barrier properties of materials, [6,7] developing biologically non-fouling surfaces,[8-11] as well as surface adhesion,[12,13] lubricity[14] and catalytic[15-18] properties of materials. Additionally, of course, enormously successful surface modifications have been achieved in the microelectronics[19-22] and semiconductor[23-26] industries.

A variety of imaginative techniques have been developed to alter the surface properties of materials. Given the volume of activity in this field, it is not practical, in the present document, to provide an exhaustive review of all the various techniques employed for this purpose. Instead a brief overview of this field is presented, identifying a number of surface treatments which could be considered to be relevant in comparison with the processes developed in the present study. For this purpose, it is convenient to divide surface treatments into: (1) non-plasma based wet-chemical methods; and (2) plasma based dry techniques.

1.2 Non-Plasma Based Wet-chemical Techniques

Commonly used non-plasma based surface modification techniques include self-assembled monolayer (SAM), surface grafting by photo-irradiation and spin coating.

1.2.1 Self-Assembled Monolayers (SAMs)

Self-assembled monolayers (SAM) have evolved as one the most popular methods employed to fabricate tailored solid surfaces. In this approach, functionalized thiol (- SH) containing compounds are chemically attached to gold plated surfaces. Typically, solutions of ~1 mmol/L alkanethiolates [alkanes containing a thiol (-SH) group at one end] are reacted with gold coated surfaces at room temperature.[36] Once the thiol ends of the molecules bind to the surface, the long alkane chains rearrange themselves in an ordered assembly, due to strong Van-der Waals attractive interactions between the adjacent non-polar chains, as depicted in Figure 1.1. Surfaces can be

functionalized with different functional groups by use of alkanethiolate molecules which contain the appropriate functional group at the other end of the

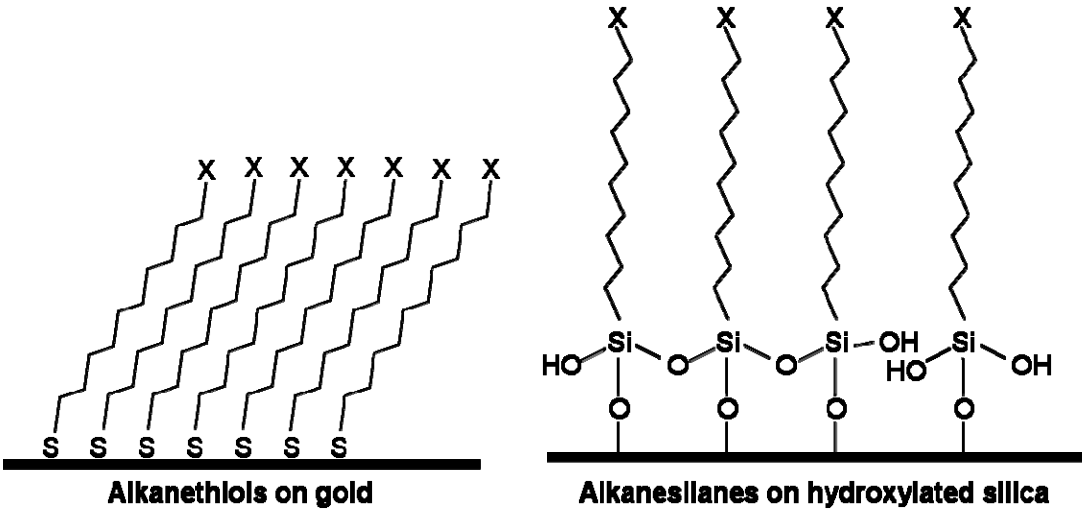

Figure 1.1 Schematic of self-assembled monolayers on alkanethiols on gold and alkanesilanes on hydroxylated silica surfaces [X indicates terminal functional groups].

molecule. Examples of such functionalized surfaces include – OH,[27-30] – COOH,[28,31,32] - NH_2,[29,33] - CH_3,[28,29,30] as well as surfaces containing a mixture[34,35] of functional groups. Surface structures obtained by this technology are generally well defined and the surface chemistry can be systematically varied for targeted applications. In more recent times, silanol (- Si-OH) chemistry has also been employed to prepare self-assembled monolayers on glass or silicon surfaces.[36,37] Self-assembled layers of alkylsiloxanes are prepared by reacting a solution of alkyltrichlorosilanes (or alkyltriethoxysilanes, or alkyltrimethoxysilanes) with hydroxylated silicon surfaces. The active chlorosilane groups react spontaneously with the surface hydroxyls to form silanols, as shown in Figure 1.1. Spatially designed SAM surfaces include structures

built by self-assembly on patterned surfaces.[38] Although SAMs have proven to be extremely useful in terms of fundamental research considerations, questions about the shelve-life, abrasion resistance and stability[39,40] of self-assembled monolayer films pose an impediment with respect to large scale utilization of this technology for practical applications.

1.2.2 Surface Grafting

Surface functionalization by graft polymerization is also a fairly common technique. Surface grafting is usually performed in two steps: initial surface activation, followed by graft polymerization.[41] Surface activation typically generates reactive free radicals which are then covalently coupled with organic precursors containing unsaturated double bonds, thus initiating the polymerization process (Figure 1.2). Surface grafting with monomers such as acrylates[42,43] and methacrylates[44,45] are now well established. A variety of techniques have been employed to achieve the initial surface activation. Examples include UV irradiation,[46-48] high energy electron beam bombardment,[49] chemical reactions,[50] plasma treatment[51,52,53] and ozone exposure.[54] Sometimes, experiments involving grafting of long polymeric chains directly onto the activated surfaces are not successful because concentration gradients and/or the bulk nature and coiling properties of the polymer molecules prevent their facile diffusion to the activated surface for the grafting processes.[41]

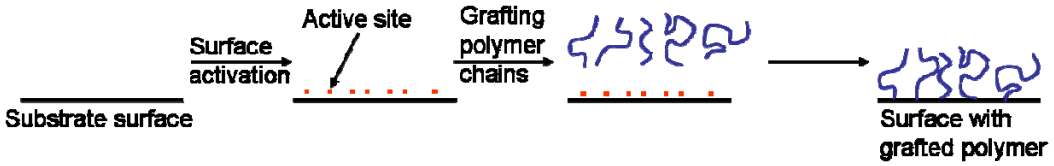

Figure 1.2 Schematic of direct coupling (grafting) of polymer chains on surfaces.

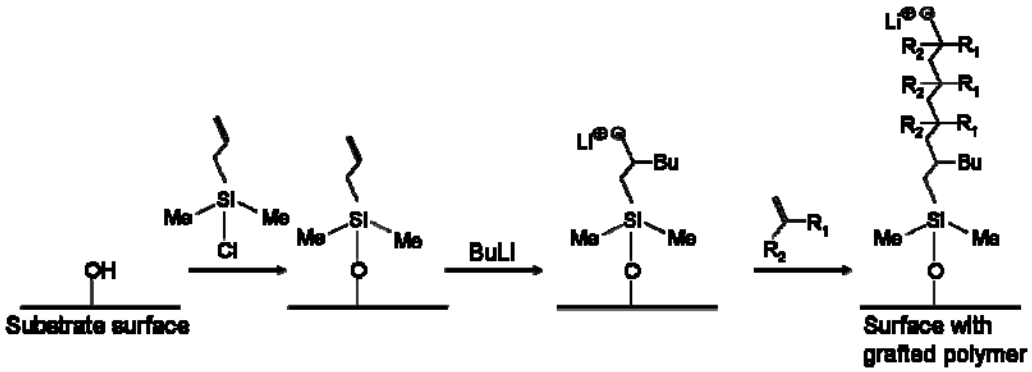

Figure 1.3 Schematic of surface initiated grafting of polymer chains on surfaces.

In contrast to the difficulties in coupling long polymer chains on activated surfaces, approaches that provide direct and controlled growth of polymer at the activated sites on the surfaces are gaining increased interest. Surface initiated ionic polymerization, free-radical polymerizations and atom-transfer-radical polymerization (ATRP) are reported to provide improved control over the structure and function of the graft polymers.[41,55-58] Surface initiated anionic polymerization technique, as depicted above in Figure 1.3, is one such example of this approach. In this example, the vinyl group in the surface bound silane compound is reacted with butyl lithium to form an anion which subsequently initiates the polymerization reaction of a vinyl monomer.

1.2.3 Spin Coating

Spin coating is most commonly employed in the microelectronics industry[59-62] and it is also used in manufacturing flat panel displays,[63] anti-reflecting surfaces[64] and compact discs.[65] Initially, a liquid solution containing a dissolved polymer is placed on the substrate, which is then rotated at very high speed to spread the solution uniformly over the sample, simultaneously promoting solvent evaporation. The film thicknesses deposited depend on the rotational speed of the disk (usually in the range of 5000 rpm to 10000 rpm), concentration and viscosity of solution and also on the nature of the solvent. Usually, surface coating by this technique is achieved in less than one minute and film thicknesses deposited typically range from 0.3 to 10 μm.[66] A serious limitation of the spin coating approach is its restriction to flat substrates. Additionally, it is generally not possible to provide ultrathin uniform films, such as those having thickness less than 100nm.

1.3 Plasma Based Dry Techniques

In addition to the liquid based coating processes noted above, all dry coating technologies are also available. Since these latter processes produce little waste, they are generally considered as being more environmentally friendly. The all-dry processes are usually based on some aspect of plasma technology. Plasma is the fourth state of matters where atoms or molecules exist in fully or partially ionized gaseous form. In plasma based surface modifications, substrates are coated by deposition of thin solid

organic and/or inorganic films directly from the gas phase unto the substrates. Among the most commoningly used plasma based surface modification techniques, those of ion implantation and deposition; sputtering; and, plasma enhanced chemical vapor deposition (PECVD) [also frequently called plasma polymerization] are discussed in this section.

1.3.1 Plasma Based Ion Implantation and Deposition (PBIID)

Ion assisted thin film deposition is an increasingly popular method to implant ions into substrates for tailoring surface characteristics.[67] There are different types of ion implantation processes, such as plasma based ion implantation (PBII), and plasma based ion implantation and deposition (PBIID). In the latter case, the ion implantation is accompanied with deposition of a film as an integral part of the surface modification.[68] The main advantages of PBII and PBIID are their simplicity for coating large surfaces or three-dimensional objects in relatively short processing time (minutes).[69,70] A disadvantage of this technique, dependent on the materials employed, is the absence of ion selectivity during the treatment, i.e., in many cases ions of all types (ionic impurities) present in the plasma are simultaneously implanted in the surface.[67] Despite this potential problem, surface modification by PBII and PBIID techniques have been employed in the fields of biomaterials,[71,72,78] metallurgy,[73,74] and modification of the electrical[75] properties of materials. Also noteworthy is the use of this technique in preparing diamond like carbon (DLC) films[76-80] for applications requiring hard, chemically inert and thermally stable surfaces.

1.3.2 Sputtering

Sputtering is another widely used, industrially important, tool for surface modifications by thin film depositions. In this process, sputtering of small particles, i.e atomic clusters, are ejected as a result of impingement of high energy particles on the surface of a target material. Obviously, the energy deposited by the incident particles must be in excess to the binding energy of the ejected atoms in the substrate. The ejected species subsequently deposit on the substrate to be coated, forming a very uniform and conformal film on the substrate. The initial target, i.e. the source of coating material, is located close to the substrate and the system is initially evacuated to a very high vacuum, typically in the range of 10^{-8} to 10^{-10} Torr background pressure. In most cases, the sputtering chamber is then backfilled with Argon gas, in a pressure range of 10 – 100 mTorr, and a high power glow discharge is ignited. A negative potential (0.5 – 5 kV) is applied to the target and the substrate is grounded in order to initiate positive-ion bombardment. For non-conducting or insulating materials, radio-frequency (RF) sputtering is preferred over direct current (DC) sputtering because charge build-up is observed in the later. An attractive feature of this technique is that, since sputtering arises from a physical exchange of kinetic energy, as opposed to chemical or thermal breakdown, virtually any material can be used as a source of coating[81] and good compositional control of the deposited films are generally available.

There are many applications involving sputtering techniques. One of its most common applications is in electron microscopy where the samples for analysis are

initially coated with a very thin gold film to make them electrically conducting. Thin film deposition by sputtering has been extensively employed to deposit metals,[82,83] metal oxides,[84,85,86] nitrides,[83,87] metal alloys[88,89,90] and polymers[91,92,93] to improve electrical, anti-corrosive, mechanical properties as well as the biocompatibility of materials.

1.3.3 Plasma Enhanced Chemical Vapor Deposition (PECVD) or Plasma Polymerization

Polymerization of volatile monomers and deposition of polymeric films by glow discharge is commonly known as plasma polymerization or plasma enhanced chemical vapor deposition (PECVD). Although formation of solid materials from electrical discharges of organic precursors was known since the advent of gas discharges, "Only since the 1960s has the formation of materials in plasma been recognized as a means of synthesizing polymers, and the process, when used to make a special coating on metals, has been referred to as plasma polymerization or glow-discharge polymerization".[94] In this process, ionized gas plasmas are generated by radio-frequency (RF),[95] microwave[96-98] or direct current (DC)[99-101] discharges under low pressure monomer conditions. In the glow discharge, random fragmentation of the gaseous molecules leads to formation of ions and free radicals which readily react with each other and undissociated monomer, ultimately depositing as polymeric films over all surface areas exposed to the plasma discharge.

From the chemical standpoint, plasma polymerization provides a wide range of flexibility in selection of monomers. In fact, virtually any monomer can be used in this

technique provided it is sufficiently volatile to provide a satisfactory operating vapor pressure (typically at least 30 mtorr) in the polymerization chamber. For comparatively low volatile monomers, for example N-isopropylacrylamide (NIPA), a heating system can be used to obtain sufficient vapor pressure to ignite the plasma discharge.[103] An advantage of the plasma approach, relative to that involved in conventional solution based polymerizations, is that the monomers employed need not have any particular functional group or structure in order to generate useful polymeric films.

The properties of plasma polymerized films are not solely dependent on the nature of the monomers, but also on the operating parameters employed at the time of the plasma polymerization. Common parameters that control the film physical and chemical properties are power input, operating vapor pressure, monomer flow rate and in some cases, location of the substrate in the reactor. The ready availability of a wide range of monomers, including volatile compounds that contain virtually every important organic functional group, is a distinct advantage of this surface modification technology and, no doubt, is an important consideration for those employing this surface modification technique. In addition, there are a number of other inherent advantages of plasma polymerizations as a coating technology. Among these advantages are the following considerations: [94,102,2]

- The processing is done in a single, dry step, a significant environmental consideration with respect to reducing waste liquids.

- The plasma deposited films are conformal. Substrates of any shape and size can be uniformly coated.
- Thickness of the plasma deposited films can be controlled from nanometer to micron scales.
- The processing is rapid and can be used as a continuous production unit.
- The films are pin-hole free which provides good barrier properties to the modified surfaces.
- Plasma surface modification is independent of the nature of the substrate. Many materials, including plastics, metals, rubbers, ceramics, glasses and even paper have been employed as substrates.
- The deposited films are resistant to delamination and exhibit good abrasion resistance.

Despite the favorable properties identified above, the plasma approach also introduces some potential limitations with respect to surface modifications. Since the monomers are exposed to an environment of highly energized electrons during the plasma discharge, monomer molecules may undergo random ionization and bond dissociation processes. As a result, control of film chemistry under continuous-wave (CW) plasma conditions is difficult to achieve, in many cases the resultant polymer films produced exhibit little resemblance to the starting monomers. However, it is significant to note that, under CW conditions, it is possible to produce unique (and useful) polymeric films which are simply not available with any other synthetic

approach. Indeed, for the first few decades of research in this area, the experimental work focused on production and evaluation of these unique polymer films. For example, highly crosslinked, polymeric films are readily obtained, from basically non-reactive monomers such as ethane or propane, under high power input plasma conditions. Such materials have been employed as moisture barrier layers and for prevention of corrosion.

In contrast to early work,[104-106] there has been a definitive increasing trend in recent years to utilize the inherent advantages of plasma polymerization technology and extend this approach to molecular tailoring of surfaces. These studies have involved not only control of overall surface chemistry but, additionally, control of the density of functional groups deposited on the surfaces during the plasma polymerization process. Among relatively recent innovations has been introduction of a variable duty cycle pulsed plasma technique employed in lieu of the conventional CW plasma approach.[108,109] In pulsed plasma depositions, plasma on and off times are independently varied. The ratio of plasma "on" time to the total plasma "on" plus "off" times is known as the plasma duty cycle. In this approach, the reactive species generated during the plasma on time undergo continued reactions during the plasma off times. It has been clearly demonstrated that significant film formation occurs during the plasma off periods, during which times significantly more selective chemistry occurs compared to that under CW conditions.[110] For example, extremely reactive ion radicals produced during the plasma on periods are replaced by neutral, significantly less

reactive radicals, during the plasma off times. In fact, the neutral free radical chemistry is similar to that observed during traditional solution based polymerization processes. It has now been clearly established, as demonstrated with a wide range of monomers, that the variable duty cycle pulsed plasma technique can be utilized to achieve exceedingly fine control of the film chemistry during plasma polymerizations.[95,107] In particular, increased retention of functional groups present in the starting monomer are observed to be present in the polymer films as the plasma duty cycle employed during film formation is decreased.

1.4 Experimental Approach and Outline of Dissertation

The emphasis of this thesis is to explore and evaluate the overall usage of variable duty cycle pulsed plasma polymerizations with respect to surface molecular tailoring of materials. At the same time, careful considerations are made to identify potential limitations and difficulties presented by this technology. The research studies conducted involved not only the preparation of novel new surfaces but, additionally, examined the utility of these surfaces for use of plasma modified surfaces in a number of new applications, with the main focus involving biomaterials research.

The experimental results obtained are presented in four separate chapters, with each chapter providing an introduction, experimental details, results and discussion. The topics examined are as follows:

a. Preparation of thermoresponsive hydrogels by pulsed plasma polymerization of a new class of organic monomers. It is demonstrated, for the first time, that by appropriate control of the plasma deposition conditions, along with the use of mixed monomers, that it is possible to synthesize thermoresponsive films having controllable lower critical solution temperatures and swelling behavior upon immersion in aqueous solutions.

b. Chapter three examines the utility of employing plasma functionalized surfaces for the express purpose of subsequent covalent attachment of biomolecules to the modified surfaces. It is demonstrated that the pulsed plasma technique does provide a very convenient avenue for this purpose, including successful application of this technology to ultrafine powders, including nanoparticles. The proof of concept provided in this study includes both the successful attachment of fluorescence labeled bovine serum albumin (BSA) as well as RL-9A T-cell receptor mimic (TCRm) antibodies. In the latter case, ELISA type assays were conducted to demonstrate that the attached antibodies retained their biochemical specificity to a very high degree.

c. The potential use of plasma surface modifications to improve tissue culture growth is presented in the next chapter. Specifically, the adhesion and proliferation of fibroblasts and human aortic endothelial cells on plasma modified surfaces was examined. As described in this chapter, it was discovered that these cells grow significantly better on plasma polymer films containing –COOH groups. Surprisingly,

it was observed that both film thickness and surface density of –COOH functional groups are effective in promoting increased growth rates of these cells.

d. In the final chapter, the utility of using pulsed plasma polymerization to synthesize bipolar films is described. An important aspect of this study was a demonstration that the pulsed plasma approach can provide exact control in deposition of ultra thin films as small as 2 nm. The dielectric constants of the films were measured to be in excess of 6, an extremely high value for an all-organic film. Given the flexibility of these films, it is suggested that they may possibly find use as gate dielectric in the fabrication of all-polymer electronic devices.

CHAPTER 2

PULSED PLASMA POLYMERIZED THIN FILM THERMORESPONSIVE HYDROGEL

2.1 Introduction

Hydrogels are three-dimensional hydrophilic polymeric structures able to absorb large quantities of water. They are synthesized by polymerization of hydrophilic monomers. The extent of the reversible swelling and deswelling properties of these materials is known to depend on the nature of both intermolecular and intramolecular crosslinking, as well as the degree of hydrogen bonding in the polymer network.[111] Increasingly, these hydrogels are being utilized in a variety of applications including drug release,[112-114] biosensors,[115-117] tissue engineering,[118-120] and pH sensors.[121,122]

To date, a variety of compounds have been utilized in synthesis of hydrogels. Examples of monomers employed for this purpose include N-isopropylacrylamide [NIPAM],[103,123-125] vinyl alcohol,[118,126] ethylene glycol,[127,128] and N-vinylpyrrolidone.[129] Of these compounds, hydrogels made from NIPAM, including some involving incorporation of co-monomers,[130-132] have been extensively studied for their thermoresponsive behavior near physiological temperature. These thermoresponsive hydrogels exhibit phase transitions when subjected to an alteration in the environmental

temperature. For example, poly-NIPAM is hydrophilic below ~30°C and becomes hydrophobic above ~35°C. The reported phase transition temperature for NIPAM is 31°-32°C.[133-135] Various approaches have been employed to immobilize these thin films on solid surfaces. These techniques include electron beam irradiation,[136,137] photoinitiated grafting,[118,138,139] use of activated and functionalized substrates,[140,141] and plasma polymerization.[103,123,142-144]

The prior plasma generated films, noted above, all involved the use of NIPAM monomer. In this chapter, the synthesis of hydrogel films from other monomers by plasma polymerization was examined. For this purpose, low molecular weight and relatively volatile monomers such as 1-amino-2-propanol (1A2P) and 2-(ethylamino)ethanol (2EAE), compounds containing both amine and hydroxyl functional groups, were selected. A variable duty cycle pulsed plasma was employed to control the film compositions obtained during the plasma polymerizations.[102] Under pulsed conditions, both the degree of film cross-linking and extent of retention of the monomers functional groups in the resultant plasma films can be controlled, to a relatively high degree. The aim of this experiment was to identify deposition conditions which would provide a compromise between the degree of polymer cross-linking and retention of the hydroxyl and amine groups and thus the extent of hydrogen bonding in the films. The compromise mentioned reflects the fact that under pulsed plasma conditions, higher duty cycles promote increase polymer cross-linking but at the expense of retention of monomer structure.[102] A second important consideration in this

work was to generate hydrogel films under conditions such that the films were strongly bonded to the substrate supports, so as to exhibit sufficient adhesion and abrasion resistance for use in future applications. Thus, both of these goals involved study and careful adjustment of plasma parameters, particularly the average power input.

As an extension to synthesis of hydrogels from the two above mentioned monomers, attempts were made to alter the thermoresponsive properties of the plasma polymerized hydrogels. Tuning the lower critical solution temperature (LCST) of thermoresponsive hydrogel is an important issue for various applications. Many attempts including addition of co-monomers such as N-*tert*-butylacrylamide,[132] crown ethers[145] and polyelectrolyte molecules[146] have been reported in attempts to modulate the transition temperature of PNIPAM hydrogels. Previous studies have shown that this temperature can be varied from a lower range (14°C) to a higher range (45.5°C) by changing the composition and ratios of the monomers. All the approaches previously studied to change the LCST of these hydrogels involved conventional solution co-polymerization techniques. Although PNIPAM has been deposited by plasma polymerization technique, no attempts were reported to control the LCST or the phase transition temperature of these hydrogels.

In the present study, the successful production of hydrogel films from pure 1A2P and 2EAE monomers was first demonstrated. With both monomers, plasma conditions could be adjusted to produce single temperature thermoresponsive films from each pure monomer. Subsequently, it was discovered that hydrogels having a

tunable range of LCSTs, ranging from ~33 °C to 58 °C are obtainable via use of 1A2P /2EAE mixtures during the plasma polymerization synthetic step. In all cases, uniform high quality films were obtained and the hydrogel and spectroscopic properties of these films were carefully examined.

2.2 Experimental

2.2.1 Preparation of the hydrogel films from pure monomers

The 1A2P and 2EAE monomers were obtained from Sigma-Aldrich, St. Louis, MO and had a stated purity of +98%. Prior to film deposition, the monomers were repeatedly freeze-thawed to remove dissolved gases. Monomer vapors were subjected to a radio-frequency (RF) plasma glow discharge, at room temperature, in a bell-shaped reactor chamber (Figure 2.1). Polished Si wafers were used as substrates for XPS studies and water contact angle measurements. ATR crystals, made from Si wafers, were employed for the ATR-FTIR spectroscopic studies.[147,148] All Si wafers were sonicated with acetone, methanol and hexane to clean the wafer surfaces prior to use. After substrates were placed inside the reactor, a background pressure of 6 mtorr was established for each run. Oxygen plasma at 100W average power input was employed to remove any carbonaceous residue left on the substrates. Monomer vapor was introduced into the reactor chamber and an RF glow discharge was maintained at 130 mtorr pressure at 150W peak power input. Three different average power input conditions were employed, namely, pulsed discharges at 10/30 and 10/10 ($t_{on}/t_{off,}$ ms) duty cycles, plus runs using a continuous wave (CW) operational mode. All samples

were prepared using the 150W power input. In the case of pulsed runs, the average power input is defined as:

Average Power = [On Time / (On + Off) Time] x Peak Power

2.2.2 Preparation of the hydrogel films from monomers mixtures

The same experimental set up was employed for preparation of hydrogel films from mixture of 1A2P and 2EAE monomers. The monomers were mixed in two proportions such as (a) 1A2P:2EAE (1:1) and (b) 1A2P:2EAE (1:2). In this experiment, only pulsed plasma conditions of duty cycle 10/30, 150W power input at 130mTorr monomer vapor pressure were employed.

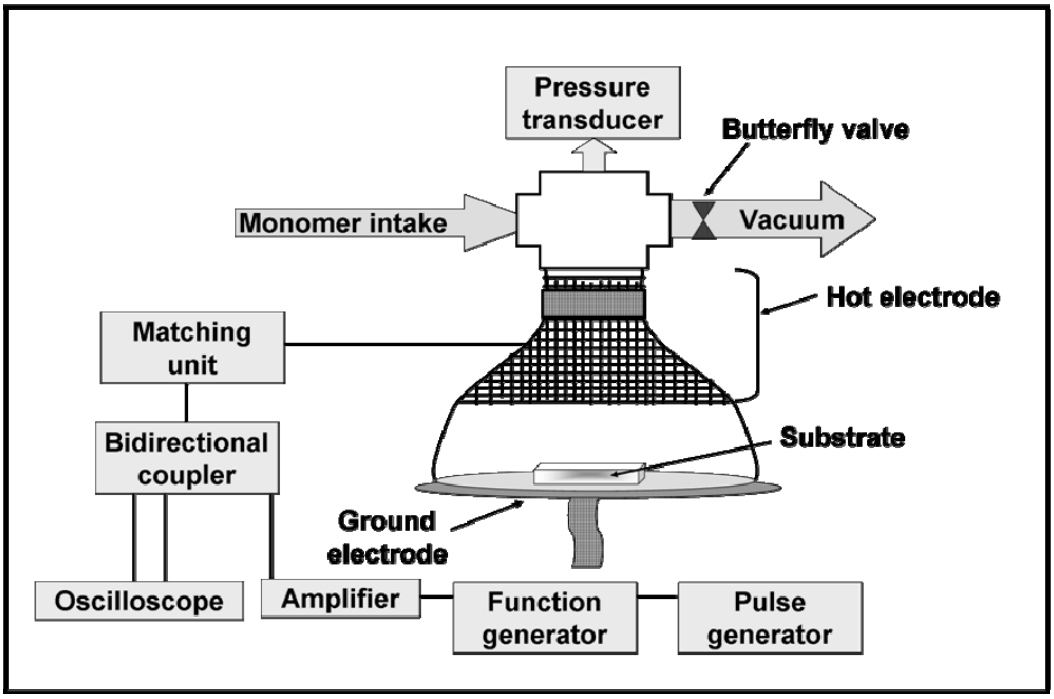

Figure 2.1 Schematic diagram of bell-shaped plasma polymerization reactor.

2.2.3 Characterization of plasma polymerized films

The 1A2P polymer films were characterized by ATR-FTIR and XPS spectroscopies, water contact angle measurement and capillary rise experiments. The ATR-FTIR spectral analyses were carried out using a Bruker Equinox 55 FT-IR Spectrophotometer. The XPS spectra were obtained using a Perkin-Elmer PSI 5000 series instrument equipped with an X-ray source monochromator. A Rame-Hart sessile drop goniometer, with a small heater and thermocouple attachment, was used to measure the contact angles of the films over a temperature range of 20°C to 70°C. Capillary rise measurements were employed to examine the hydrophilic/ hydrophobic transition behavior of the thin films with temperature.[103,139] Glass capillaries, 1.5 x 50mm in size, were used for this purpose. Ultra-pure water was used for the contact angle and capillary rise measurements.

2.3 Result

The initial studies focused on the 1A2P monomer and the following results were obtained.

2.3.1 Energy Efficiency of Film Formation under Pulsed and CW Conditions

It was observed that the polymer film thickness obtained under the 10/30 and 10/10 conditions varied linearly with deposition time. This was not true for the CW films which revealed a decrease in the rate of film formation with increasing deposition times. The decreasing rate with time under CW conditions presumably arises from an

increasing contribution from film ablation at the relatively high power employed, an observation which has been made in numerous prior plasma polymerization studies. The variations of film thickness with deposition times are shown in Figure 2.2. From these data, the energy efficiency of film formation was calculated for each duty cycle and the results are shown in Figure 2.3, revealing a clear increase in efficiency with decreasing duty cycle. Also, as illustrated in Figure 2.3, the energy efficiency for film formation under pulsed conditions remains essentially independent of the total deposition time employed in each run. The energy efficiency results obtained in this study are comparable to those reported in other pulsed plasma studies, and have been interpreted as evidence for significant film formation during plasma off times under pulsed conditions.[102]

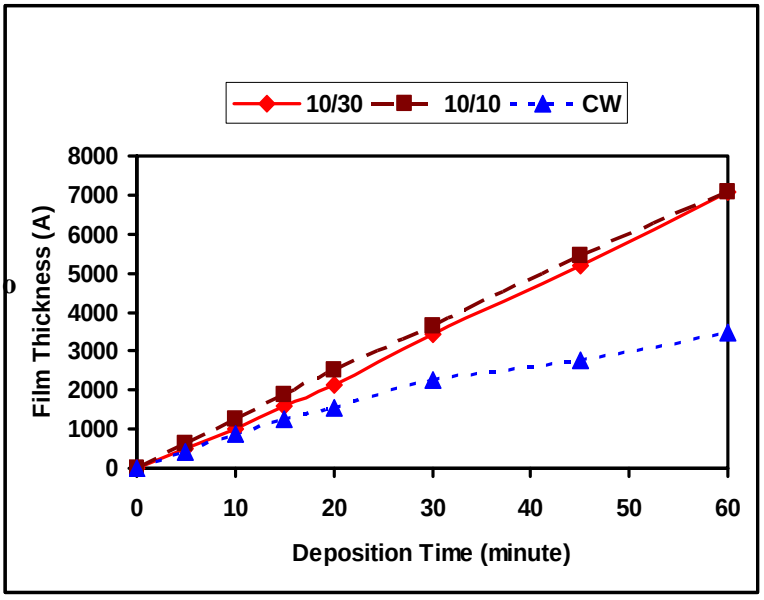

Figure 2.2 Deposition rate of plasma polymerized 1A2P films.

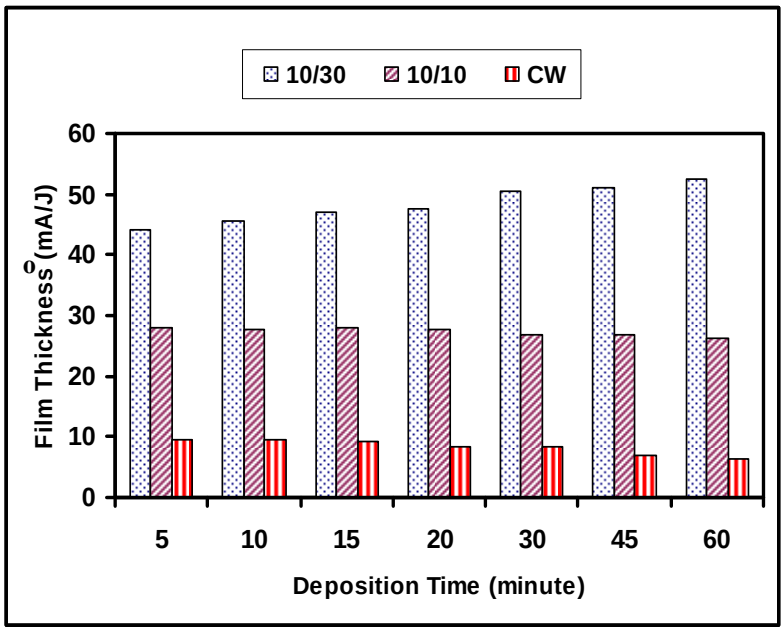

Figure 2.3 Energy efficiency plot for formation of 1A2P films as a function of plasma duty cycles. Efficiency is expressed in terms of film thickness per J of power input.

2.3.2 ATR-FTIR Characterization

ATR-FTIR spectra of 1A2P films were studied as a function of exposure time to purging by a stream of dry nitrogen. These spectra were recorded after the films had been exposed to the atmosphere sufficiently long to equilibrate with respect to moisture adsorption. The resulting spectra are shown in Figure 2.4 [a-c] for films synthesized under the two pulsed plasma and CW conditions. FT-IR spectra of each film (thickness ~200nm) were obtained of the initially prepared moisture saturated plasma films, followed by spectra recorded after 2, 5 and 10 minutes of dry nitrogen gas purging. As shown in Figure 4, sequential changes in absorption peak intensities were observed with increasing N_2 purging times. Peak assignments for these spectra are as follows: (a) the

region from 3600 to ~3000 cm^{-1} (N-H and O-H stretching modes); (b) 2970 cm^{-1} (-CH_3 asymmetric stretch); (c) 2930 cm^{-1} (–CH_2– asymmetric stretch, (d) 2866 cm^{-1} (-CH_3 symmetric stretch); (e) 2240 cm^{-1} (–C≡N stretch); (f) 2180 cm^{-1} (–N≡C stretch); (g) ~1650 cm^{-1} (amide C=O stretch). Atmospheric absorptions by CO_2 and H_2O were eliminated by recording a background spectrum on an uncoated ATR crystal which was then subtracted from each of the polymer film absorptions. As shown in Figure 2.4, substantial decreases in peak intensities were observed in both the 3600-3000 cm^{-1} and below 1700 cm^{-1} region with increasing purge times.

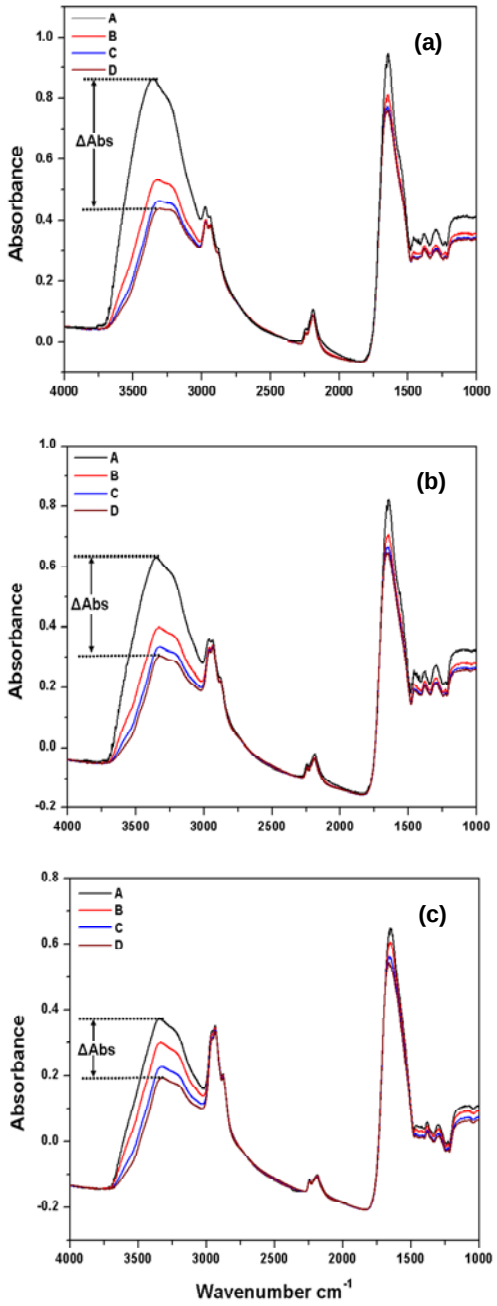

Figure 2.4 ATR-FTIR spectra of plasma polymerized 1A2P films deposited under (a)10/30 ms; (b) 10/10 ms; (c) CW conditions. The A, B, C., and D spectra shown for each duty cycle represent the sequence as deposited, and after 2, 5, and 10 minute dry N_2 purge.

2.3.3 XPS Characterization

The atomic compositions of the films produced under the different deposition conditions are shown in Table 2.1. The high resolution C(1S) XPS spectra of films obtained from the 1A2P monomer are shown in Figure 2.5, arranged in order of increasing plasma duty cycle employed during deposition, reading top to bottom. As shown in this Figure, there is a significant decrease in the relative contribution of higher binding energy C(1S) peaks as the plasma duty cycle employed was increased. Analyses of the deconvoluted C(1S) spectra, shown in Table 2.2, provides a more quantitative measure of the relative variations in the higher binding energy peaks. The peak centered at 284.6 eV represents carbon atoms not bonded to heterogeneous atoms, in this case neither nitrogen nor oxygen. Other peak assignments are C-N at 285.5 eV, C-O plus C≡N at 286.3 eV and N-C=O at 287.8 eV. The progressive relative increase in the peak at 284.6 eV, as the plasma duty cycle is increased, is consistent with the progressive decrease in the heteroatom content of the films, and thus an increase in polymer cross-linking, with increasing average power input. The peak assignments shown in Table 2.2 are in accord with known functional group binding energies.[149]

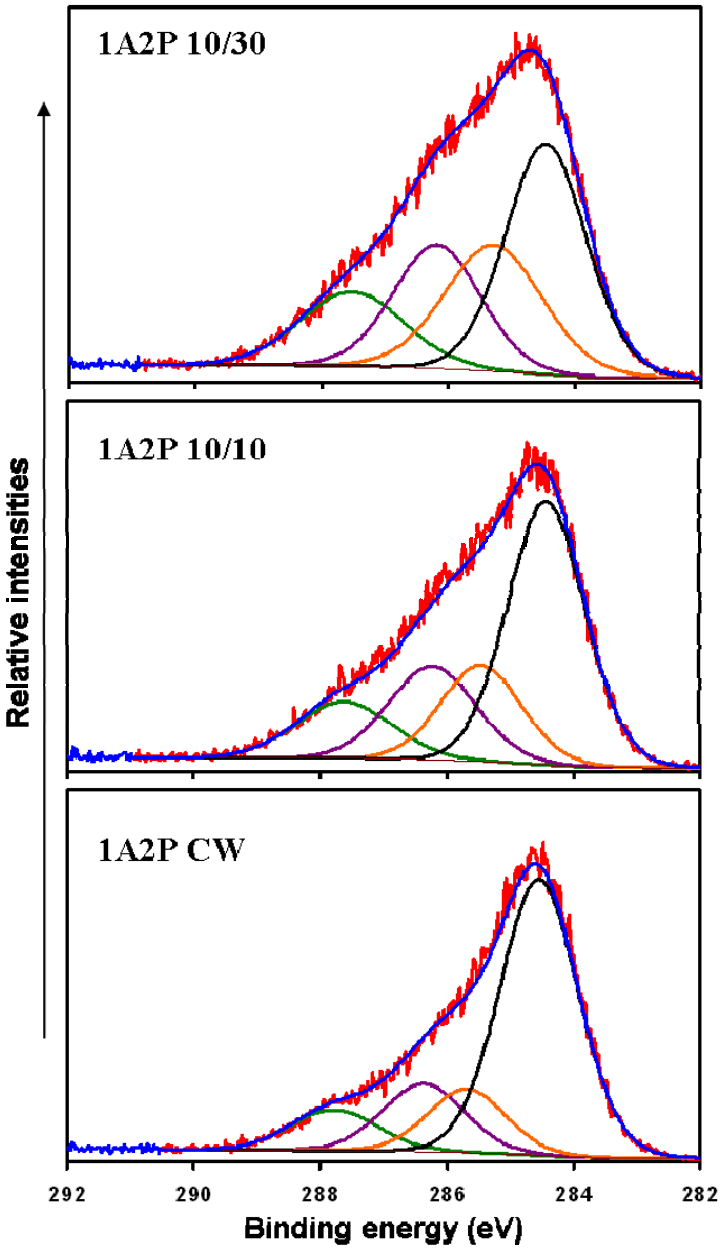

Figure 2.5 High resolution C(1s) X-ray photoelectron spectra of 1A2P films deposited at 10/30, 10/10 pulsed and CW conditions, as shown.

Table 2.1 Percent atomic composition of plasma polymerized 1A2P films produced by varying plasma conditions.

Plasma condition	**% C**	**% N**	**% O**
10/30	70.7	17.6	11.7
10/10	70.4	17.2	12.4
CW	75.6	13.7	10.7

Table 2.2 Percent carbon surface functionalities from high resolution XPS C(1s) spectra of different 1A2P films.

Plasma condition	**C-H 284.6 eV**	**C-N 285.5 eV**	**C-O/C≡N 286.3 eV**	**N-C=O 287.8 eV**
10/30	37.5	24.9	21.9	15.7
10/10	48.8	18.7	19.6	12.9
CW	60.3	13.9	15.6	10.2

2.3.4 Contact Angle and Capillary Rise Measurements:

Static, sessile water drop contact angle measurements were recorded at temperatures ranging from 20° to 60°C for 1A2P films deposited at the three aforementioned plasma duty cycles. The results of these measurements are shown in Figure 2.6. Notable differences in contact angles, and their temperature dependence, are clearly apparent. The low temperature contact angles increased significantly with higher power input, ranging from 45° for the 10/30 sample, to 55° for the 10/10 sample, to a value of 60° for the film deposited under CW conditions. The increasing film hydrophobicity, with increasing power input during film formation, is in accord with the

XPS results which reveal a progressive decrease in hetero atom content, and thus less polar groups, in the film sequence 10/30, 10/10, CW. More significantly, a dramatic increase in contact angle is observed for the 10/30 film, with a sharp change in wettability occurring over the temperature interval from 30° to 35°C. In contrast, no measurable change in film wettabilities were observed with increased temperature for the other two films. A constant time period (30 sec) was employed for each individual measurement to permit equilibration of the film with the sessile drop and, at the same time, to minimize evaporation of water from the hydrogels at higher temperature.

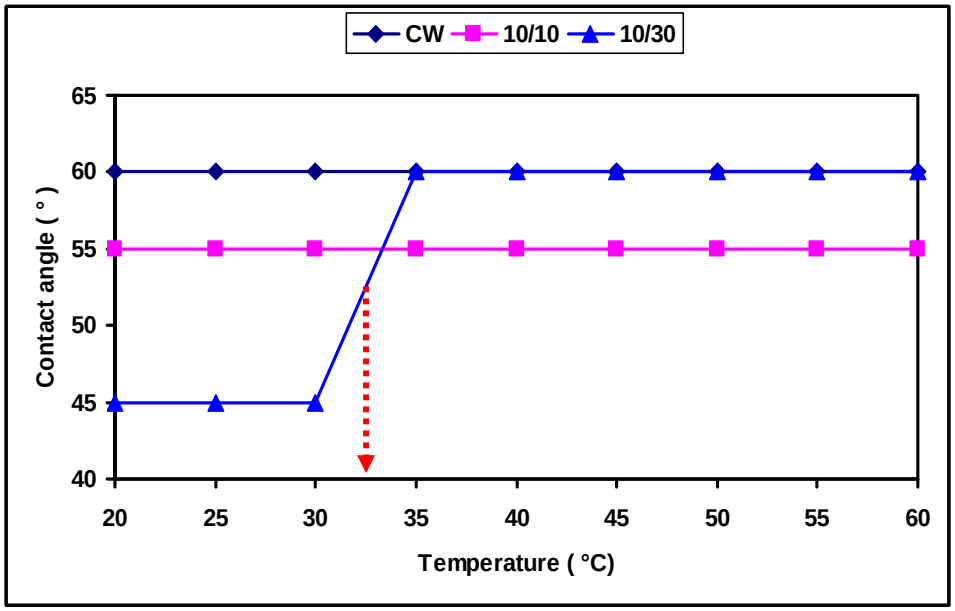

Figure 2.6 Static water contact angle measurements as a function of temperature for plasma polymerized 1A2P films produced under 10/30, 10/10 ms pulsed and CW modes.

The differences in surface wettabilities of the films noted in the contact angle measurements were confirmed by the capillary rise measurements. Figure 2.7 shows

the variation in heights of water column rise in capillaries coated with the three different 1A2P plasma polymers. These measurements were made with the capillary tubes immersed in water in a petridish. As shown in Figure 2.7, the rise heights clearly show the increased film hydrophobicity as the plasma duty cycle employed during deposition is increased. Additionally, although the 10/10 and CW films exhibit virtually no change in rise height when measurements are made at 40°C, the 10/30 film shows a sharp drop (i.e. increased hydrophobicity) at this higher temperature. The 6.5 mm decrease in capillary rise height level observed is consistent with the sharp increase in water contact angle for this film with increasing temperature, as shown in Figure 2.6.

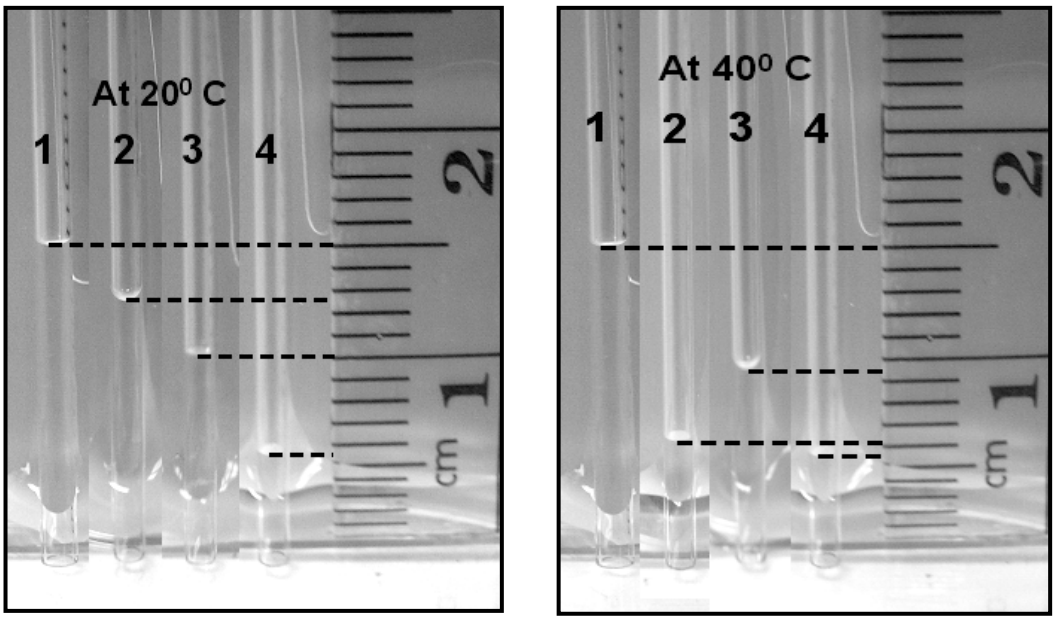

Figure 2.7 Capillary rise experiment of (1) uncoated capillary, (2) capillary coated with 1A2P (10/30), (3) capillary coated with 1A2P (10/10), (4) capillary coated with 1A2P (CW) at 20°C and 40°C.

Finally, it is interesting to note that a distinctive color change is observed for the 10/30 films but not for the other two films. The color change for the 10/30 samples occur shortly after the samples are removed from the plasma reactor. An example of this color change is shown in Figure 2.8 for samples deposited on polished silicon substrates. The bright colors shown result from interference effects due to reflection from the polished Si substrate. It is felt that the color changes arise from water absorbed thickness change and not from a change in refractive index. The polymer films, deposited on a transparent substrate, were light yellow in color. The actual color changes observed depend on the film thickness but they always occur spontaneously, over a short time period, with simple exposure of the sample to the atmosphere. This color change is completely reversible with respect to repeated heating and cooling. It is significant to note that no such color change was observed with samples of films produced under the 10/10 and CW conditions.

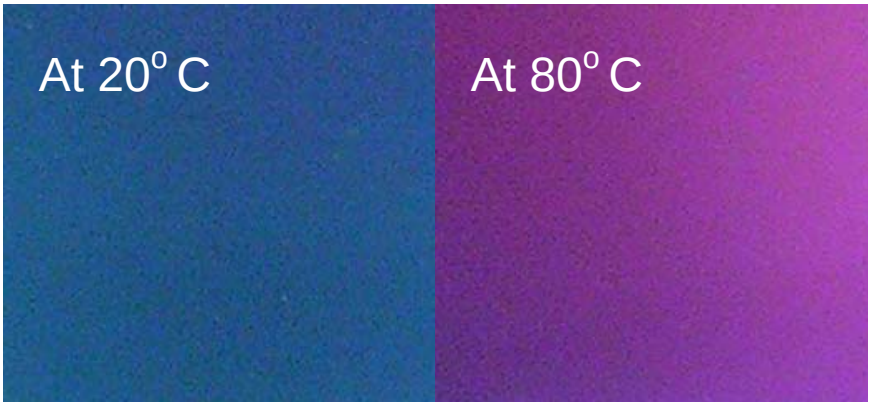

Figure 2.8 Color of plasma polymerized 1A2P (10/30) film at 20°C and 80°C.

2.3.5 Swelling studies of 1-amino-2-propanol films:

1A2P films of 1 micron thickness were deposited on tared PET cover slips of 22 x 60 mm size and weighed after exposure to the atmosphere to permit water adsorption. Subsequently, each film was placed in a petridish and immersed with 20 ml of deionized distilled water at room temperature for 48 hours. The weight of swollen films was measured after the moisture on their surfaces was carefully wiped with a tissue paper. Swelling ratios (SR) were calculated using SR = Ws/Wd, where Ws and Wd are the weights of the swollen and dry 1A2P films.[150] The swelling ratio results are summarized in Table 2.3.

Table 2.3 Comparison of swelling ratio of 1A2P films polymerized at different plasma conditions.

Plasma conditions **ms/ms**	**Swelling ratio (Ws/Wd)**
10/30	28 ± 2
10/10	12 ± 3
CW	7 ± 1

2.3.6 Plasma Polymerization of 2-(ethylamino) ethanol monomer

To further test the generality of hydrogel film synthesis via plasma polymerization, this study was extended to include a limited number of experiments with a second monomer. For this purpose, polymer films were generated using 2-(ethylamino) ethanol (2EAE), monomer. The 2EAE monomer contains structural

features (N-H and O-H groups) in common with the 1A2P compound. The 2EAE experiments included both pulsed and CW runs, under the same deposition conditions employed with the 1A2P monomer, namely pulsed runs at 10/30 and 10/10 ms, on/off ratios and CW, all runs carried out at 150 W peak RF power. These films were also characterized using ATR-FTIR, XPS and static water contact angle measurements.

2.3.6.1 ATR-FTIR Characterization of Plasma Polymerized of 2EAE films

The IR spectra observed were essentially identical to those obtained from the 1A2P compound, with respect to the absorption bands. Although the same absorption bands are observed with both monomers, the intensities of the high wave number 3500 to 3100 cm^{-1} peaks, relative to the peak centered around 1600 cm^{-1}, were significantly higher in the case of 1A2P than the 2EAE films. As in the case of the 1A2P films, the 2EAE films also exhibited the spontaneous absorption of water, as evidenced by the decreased absorption in the high wave number region after purging of the samples with dry N_2. As shown in table 2.4, the relative decrease in the high wave number absorption intensity, as a function of the plasma deposition conditions with purging, is in the order: 10/30 > 10/10 > CW, the same sequence as observed with the 1A2P compound.

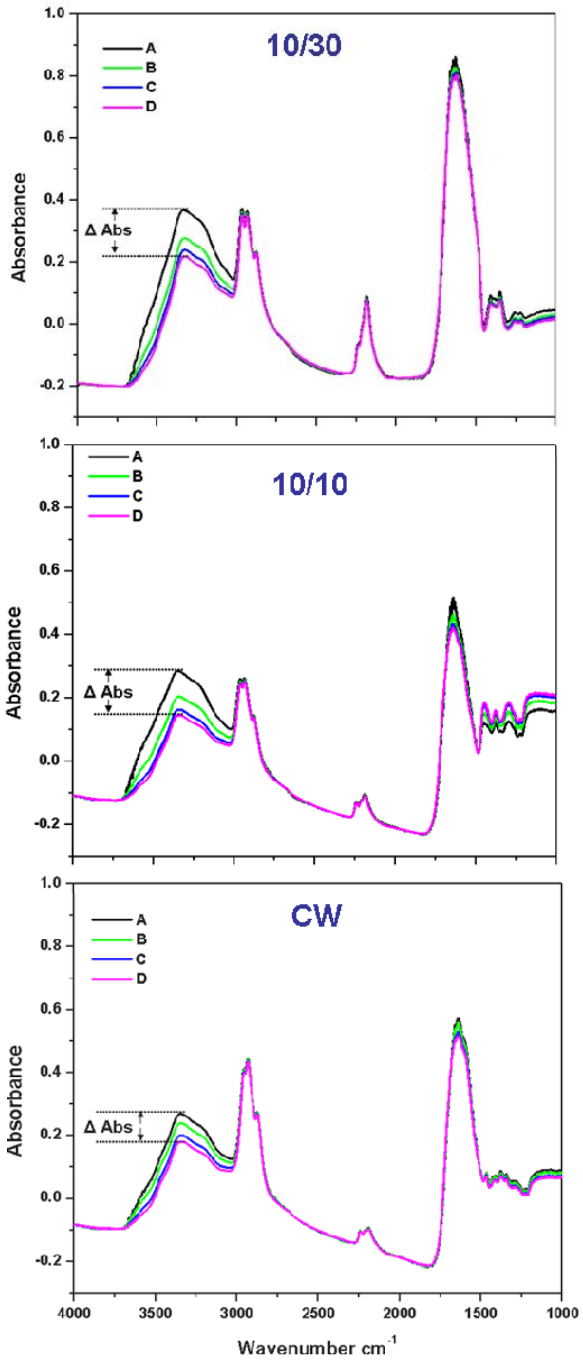

Figure 2.9 ATR-FTIR spectra of plasma polymerized 2EAE films deposited under (a) 10/30 ms; (b) 10/10 ms; (c) CW conditions. The A, B, C., and D spectra shown for each duty cycle represent the sequence as deposited, and after 2, 5, and 10 minute dry N_2 purge.

Table 2.4 Comparison of change in relative absorbance of the 3600-3100 cm^{-1} peaks after dry N_2 purge, all polymer films deposited at 150W peak power.

Plasma condition		**Δ Absorbance**	
Duty cycle	**Average power (W)**	**1A2P**	**2EAE**
10/30	37.5	0.44	0.17
10/10	75	0.33	0.14
CW	150	0.18	0.08

2.3.6.2 XPS Characterization of Plasma Polymerized 2EAE films

The atomic compositions of the poly-2EAE films produced under the different deposition conditions are shown in Table 2.5. The high resolution C(1S) XPS spectra of films obtained from the 1A2P monomer are shown in Figure 2.10, arranged in order of increasing plasma duty cycle employed during deposition, reading top to bottom. As shown in this Figure, there is a significant decrease in the relative contribution of higher binding energy C(1S) peaks as the plasma duty cycle employed was increased. Analyses of the deconvoluted C(1S) spectra, shown in Table 2.6, provides a more quantitative measure of the relative variation in the higher binding energy peaks. The peak assignments are identical to the 1A2P films, such as C-N at 285.5 eV, C-O plus C≡N at 286.3 eV and N-C=O at 287.8 eV. The progressive relative increase in the peak at 284.6 eV, as the plasma duty cycle is increased, is consistent with the progressive decrease in the heteroatom content of the films, and thus an increase in polymer cross-linking, with increasing average power input.

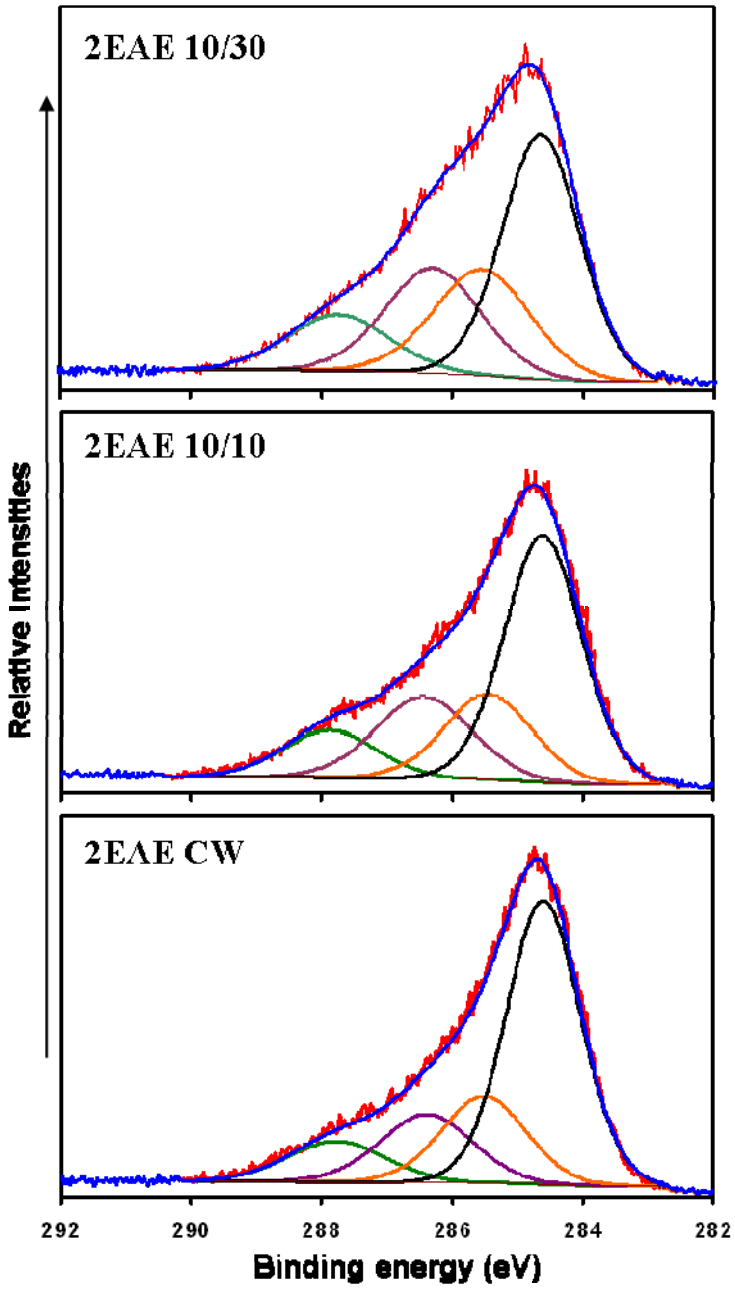

Figure 2.10 High resolution C(1s) X-ray photoelectron spectra of 2EAE films deposited at 10/30, 10/10 pulsed and CW conditions, as shown.

Table 2.5 Percent atomic composition of plasma polymerized 2EAE films produced by varying plasma conditions.

Plasma condition	**% C**	**% N**	**% O**
10/30	71.9	15.4	12.7
10/10	74.2	10.6	15.2
CW	75.3	9.4	15.3

Table 2.6 Percent carbon surface functionalities from high resolution XPS C(1s) spectra of different 2EAE films.

Plasma condition	**C-H 284.6 eV**	**C-N 285.5 eV**	**C-O/C≡N 286.3 eV**	**N-C=O 287.8 eV**
10/30	42.6	22.7	22.3	12.4
10/10	49.4	19.4	20.1	11.1
CW	54.7	19.1	16.2	10.1

2.3.6.3 Contact Angle and Capillary Rise Measurements:

The measurement of the temperature dependent water contact angles, shown in Figure 2.11, reveal a dramatic change in surface wettability for the 10/30 sample but no notable change for the 10/10 and CW samples. Although this same trend was also observed with the 1A2P, the ~57°C transition temperature observed with the 2EAE is significantly higher than that obtained for the 1A2P films.

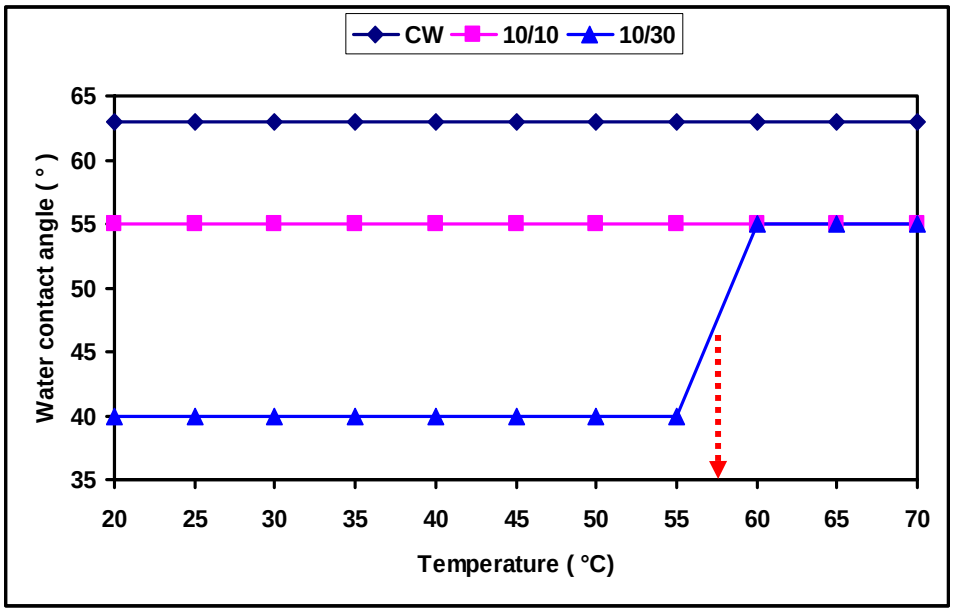

Figure 2.11 Static water contact angle measurements as a function of temperature for plasma polymerized 1A2P films produced under 10/30, 10/10 ms pulsed and CW modes.

2.3.7 Plasma Polymerization of 1A2P and 2EAE monomer mixtures

As noted above, different LCSTs were observed for hydrogel films obtained by pulsed plasma polymerization of the two pure monomers, namely ~33°C for poly-(1-amino-2-propanol) and ~57°C for poly-(2-ethylaminoethanol). In light of these observations, experiments were conducted to determine if combinations of these two monomers might provide hydrogel films having variable, but controlled, LCSTs,

In these experiments, the two monomers 1A2P and 2EAE were combined in the ratio 1:1 and 1:2, respectively, and subsequently polymerized under pulsed plasma conditions. The same plasma conditions namely duty cycle 10/30 (t_{on}/t_{off}, ms), 150W power and 130 mTorr pressure were employed for both depositions. In all runs, uniform

films of ~ 200 nm thickness were deposited on silicon wafer substrates. Static water contact angel measurements with variable temperature were performed to observe any change in hydrophilic / hydrophobic behavior of the thin hydrogel films. X-ray photoelectron spectroscopy was employed to analyze the chemical composition of the deposited hydrogels.

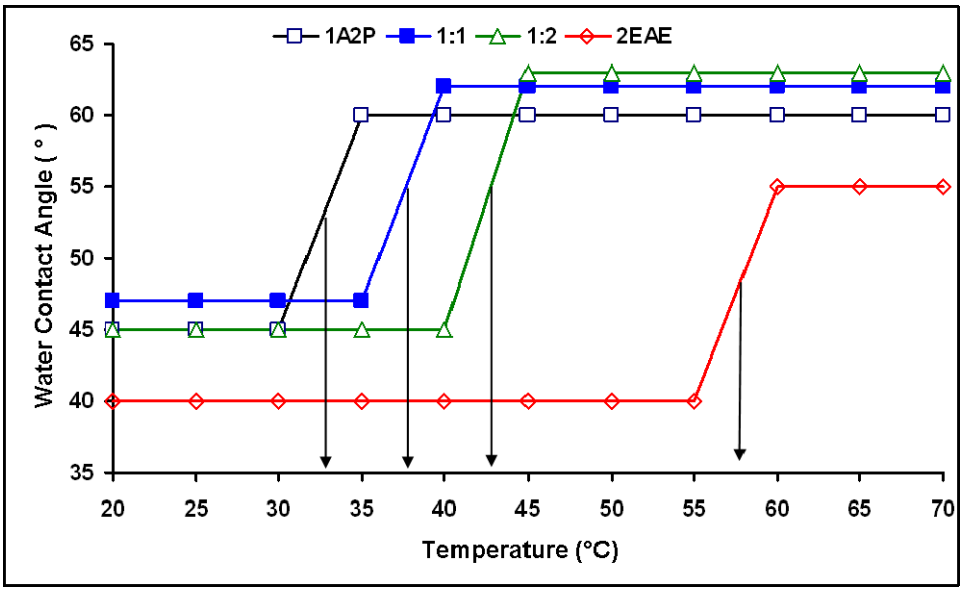

Figure 2.12 Static water contact angle measurements as a function of temperature for plasma polymerized 1A2P, 2EAE monomers and their mixtures.

Figure 2.12 shows the variation of static water contact angle of plasma deposited hydrogel films as a function of temperature, for both the two mixtures and, for comparison, the two pure monomers. The projected lines indicate the temperature at which the films are transitioning from more hydrophilic (lower contact angle) states to their more hydrophobic (higher contact angle) states, i.e. the LCSTs. It is interesting to note that, as the concentration of 2EAE increases in the feed monomer composition, the

transition temperature also increases. Therefore, the transition temperature can be tuned by adjusting the ratio of the feed monomers. An increase in LCST may be explained from the molecular structure of the monomers. 2EAE has one ethyl-substituted secondary amine which is providing more hydrophobic groups in the hydrogel. The IR spectra observed for these polymers were essentially identical with respect to the absorption bands. Therefore, it is difficult to distinguish the molecular structure of the plasma deposited polymeric films from IR spectra.

The elemental composition of the mixed monomer films, as obtained from X-ray photoelectron spectroscopy (Table 2.7), shows variations in the % C and hetero atoms (N and O). Percent carbon content increases as the proportion of 2EAE increases in the monomer mixture.

Table 2.7 Percent atomic composition of plasma polymerized (1A2P + 2EAE) films produced by varying plasma conditions.

Plasma condition	**% C**	**% N**	**% O**
1A2P:2EAE (1:1)	70.4	16.0	13.6
1A2P:2EAE (1:2)	72.5	14.8	12.7

Figure 2.13 shows the deconvoluted high resolution C(1S) spectra for the two mixtures. Both spectra are almost identical with a small variation in % composition of carbon surface functional groups as depicted in table 2.8. The percent surface carbon functional group composition is consistent with the percent elemental composition.

Relative quantities of functional groups containing hetero atoms decrease as the ratio of 2EAE monomer increases in the monomer mixture.

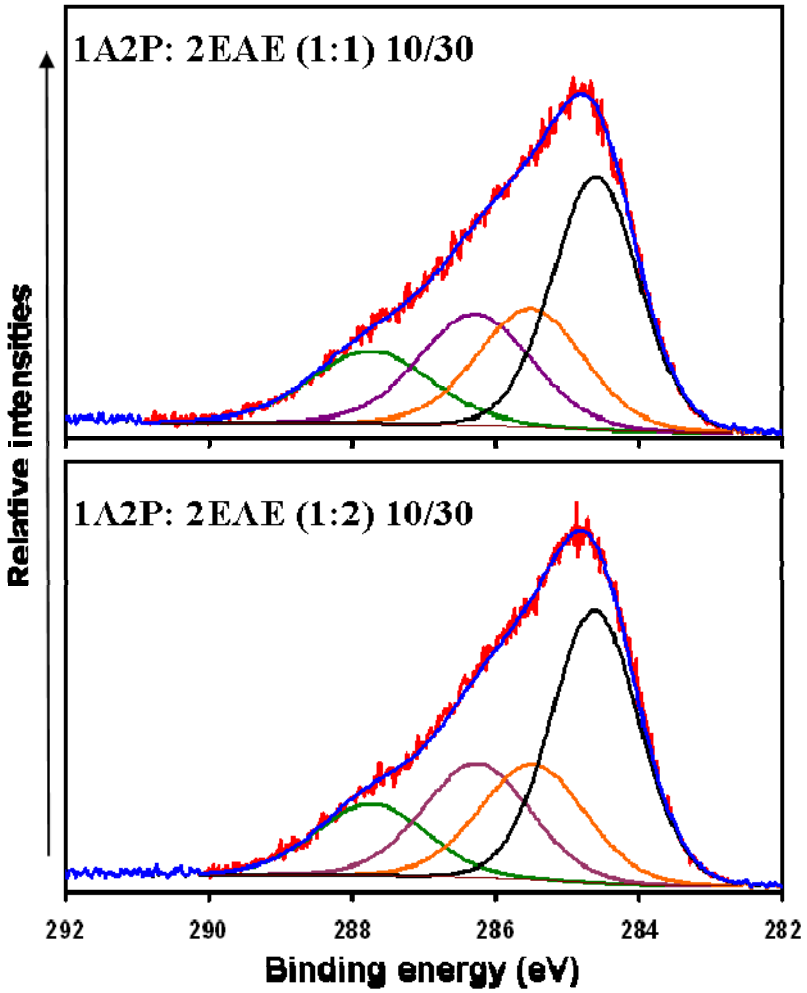

Figure 2.13 High resolution C(1s) X-ray photoelectron spectra of (1A2P + 2EAE) films deposited at 10/30 pulsed conditions as shown.

Table 2.8 Percent carbon surface functionalities from high resolution XPS C(1s) spectra of different (1A2P + 2EAE) films.

Plasma condition	**C-H 284.6 eV**	**C-N 285.5 eV**	**C-O/C≡N 286.3 eV**	**N-C=O 287.8 eV**
1A2P:2EAE (1:1)	39.3	22.6	22.4	15.7
1A2P:2EAE (1:2)	42.6	21.7	21.7	14.0

In an attempt to rationalize the thermoresponsive behavior of the hydrogel films obtained by plasma polymerization of the pure monomers and the mixtures at pulsed duty cycles (10/30 and 10/10) and CW mode, a more detailed analysis of the XPS data was performed. Table 2.9 shows the ratio of different atom percentage and different surface carbon functional groups for all the hydrogel films. In order to illustrate these data, these ratios are plotted in Figure 2.14.

Table 2.9 Ratio of percent elemental composition and carbon surface functionalities from high resolution XPS C(1s) spectra of different hydrogel films.

Monomer *Duty cycle*	Ratio of % C, %N, %O and % surface carbon functional groups							
	C:O	C:N	N:O	C-N : C-O/C≡ N	C-N : N-C=O	C-H : N-C=O	C-H : C-O/C≡ N	C-H : C-N
1A2P *10/30*	6.04	4.02	1.50	1.14	1.59	2.39	1.71	1.51
1A2P *10/10*	5.68	4.09	1.39	0.95	1.45	3.78	2.49	2.61
1A2P *CW*	7.07	5.52	1.28	0.89	1.36	5.91	3.87	4.34
2EAE *10/30*	5.63	4.68	1.20	1.02	1.83	3.42	1.91	1.87
2EAE *10/10*	4.90	6.98	0.70	0.97	1.75	4.45	2.46	2.55
2EAE *CW*	4.92	7.99	0.62	1.18	1.89	5.42	3.38	2.86
1:1 *10/30*	5.15	4.41	1.17	1.01	1.44	2.51	1.76	1.75
1:2 *10/30*	5.71	4.89	1.17	1.00	1.55	3.05	1.96	1.97

In Figure 2.14, it is clearly noticed that the ratio of C:O, C:N and C-H:N-C=O are quite similar for all the hydrogel films deposited at 10/30 duty cycle (as shown in blue circle) whereas, the value of these ratios are inconsistent for the non-thermoresponsive hydrogel films. A similar trend is observed for the ratio of N:O, C-N:C-O/C≡ N, C-N:N-C=O, C-H:C-O/C≡ N and C-H:C-N for the films synthesized at 10/30 duty cycle (as shown in red circle). However, these ratios for the non-thermoresponsive films exhibit significantly different values than those observed from the thermoresponsive films. It would appear that it is the ratio of these functional groups and atom percents which are responsible for thermo- or non-thermoresponsive behavior.

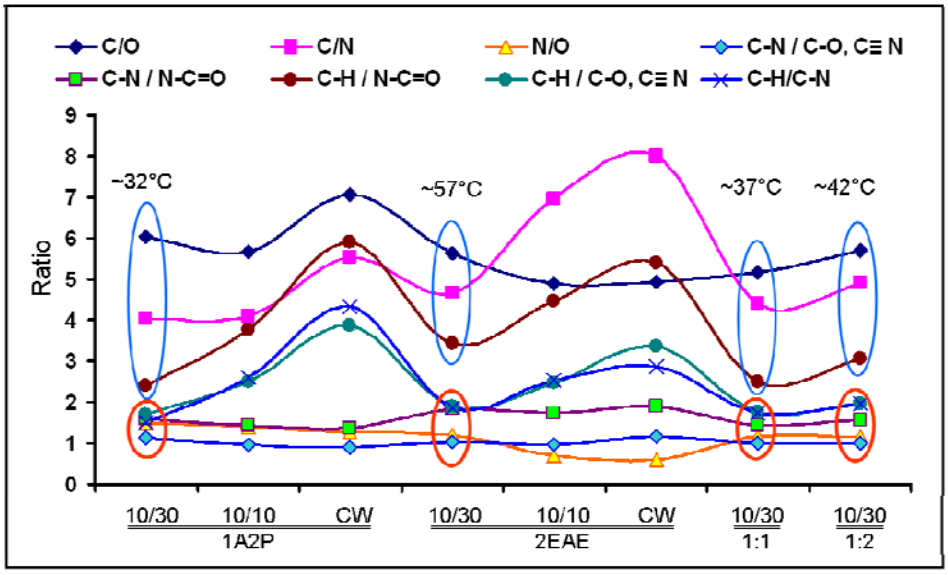

Figure 2.14 Plot of ratio of percent elemental compositions and carbon surface functionalities from XPS analysis of different hydrogel films.

2.4 Discussion

The films generated from the two monomers employed in this study exhibited similar properties in terms of IR spectra and surface energy changes upon warming. Both sets of polymer films exhibited a pronounced tendency towards spontaneous atmospheric water adsorption, which is subsequently readily released upon exposure to a flow of dry N_2. A more quantitative measurement of the variation in extent of water adsorption with duty cycle changes was obtained by measurement of the weight gain by the films, with and without adsorbed water. The weight changes observed for the 1A2P films are shown in table 2.4, in which the swelling ratio is significantly higher for the 10/30 film than the other two samples. The IR absorption peak frequencies observed are essentially identical with both monomers, although there is some difference in the

relative band intensities and the magnitude of water adsorbed upon exposure to air. The extent of spontaneous water adsorption is considerably more pronounced with films from the 1A2P monomer relative to those from 2EAE, as revealed in Table 2.3.

A second important distinction between the 1A2P and 2EAE films, as shown by a comparison of Figures 2.6 and 2.9, is the temperature difference required for the hydrophilic to hydrophobic phase transition for the 2EAE film relative to that of the 1A2P. Presumably, the higher transition temperature exhibited by the 2EAE film reflects the somewhat higher cross-linking, and thus the aforementioned less H_2O adsorption, in this film compared to the 1A2P sample.

The results obtained in this study provide strong confirmation of the utility of the plasma polymerization technique as a viable approach to synthesis of hydrogel films. Prior work in the area of hydrogel synthesis via plasma polymerizations has focused on NIPAM, including a recent thorough study of the effects of power input and reaction temperatures on the composition and thermal responsive behavior of polymer films produced.[144] The present study identifies two new monomers which provide hydrogel films under appropriate plasma conditions. It differs from the NIPAM work in that the volatility of the monomers eliminates the need for heating of the monomer or the reactor chamber. As demonstrated in the present study, in common with the NIPAM work, the production of films which exhibit thermoresponsive hydrogel behavior is strongly dependent on the plasma conditions employed. With both monomers, the characteristic hydrogel property of a phase transition with temperature change is

observed only at the lowest average power inputs employed. Attempts to produce hydrogel films at even lower average power inputs were unsuccessful in that those films exhibited significant solubility in water, even at room temperature. Overall the picture which emerges from this investigation is that with judicious control of the plasma deposition parameters, in this case the plasma duty cycles, it is possible to produce films which possess significant H-bonding to exhibit hydrogel properties, and at the same time, are sufficiently cross-linked to be insoluble in water. For example, the films used in the present study have exhibited long term stabilities with respect to immersion in aqueous solutions, as well as to repetitive cycling between wet and dry states.

The film chemistry variations observed with changes in plasma duty cycles are consistent with many prior studies of film chemistry control, covering a wide range of monomers, made available by the variable duty cycle pulsed plasma approach. As revealed by the XPS, IR and water contact angle measurements, a decrease in plasma duty cycle provides an increased retention of the heteroatoms of the monomers in the polymer films, and thus the degree of polarity in these polymers. The increased retention of monomer structure in the polymer films with decreasing plasma duty cycles is believed to arise from the increased importance of film formation under plasma off times, as revealed by the energy efficiency data (Figure 2.3). The less energetic conditions which prevail during plasma off times limit monomer fragmentation. As illustrated in the present study, this film chemistry control is of pivotal importance in achieving a true thermoresponsive hydrogel state via the plasma polymerization route.

At the same time, given the relatively minor variations in atomic compositions (Table 2.1) it is clear that the film properties are determined by the relative amounts of functional groups present, shown in Table 2.2. It is interesting to note that the thermo responsive hydrogel properties are only observed for one of the three samples with each monomer. Clearly, the present results suggest that relatively small changes in molecular structure can produce very significant film behavior with respect to the thermal induced hydrophilic to hydrophobic phase transitions.

In summary, an all-dry single step, plasma polymerization route to synthesis of thermoresponsive hydrogel thin films from the monomers 1-amino-2-propanol and 2-ethylaminoethanol and their mixtures has been successfully demonstrated. In particular, thermoresponsive hydrogels exhibiting a controlled range of lower critical solution temperature have been synthesized for the first time using plasma polymerization technique. It seems reasonable to speculate that the film chemistry control provided by the variable duty cycle pulsed plasma technique should provide opportunities to generate hydrogel films from many other monomers. In particular, given the different phase transition temperature observed in the present work, identification of other monomers may well provide a spectrum of hydrogels having transition temperatures covering a wide range of values.

2.5 Conclusion

A new class of monomers has been used to prepare plasma polymerized hydrogel films. Molecular structure of the films has been characterized by ATR-FTIR

and XPS spectroscopies. Variable duty cycle pulsed plasma polymerization has been shown to be an effective route to control moisture uptake and thermoresponsive behavior of the films.

CHAPTER 3

IMMOBILIZATION OF BIOMOLECULES TO PLASMA POLYMERIZED SURFACES

3.1 Introduction

Immobilization of biologically important molecules such as cell receptor ligands, antibodies, enzymes, DNA fragments and drugs on solid surfaces has many biomaterials, therapeutic, bioprocessing and biochemical applications. A few examples in which surface chemistry plays an ever increasing role include probing cell-biomaterials surface interactions,[151-153] inflammatory responses to implants,[154,155] biosensors,[156-158] bioseparations,[159,160] DNA arrays,[161,162] bioreactors,[163] targeted drug deliveries.[164,165,166] A more extensive listing of current research involving immobilized biomolecules is provided in Table-3.1.

Typically there are three general methods employed to incorporate biomolecules on solid substrates, namely: physical adsorption; entrapping biomolecules within the substrate matrix; and, covalent attachment of molecules by chemical methods. In physical adsorption of biomolecules, surface physical properties, such as surface hydrophilicity/ hydrophobicity, porosity and morphology influence the extent of protein adsorption. Additionally, chemical properties such as the nature of the surface

functional groups, also affect the amounts of adsorbed proteins. In general, passive physisorption is usually uncontrolled, and adsorbed films are generally unstable to denaturation and desorption or displacement.[167,168] As a result, direct passive adsorption of proteins has become of increasingly less use as other surface modification techniques are developed.

Biomolecules can also be immobilized within a polymer matrix by entrapping them within the polymer porous structure through simple absorption or encapsulation techniques.[169,170,171] This method is commonly employed in drug delivery applications where desorption or diffusional release of the entrapped molecules are required. The release of entrapped or encapsulated molecules depends on their size, molecular nature and matrix porosity. However, a better control of the release of the biomolecules can be achieved by polymerizing biomolecule conjugated monomer(s). In this way, the entrapped biomolecules are covalently bonded to the host matrix.[172,173] Subsequently, under certain conditions, these covalent bonds may undergo hydrolysis or dissociation thus releasing the biomolecule. In this approach, the release profile depends on the chemical nature of the bonds between the biomolecules and the matrix.

In recent years, the third approach noted above namely, covalent bonding of biomolecules to substrate surfaces, has gained increased attention. In these studies, biomolecules are attached to the substrate surface via strong covalent bonds, thus essentially eliminating subsequent leaching of active components from the modified surfaces. Although this covalent attachment can be achieved, the conjugation process is

frequently accompanied by loss or decrease in biological activity of the attached molecules, such as denaturation of proteins.[167,168] To help minimize denaturation and thus improve retention of biomolecule structures and functions, an intermediate, generally short chain linker, is often employed to tether the biomolecules to the substrate. The linker molecules, also known as spacer groups or arms, are intended to help retain the stereochemical freedom of the attached molecules by minimizing their interactions with the solid supports. In practice, bifunctional spacer molecules are commonly used to tether biomolecules to the surface. Bifunctioalized polyethylene glycols, possessing reactive groups at both ends of the molecule, are among the most popular compounds used for this purpose. For example, surface tethered cell adhesion peptides (RGD, RGDS etc.) show significantly greater response when spacers of optimum chain length are used.[174,175]

The aim of the research studies described in this chapter was to determine if plasma surface modification technology could be successfully employed to covalently attach biomolecules to surfaces, without undue compromise of the biological activity of the attached molecules. A significant driving force in undertaking this work is the fact that the plasma surface modifications are completely conformal in nature, thus not limiting the covalent attachment process simply to flat objects. This is an important consideration given the fact that biomaterials surface modifications increasingly involve objects of unusual shape. For example, vascular stents plus many other implants, scaffolds for cell growth, and fine particles for directed drug delivery are but a few of

the current highly active research areas which would benefit from conformal coatings of non-planar substrates.

The pulsed plasma polymerization technique was used to deposit thin polymeric functionalized films on targeted surfaces. The functionalized surfaces were then either used directly for biomolecule conjugations, or, in other cases, were functionalized with linker molecules for subsequent tethering of the biomolecules to the functionalized surfaces. After evaluation of various potential functionalized monomers, it was determined that plasma polymerization of vinyl acetic acid provided an opportune route to introduce reactive –COOH groups unto the surfaces for the subsequent attachment of biomolecules. Plasma polymerization was operated under pulsed conditions in order to obtain optimized film chemistry in terms of maximum surface functional group density consistent with sufficient cross-linking in the polymeric films. Crosslinking in the deposited polymer was required to prevent it from dissolution during further derivatization reactions by wet-chemistry and subsequent biomaterials applications. Once the integrity of the plasma deposited films were verified, bovine serum albumin (BSA) and RL-9A TCRm antibody were attached to the modified surfaces, as proof of concept tests of the overall utility of this approach.

BSA was selected for this experiment because it is an abundant, less expensive and commonly used protein of molecular weight ~67kDa. BSA has been immobilized on solid surfaces, by both physical and chemical methods, for many applications. For example, in enzyme linked immunosorbent assays (ELISA) to minimize non-specific

adsorption of other proteins,[176,177] in enantiomeric separations on ion-exchange stationary phases,[178] to study drug-protein interactions in affinity column chromatography,[179] and in biosensor for trace lead detections.[180]

The RL-9A TCRm antibody employed was selected for its availability in highly purified form, coupled with the fact, that an assay exists to measure the biological activity of these antibodies,[181,182] as developed by collaborators at Texas Tech University. RL-9A antibody is a T cell receptor mimic, having a molecular weight of 150kDa. It has specific binding ability to the HLA-A2/NY-ESO-1 peptide complex which exists in malignant tumor cell lines. In the present study, the RL-9A antibodies were covalently coupled to iron oxide nanoparticles. The choice of Fe_2O_3 nanoparticles was based on their supermagnetic properties when exposed to a magnetic field. In this way, functionalized particles can be conveniently collected or localized via simple exposure to an appropriately focused magnetic field.

In both sets of coupling reactions, a bifunctional 6-carbon spacer molecule, 6-aminohexanoic acid, was used to keep the immobilized biomolecules positioned away from the substrate surface. Water soluble carbodiimide chemistry[183] (Figure 3.1a and Figure 3.1b) was employed to perform both the conjugation reactions, such as tethering spacer molecules to –COOH groups on plasma polymeric films and BSA or RL-9A TCRm antibody attachment to surface immobilized spacer molecules.

Table 3.1 Application of Immobilized Biomolecules and Cells.[184]

Enzymes	Bioreactors (Industrial, biomedical) Bioseparations Biosensors Diagnostic assays Biocompatible surfaces
Antibodies, peptides, and other affinity molecules	Biosensors Diagnostic assays Affinity separations Targeted drug delivery Cell culture
Drugs	Thrombo-resistant surfaces Drug delivery systems
Lipids	Thrombo-resistant surfaces Albuminated surfaces
Nucleic acid derivatives and nucleotides	DNA probes Gene therapy
Cells	Bioreactors (industrial) Bioartificial organs Biosensors

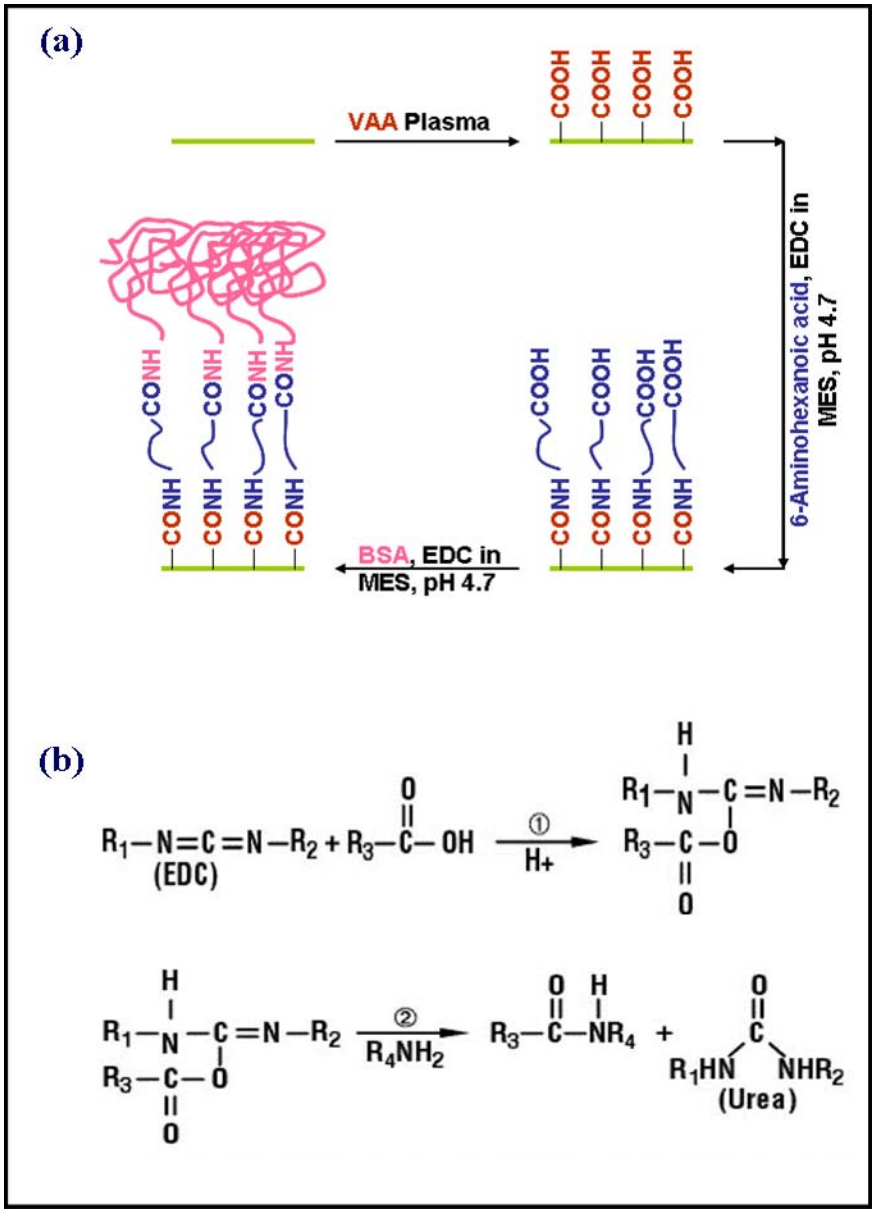

Figure 3.1 (a) Schematic diagram of the process of BSA immobilization on solid surface, (b) Reaction scheme of 1-Ethyl-3-(3-dimethylaminopropyl)-carbodiimide.

3.2 Experimental

3.2.1 Materials

Vinyl acetic acid, 6-aminohexanoic acid and BSA were purchased from Sigma-Aldrich, St. Louis, MO. EDC (1-ethyl-3-(3-dimethylaminopropyl) Carbodiimide.HCL) and MES (2-(N-morpholino) ethanesulphonic acid) buffer were purchased from Pierce, Rockford, IL. The RL-9A antibodies were supplied by Professor Jon Weidanz, of the Texas Tech School of Pharmacy. Polypropylene microparticles (~35μm) and iron oxide nanoparticles were purchased from Polysciences Inc., Warrington, PA and Alfa-Aesar, Ward Hill, MA respectively.

3.2.2 Plasma Polymerization

An ATR crystal and 1 cm^2 sections of Si wafer were placed inside a 360° rotating plasma reactor (Figure 3.2). The reactor was evacuated to 2 mTorr background pressure. Vinylacetic acid (VAA) monomer was then introduced into the reactor. Plasma was ignited at a constant monomer pressure of 80 mTorr. VAA was plasma polymerized under pulsed conditions. The optimum plasma duty cycle, with respect to maximizing the –COOH film surface density and, at the same time, achieving sufficient polymer cross-linking to provide film stability upon immersion in aqueous solutions, was determined to be 0.75ms/20ms (t_{on}/t_{off}) and 200W peak power input. Polypropylene microparticles (35 micron) were coated with plasma polymerized (PP) VAA to immobilize BSA molecules, whereas 30 nm Fe_2O_3 particles were employed in the antibody work. Typically, 50 nm thick films were deposited on the polypropylene

particles but much thinner films, 5 to 10 nm, on the iron oxide particles. The VAA polymers were also deposited on other substrates for spectroscopic characterization of the thin films. These included polished silicon, for XPS and surface wettability measurements, and quartz crystals for ATR-FTIR measurements. A home built 360° rotatable reactor plasma system was employed for the particle coating experiments. Thin ledges, on the inside walls of the reactor, were employed to transport and provide continuous exposure of the particle surfaces to the plasma discharge. The constant particle agitation was necessary to help overcome the natural tendency for the particles to aggregate. This is particularly true for the nanoparticles, as aggregation becomes increasingly more pronounced as the particle size is decreased. A schematic diagram of the reactor system employed is shown in Figure 3.2.

3.2.3 Reaction of PP VAA with 6-Aminohexanoic acid

The PP VAA coated samples, including ATR crystals, silicon wafers, polypropylene microparticles and iron oxide nanoparticles, were thoroughly washed, 3 times with 30 minutes moderate shaking, with deionized water and MES buffer (pH 4.7) separately to remove any loosely bound/ adsorbed VAA oligomers/ monomers. The $-NH_2$ end of 6-aminohexanoic acid was reacted with the surface –COOH using standard carbodiimide chemistry in aqueous medium at pH 4.7.[176] Subsequently, the samples were washed repeatedly with buffer solution and deionized water to remove any unreacted components.

For the carbodiimide coupling reactions of BSA to the polymer surfaces, the concentrations of spacer and EDC were maintained at 10mg/ml and that of BSA at 2 mg/ml of the solution buffer. For PP particles, 100mg of washed particles were dispersed in 5ml of MES buffer. Fifty mg of EDC were then added and stirred for 2 minutes to allow dissolution and reaction of EDC with the –COOH groups. Subsequently, 50 mg of spacer (6-aminohexanoic acid) were added. This reaction mixture was allowed to continue, with moderate shaking, for 2 hours. The particles were then washed three times with deionized water followed by 3 washings with MES buffer. All the supernatant liquids were discarded.

In the experiments with RL-9A TCRm antibodies, varying amounts of VAA coated iron oxide nanoparticles were employed in reactions with a fixed quantity of antibodies. This approach was employed since the absolute surface number of the –COOH groups on the particle surfaces was not known. The amounts of Fe_2O_3 employed in the separate tubes were 5 mg, 15 mg, 30 mg, 40 mg and 50 mg, respectively. The particles were dispersed in 2 ml MES and washed, as mentioned above, to remove any low molecular weight oligomers or even monomer molecules of VAA adsorbed on the particles from the plasma process. Following the washing procedure, 2 ml of MES buffer were added to each vial followed by addition of 20 mg of EDC. After 2 minutes of stirring, 20 mg of spacer were added and the reaction was continued for 2 hours. The solution was then discarded and particles were washed 5

times with MES buffer and 5 times with deionized water in order to remove any unwanted species (such as excess spacer, EDC and byproducts).

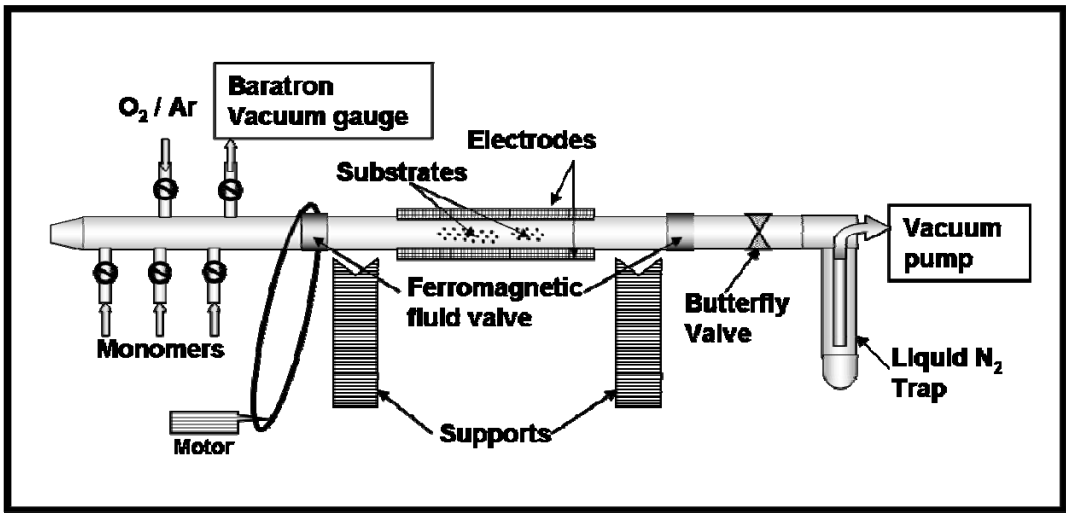

Figure 3.2 Schematic diagram of 360° rotating plasma reactor.

3.2.4 Immobilization of BSA and antibodies

The PP particles, functionalized with the covalently attached 6-aminohexanoic acid spacers, were redispersed in 4 ml of fresh MES buffer. Fifty mg of EDC were added to the dispersion, stirred for 2 minutes and 1ml of BSA or FITC-BSA (2mg/ml) was then added to the mixture. The reaction was allowed to continue for 2 hours with continuous shaking. The polypropylene particles, along with several functionalized flat substrates, were washed several times with buffer solution, deionized water and finally 1% SDS (sodium dodecyl sulfate) solution to remove any non-covalently linked BSA from the surfaces.

To immobilize RL-9A antibodies, spacer attached iron oxide nanoparticles were redispersed in 1 ml MES buffer, and 20 mg of EDC were added and stirred for 2

minutes. One ml of RL-9A antibody (2mg/ml) was added to each of the 5 vials containing Fe_2O_3 nanoparticles quantities ranging from 5 to 50 mg, as described above. The covalent coupling of the antibodies to these particles was allowed to continue for 2 hours with continuous shaking. The RL-9A antibody conjugated iron oxide nanoparticles were washed 5 times with MES buffer, followed by 5 times washing with PBS (phosphate buffer saline, pH 7.2) solution. The particles were redispersed in 1 ml PBS solution for further studies. Table-3.2 describes the varying concentration of nanoparticles used in this experiment.

Table 3.2 Description of nanoparticle concentration in the RL-9A conjugation reactions.

Sample name	Amount of nanoparticles used	Description
5 RL-9A	5 mg	2mg RL-9A antibody conjugated to 5 mg of nanoparticles.
15 RL-9A	15 mg	2mg RL-9A antibody conjugated to 15 mg of nanoparticles
30 RL-9A	30 mg	2mg RL-9A antibody conjugated to 30 mg of nanoparticles
40 RL-9A	40 mg	2mg RL-9A antibody conjugated to 40 mg of nanoparticles
50 RL-9A	50 mg	2mg RL-9A antibody conjugated to 50 mg of nanoparticles

3.2.5 Characterization

The initially produced plasma thin films, as well as the subsequent modification of these films, were analyzed by ATR-FTIR spectroscopy using a Bruker Equinox 55 Spectrophotometer. Additionally, X-ray Photoelectron Spectroscopy (XPS) data for the surfaces were obtained using a Perkin Elmer PSI 5000 series instrument equipped with

a monochromator. Fluorescence images of the polypropylene microparticles were taken in a Leica fluorescence microscope (Leica Microsystems, Wetzlar, GmbH) equipped with a Nikon E500 Camera (8.4V, 0.9A, Nikon Corp., Japan).

3.3 Results and discussion

The characterization and evaluation of the BSA coupled samples are described below.

3.3.1 ATR-FTIR Spectroscopy

Figure 3.3 shows the ATR FT-IR spectra of a sample taken at various stages of reaction. The PP-VAA spectrum represents the FT-IR spectrum of plasma deposited vinylacetic acid film. The distinct, sharp, intense peak at 1708 cm^{-1} and the broad peak at ~3000 cm^{-1} – 3500 cm^{-1} are absorptions of >C=O and -O-H characteristic of carboxylic acid groups.[185] The next spectrum, identified as *reacted with spacer,* was taken after the spacer molecules were attached to the poly(vinylacetic acid) film. The intensities of >C=O and -O-H peaks decreased somewhat, most probably as a result of dissolution of a portion of the polymer film polymer and/or trapped oligomers in the polymer during the washing procedure. Of more significance are the two new peaks of low intensity, at 1650 cm^{-1} and 1530 cm^{-1}, shown in the inset. These two peaks are characteristic of amide carbonyls (>C=O)[185] as a result of the formation of amide bonds by the reaction of –COOH groups of VAA with the $-NH_2$ terminal group of the 6-aminohexanoicacid spacer molecule. The presence of these two peaks confirms the

successful attachment of the hexanoic acid spacer through the EDC coupling process. Finally, the presence of BSA on the polymer film (labeled *BSA attached PP VAA*) is confirmed by the appearance of very much enhanced amide carbonyl peaks (1654 cm^{-1} and 1528 cm^{-1}) and characteristic N-H stretching frequency (3305 cm^{-1}) due to presence of amide bonds in BSA.

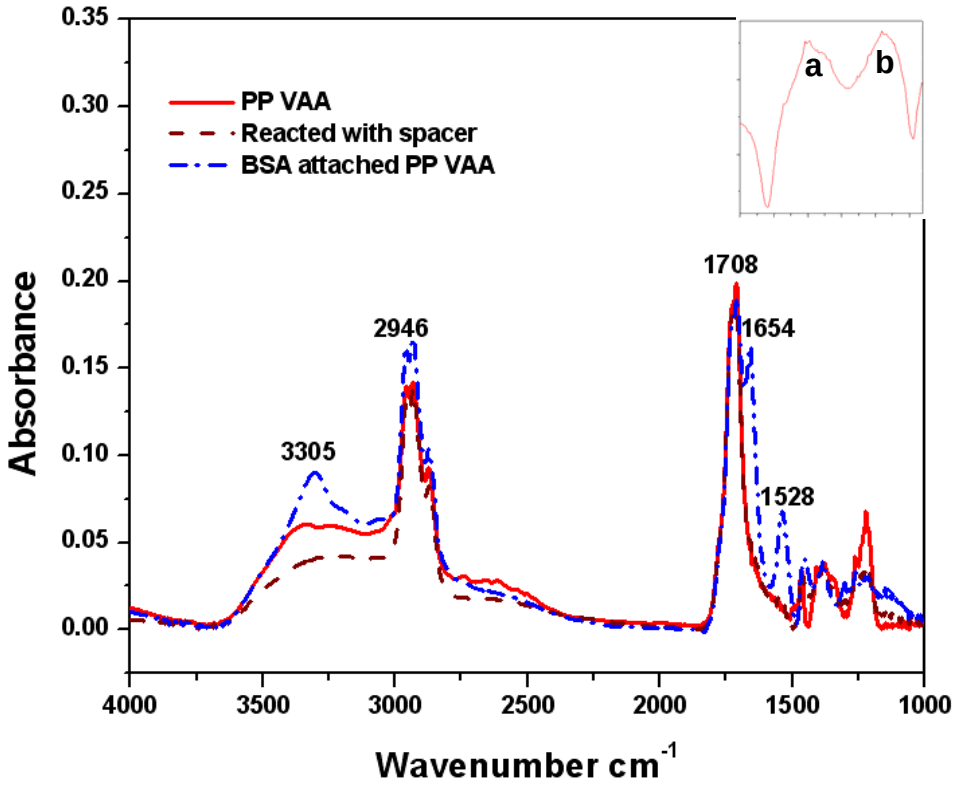

Figure 3.3 ATR-FTIR Spectra of unmodified PP VAA, PPVAA reacted with spacer and BSA attached PPVAA. [Inset: characteristic peaks of amide carbonyl at (a) 1650 cm^{-1} and (b) 1530 cm^{-1}].

To ascertain that the protein molecule is covalently bound to the substrates, and not simply physically adsorbed, the BSA conjugated films were washed with a 1% sodium dodecyl sulphate (SDS) surfactant solution. SDS is a well known surfactant used to remove any physically adsorbed or unconjugated proteins from surfaces. In this case, BSA attached films were placed in 1% SDS solution for 4 hours and ATR-FTIR spectra of the sample were recorded at 1hr, 2hr and 4 hr time periods to observe any change in the intensities of the FT-IR peaks from the attached BSA molecules. Figure 3.4 shows the subtracted spectra of attached BSA molecules as obtained by subtracting the *Reacted with spacer* spectrum from each individual spectrum taken after each 1% SDS washing steps. That is, Figure 3.4 represents only BSA molecules present on the surface after the successive washing periods. It is clearly noted that the intensity of amide carbonyl peaks (1654 cm^{-1} and 1528 cm^{-1}) and characteristic N-H stretching frequency (3305 cm^{-1}) remain essentially constant with SDS washing, thus confirming the covalent nature of the conjugation and the absence of physically adsorbed BSA on the surface.

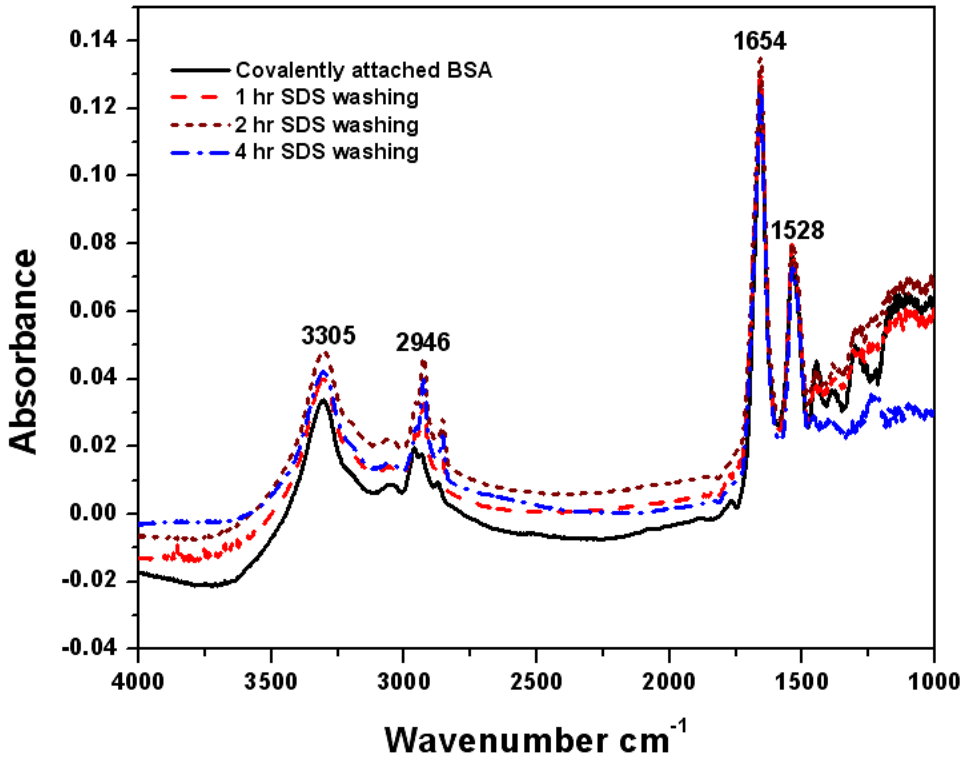

Figure 3.4 ATR-FTIR subtracted spectra of bovine serum albumin after covalent attachment to PPVAA surface at different interval of 1% SDS washing.

3.3.2 X-ray Photoelectron Characterization of the Chemically Modified Surfaces

Table 3.3 represents the change in percent atomic composition of the films obtained from the XPS survey scan at various stages of the BSA conjugation process. The initial, as formed, plasma deposited poly(vinylacetic acid) film, i.e. PP VAA, as expected, has no nitrogen in its chemical composition. A noticeable increase (2.6%) in nitrogen is observed in the sample after 6-aminohexanoic acid spacer molecule is attached to the polymer film. Appearance of 2.6 % nitrogen is consistent with that expected from the 6-aminohexanoic acid molecules. Surface %C content increased from

76% to 79.4%. with spacer attachment. The presence of increased carbon, after the attachment of the spacer molecule, is as expected from the six carbon atoms of the hexanoic acid. A relatively higher increase in N atom content (~6%) is obtained after BSA was coupled to the surface, a reasonable increase given the large molecular weight of the bound protein. The XPS data were obtained after thorough washing and drying of the protein coupled sample with the SDS solution.

Further confirmation of this covalent BSA attachment is revealed in the high resolution C(1s) XPS spectra, shown in Figure 3.5, which contrasts results from the initial PP VAA film and the surface after BSA attachment. As shown in Figure 3.5, the 288.8 eV peak in the PPVAA film, characteristic of –COOH groups, has been replaced with a peak at lower binding energy, 288.0 eV, which is consistent with conversion of –COOH groups to –CONH functionalities after the coupling reaction.

Table 3.3 Atomic composition at different stages of reactions.

Sample	**%C**	**%N**	**%O**
PP VAA	76.0	0.0	24.0
PP VAA + Spacer	79.4	2.6	18.0
PP VAA + Spacer + BSA	74.0	8.7	17.3

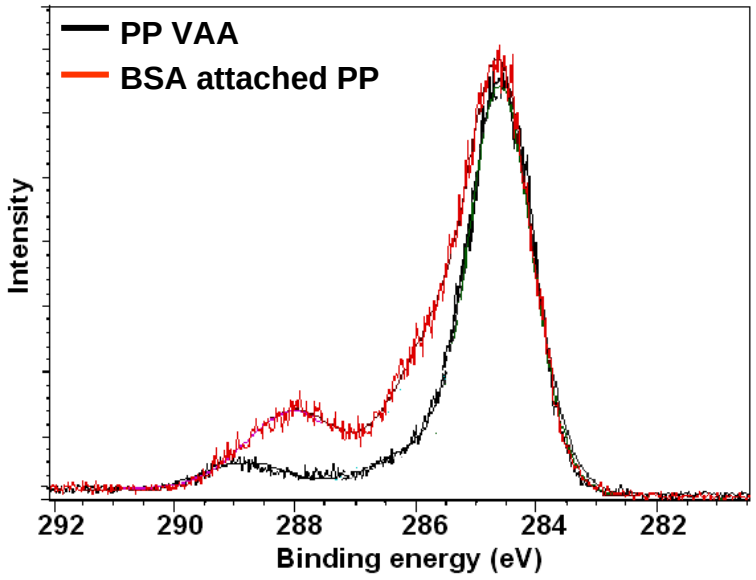

Figure 3.5 High resolution C1s X-ray photoelectron spectra of PP VAA and BSA attached PP VAA.

3.3.3 Fluorescence Microscopy

Fluorescence images of polypropylene (PP) microparticles were taken, as shown in Figure 3.6. Plasma modified PP VAA particles unexpectedly exhibit a slight fluorescence (Figure 3.6b). Possibly, this fluorescence is due to the presence of conjugated unsaturated groups generated during the plasma deposition or perhaps associated with the relatively high surface density of –C=O groups. Exposure of the VAA modified surfaces to FITC labeled BSA molecules resulted in some surface adsorbed BSA molecules, as shown by the relatively weak green fluorescence in Figure 3.6c. In contrast, covalent coupling of the labeled BSA molecules to the PP VAA surfaces, again via EDC chemistry, produced the intense green fluorescence shown in Figure 3.6d. The fluorescence measurements of both the adsorbed and covalently bound

BSA were made only after extensive washing of the samples with 1% SDS solution, thus eliminating potential contributions to the fluorescence from loosely bound BSA molecules. As shown in Figure 3.6, it is clear that a very significant enhanced fluorescence of the FITC labeled BSA molecules is achieved in the covalent coupling experiments. Overall, the FT-IR, XPS and fluorescence labeled spectroscopic results clearly confirm the utility of employing the plasma surface modification approach as a viable route to covalent attachment of biomolecules to surfaces.

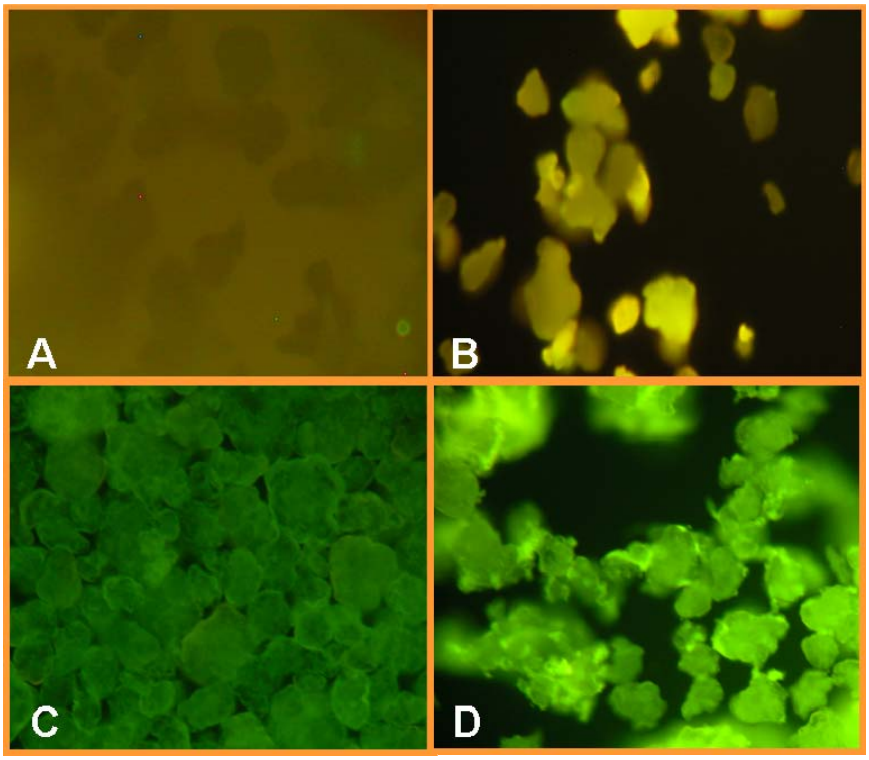

Figure 3.6 Fluorescence images of polypropylene microparticles (A) unmodified, (B) PP VAA coated, (C) incubated with FITC-BSA and washed, (D) conjugated with FITC-BSA and washed.

3.3.4 Sandwich ELISA experiments for RL-9A conjugated nanoparticles

As a far more stringent test of the efficacy of the pulsed plasma surface modification technique, experiments were conducted in which biomolecules, in this case RL-9A antibodies, were covalently attached to nanoparticles. The goal of this work was to examine the following key questions: 1. Is it possible to functionalize the surfaces of nanoparticles with polymer films containing sufficient reactive functional groups which might subsequently be used for conjugation of biomolecules to these particles? 2. If the answer to the first question is yes, will the biomolecules so attached maintain their biological activity to a sufficiently useful degree? With respect to practical considerations these two questions are extremely relevant in view of current interest in applications of nanotechnology to various medical applications, particularly in the area of targeted drug delivery.[186]

As noted earlier, Professor Jon Weidanz, of the Texas Tech School of Pharmacy, supplied the antibodies and agreed to measure and evaluate the specific biological activity of the antibodies after their conjugation to the nanoparticles. Iron oxide (γ-Fe_2O_3) nanoparticles, having an average diameter of ~25nm, were employed as substrate.

Sandwich ELISA experiments were performed using different quantities of RL-9A conjugated nanoparticles. The biological activity of the antibodies conjugated to the nanoparticles was determined using its binding specificity with the relevant HLA-A2/peptide complex. Irrelevant HLA-2/peptide complexes served as negative control

and unconjugated pure RL-9A antibody was used as positive control. A secondary antibody, goat antimouse HRP, was used at a dilution factor 1:1000 and ABTS was added to generate the color. Absorbances were monitored at 405 nm wavelength. Table 3.4 shows the absorbance values as obtained from the ELISA tests. It is clear from the data that all samples of nanoparticles containing covalently bound RL-9A antibodies exhibited significantly higher specificity against the relevant peptide SLLV compared to the irrelevant peptides and blank nanoparticles control samples (Table 3.4).

In order to evaluate an optimum concentration of RL-9A antibody conjugated particles in the test media, an additional experiment was performed. In this method, the antibody conjugated particles were dispersed in solution in three different concentrations, such as 200ng, 20ng and 2ng each in 100µl buffer and employed in the ELISA experiment. From the ELISA data, as shown in table 3.4, it is clearly observed that the higher concentration of nanoparticles (200ng/100µl buffer) showed significantly higher absorbance values compared to the diluted ones in every set of samples. Absorbance of pure RL-9A antibody for 200ng and 20ng/100µl buffer could not be monitored because they were too high and beyond the limit of the experimental set-up. Additionally, a decrease in the absorbance is also observed down the column from sample 5 RL-9A to 50 RL-9A for the relevant peptide SLLV. It is consistent with the fact that, 5 RL-9A particles have more number of antibodies on their surfaces than 50 RL-9A. This is a reasonable result given the fact that the very small amount of antibody (2mg) had to be shared by a much larger number of functionalized particles in the 50

RL-9A experiments relative to the 5 RL-9A system, thus producing a somewhat lower surface density of antibodies in the samples containing more particles. However, apparently no changes in the absorbance values are found for irrelevant peptides and blank nanoparticles which also confirm the activities of the antibody conjugated particles.

Table 3.4 Results observed in the ELISA experiment with RL-9A relevant peptide SLLV, two irrelevant peptides YLL and EIF-4G, and pure RL-9A antibodies.

Sample name	Dilution factors	Total absorbance as monitored at 405 nm wavelength					
		Relevant peptide	Irrelevant peptides		Blank nanoparticles		
		SLLV	YLL	EIF-4G	SLLV	YLL	EIF-4G
5 RL-9A	200ng/100 µl	2.210	0.142	0.118	0.153	0.092	0.106
	20ng/100 µl	1.709	0.138	0.135	0.121	0.104	0.106
	2ng/100 µl	0.146	0.122	0.112	0.107	0.095	0.136
15 RL-9A	200ng/100 µl	1.856	0.138	0.122	0.475	0.095	0.149
	20ng/100 µl	0.186	0.119	0.097	0.119	0.097	0.098
	2ng/100 µl	0.118	0.121	0.118	0.110	0.106	0.146
30 RL-9A	200ng/100 µl	1.777	0.115	0.173	0.128	0.124	0.149
	20ng/100 µl	0.257	0.118	0.110	0.110	0.109	0.136
	2ng/100 µl	0.114	0.116	0.117	0.116	0.127	0.135
40 RL-9A	200ng/100 µl	*3.492*	0.145	0.167	0.117	0.103	0.127
	20ng/100 µl	*1.426*	0.130	0.111	0.104	0.095	0.093
	2ng/100 µl	0.119	0.125	0.110	0.112	0.094	0.097
50 RL-9A	200ng/100 µl	0.484	0.092	0.103	0.119	0.094	0.089
	20ng/100 µl	0.153	0.099	0.101	0.101	0.093	0.086
	2ng/100 µl	0.113	0.098	0.152	0.091	0.085	0.087
RL 9A	200ng/100 µl	N/A	0.213	0.106	-	-	-
	20ng/100 µl	N/A	0.122	0.103	-	-	-
	2ng/100 µl	1.067	0.101	0.097	-	-	-

3.3.5 Flow cytometry experiments for RL-9A conjugated nanoparticles

In order to examine the binding specificity of RL-9A conjugated nanoparticles to tumor cell lines, a NY-ESO-1 positive tumor cell line KSM 11 was employed.

Unattached RL-9A antibody was used as a positive control whereas a NY-ESO-1 negative cell line SW620 was selected as a negative control. RL-9A conjugated nanoparticles containing the highest number of antibodies, i.e. sample number 5 RL-9A, was used for the flow cytometry experiments because it showed the highest activities (table 3.4). Goat antimouse IgG was used as a secondary antibody to detect RL-9A conjugated nanoparticles on the cells.

A positive shift in the flow cytometry with NY-ESO-1 positive tumor cell line KSM 11 was observed when RL-9A antibody was used as a positive control (Figure 3.7). The same trend was observed when NY-ESO-1 positive tumor cell line KSM 11 was stained for the antibody conjugated nanoparticles. It also exhibited specific recognition (a positive shift) of the HLA-2/peptide complex. In contrast, the NY-ESO-1 negative cell line SW620 did not show significant shift when exposed to the conjugated RL-9A nanoparticles. The flow cytometry data provide additional strong evidence that the RL-9A antibodies maintain their binding specificity and biological activities even after covalent conjugation to plasma functionalized nanoparticles.

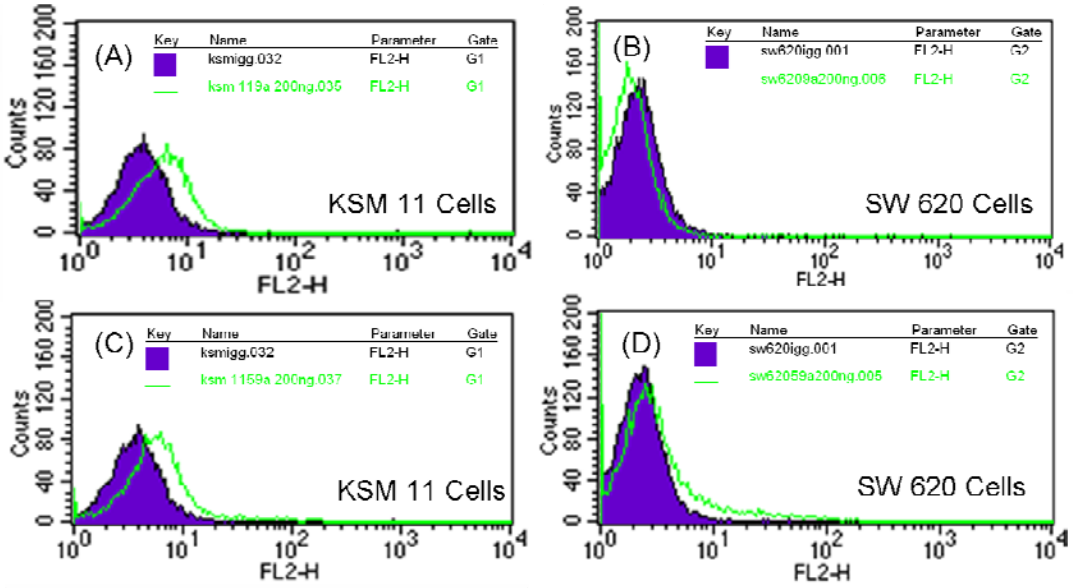

Figure 3.7 Flow cytometry data of staining two cell lines, KSM 11 and SW620. (A) and (B) show the effects of RL-9A antibodies on the two cell lines; (C) and (D) show the effects of RL-9A antibody conjugated nanoparticles on the two cell lines.

3.4 Conclusion

As demonstrated in this chapter, plasma polymerization provides an unusually simple approach to functionalization of surfaces with reactive functional groups. These groups are then available for use in further coupling reactions. The plasma technique involves a single, solventless coating procedure, providing a conformal and pin-hole free surface. Furthermore, it is applicable to any solid substrate. In the present case, the versatility of this approach was demonstrated on particle substrates, including the challenging task of molecularly tailoring nanoparticles. The polymerization of vinyl acetic acid has been shown to provide reactive surface –COOH groups, and thus a convenient route to covalent attachment of target molecules via simple derivatization reactions. Although the utility of this approach has been illustrated in this "proof of

concept" work with protein and antibody attachment, the technology employed is perfectly general in nature and can be applied to covalently attach a host of other compounds to a variety of surfaces. Furthermore, the surface density of the –COOH groups can be controlled via appropriate adjustment of plasma parameters, particularly the plasma duty cycle employed during the initial film formation. Such surface chemistry controllability is useful in quantifying interactions of modified surfaces with cells and tissue, as described in the next chapter. Additionally, as illustrated in this work, the length of separation of the bound molecules from the surface can be conveniently varied via use of a bifunctional tethering compound. Finally, it should be noted that the pulsed plasma technique can be used to introduce a variety of other surface functional groups, as dictated simply by appropriate choice of the initial monomer, thereby extending significantly the range of chemical procedures which can be employed to covalently couple target molecules to surfaces.

CHAPTER 4

EFFECTS OF –COOH SURFACE DENSITY AND POLYMER FILM THICKNESS ON CELL ADHESION AND PROLIFERATION

4.1 Introduction

Surface modifications have become an increasingly important component in advancing tissue-engineering technology. For example, surface chemistry has been shown to provide both improved cell adhesion and accelerated cell growth on biomaterials in a variety of cell types.[187,188] Despite significant advances in this field, further improvements in the surface treatments of biomaterials are very much needed. Two prominent examples involving endothelial and fibroblast cells can be cited as illustrations of desired improvements in this field. A particularly striking example of this need pertains to culturing endothelial cells, which are known to exhibit relatively poor adhesion and slow growth on biomaterials. Arterial endothelium, which consists of an ultra thin monolayer of endothelial cells, is known to play a pivotal role in maintaining vascular homeostasis, as manifested in a variety of ways. For instance, the endothelium serves as a natural barrier to prevent platelet adhesion and thrombosis. It is also involved in relaxation of underlying smooth muscle cells in response to biomechanical forces exerted on arterial walls. Disruption of the endothelium, such as

that encountered in vascular stent implantation, can lead to thrombosis, inflammation and restenosis.[189,190] Although drug eluting stents (DES) are now employed to minimize restenosis, there are increasingly reports of late-stent thrombosis and restenosis associated with the use of DES.[191,192] It is believed that these late term effects reflect the slow growth of the endothelial cells required to regenerate the protective endothelium monolayer. Fibroblasts represent a second important example in which more rapid adhesion and proliferation of cells would provide a highly useful advance. Examples include numerous situations encountered in dealing with a variety of wound healing applications, such as those encountered with burns and diabetes associated ulcers.

In light of needs such as those noted above, surface physical and chemical properties have been examined extensively to improve the overall biocompatibility of materials. In particular, a variety of surface functional groups have been evaluated to improve cell adhesion and growth. Examples of such studies include amines (-NH_2),[193,194] imines (=NH),[195] hydroxyls (-OH),[196-201] esters (-COOC-),[199,200] and carboxylic acids (-COOH).[201-203] A number of such studies have included comparisons of the effect of surface functional groups on cell adhesion and proliferation.[204-208] In particular, several studies have shown that the presence of surface –COOH groups promote both improved cell attachment and growth compared to unmodified controls.[204,206,207] Additionally, to some extent, the –COOH surface improvement has also been reported in comparison with other functional groups, such as thiol (-SH), alcohol, esters, and hydrocarbons.[205,208] However, it should also be noted, other reports

have indicated that -COOH functionalized surfaces can reduce cell adhesion and proliferation, relative to the control surfaces, as reported in studies involving smooth muscle cells,[201] endothelial cells[205] and fibroblasts.[209]

A variety of innovative approaches have been employed to immobilize different functional groups on solid surfaces. Examples of techniques employed for this purpose include self-assembled monolayers (SAM's),[204-209] photoinitiated grafting,[210] grafting,[201] radio frequency glow discharge (RFGD), also identified as plasma enhanced chemical vapor deposition (PECVD) or plasma polymerization,[193,196,197,202,203,211] and thermally initiated chemical vapor deposition.[212]

The present study utilized the RFGD approach to deposit polymeric films containing –COOH groups, as obtained by the plasma polymerization of vinyl acetic acid. Tissue culture studies were carried out with these functionalized surfaces using endothelial and fibroblast cells. A distinguishing feature of the present work, relative to prior studies of this type, is that cell adhesion and proliferation were examined as functions of both *surface density* of the –COOH groups and *thickness* of the plasma deposited polymer films. For this purpose, a pulsed plasma discharge was employed, in addition to the conventional continuous-wave (CW) operational mode. As shown previously, with a variety of monomers, variation of the plasma duty cycle during the polymer formation provides an unusually convenient and exact method to control film composition.[95,8,213,214,102] In the present work, the compositional control of interest was the extent of retention of monomer –COOH groups in the resultant films. Additionally,

under a given pulsed plasma condition, the film deposition rate varies linearly with deposition time, thus providing a convenient control of film thickness.[102]

4.2 Experimental

4.2.1 Deposition of poly(vinylacetic acid) film by RFGD plasma polymerization

Vinylacetic acid (CH_2=CH-CH_2-COOH) (abbreviated as VAA) was purchased from Sigma-Aldrich, St. Louis, MO and had a stated purity of 97%. The monomer was repeatedly freeze-thawed to remove any dissolved gases prior to use. Monomer vapor was subjected to radio frequency glow discharge (RFGD), at room temperature in a bell-shaped reactor chamber, as shown in Figure 2.1. After placement of substrates inside the reactor, the system was evacuated to a background pressure of 4 mtorr. Monomer vapor was introduced into the chamber and an RF plasma glow discharge ignited. Three different power input conditions were employed, namely, pulsed discharges at duty cycles of 2/30 and 10/30 (time on/time off, ms), plus runs using the CW operational mode. All samples were prepared using a 150 W power input. Although all runs were carried out at a 150 W peak power, it is important to note that the average power input differs significantly in contrasting the pulsed and CW depositions. The average power is computed from the plasma duty cycle (ratio of on time to the sum of the on plus off time) multiplied by the peak power. Thus the average power inputs were 9.4 and 37.5 W for the 2/30 and 10/30 runs, respectively, compared to the 150 W for the CW experiments. Monomer pressure of 160 mtorr was employed for the 2/30 duty cycle polymerizations and 40 mtorr for the 10/30 duty cycle and CW

runs. In the initial experiments, deposition times were adjusted to deposit ~ 100nm thick films for each set of plasma conditions employed. In the second set of experiments involving film thickness variation, a single duty cycle (2/30) pulsed plasma was employed to polymerize VAA, and the deposition time was varied accordingly to obtain different film thicknesses ranging from 25nm to 300nm. In all experiments, standard polystyrene tissue culture well-plates (TCPS) were used as substrate for the plasma deposited films, as well as the control samples in the cell culture studies. Polished silicon wafers were used as substrates for XPS, AFM and water contact angle measurements. All silicon wafers were treated with acetone, methanol and hexane to clean the wafer surface prior to use.

4.2.2 Characterization of plasma deposited poly(vinylacetic acid) films

The VAA polymeric films were characterized by FT-IR spectroscopy, X-Ray Photoelectron Spectroscopy (XPS), Atomic Force Microscopy (AFM) and water contact angle measurements. The FT-IR spectral analyses were carried out using a Bruker Vector-22 FT-IR spectrophotometer, operated at 4 cm^{-1} resolution, on polymer films deposited on KBr disks. XPS spectra were obtained using a Perkin-Elmer PSI 5000 series instrument equipped with a monochromator and 8.95 eV pass energy. A neutralizer was used for all measurements since the samples were non-conductive. The high resolution XPS spectra were analyzed using Casa XPS software. The binding energy of the carbon atoms not directly bonded to heteroatoms were centered at 284.6 eV. Surface roughness of the deposited films was determined using an AFM-SPM

Nanoscope from Veeco. A phosphorus (n) doped silicon tip (RTESP from Veeco Probes) was used to scan the surfaces under tapping mode operation. A Rame-Hart sessile drop goniometer was used to measure the static water contact angle of the polymeric films. Film thickness measurements were obtained using a Tenchor Alpha step 200 profilometer. A metal tipped pen was employed to scratch a thin line in the polymer films deposited on polished silicon wafers. The thickness of the films reported is an average of three measurements taken for each sample.

4.2.3 Cell culture

The cell culture studies were carried out in the laboratory of Professor Kytai Nguyen, UTA, Department of Biomedical Engineering. In this work, endothelial cells (HAECs) (Cascade Biologics Inc., OR) were grown at 37ºC in Medium 199 (Invitrogen Corp., CA) supplemented with 5% FBS (Hyclone, UT), Endothelial Growth Supplement (Cascade Biologics, OR), and 1% penicillin-streptomycin (Invitrogen, CA). 3T3 fibroblasts (ATCC, #CCL-92, VA) were grown at 37ºC in Dulbecco's Modified Eagle's Medium (DMEM, Invitrogen, CA) supplemented with 10% FBS (Hyclone, UT), and 1% penicillin-streptomycin (Invitrogen, CA). Cells between passage 5 and 10 were used for all experiments.

4.2.4 Cell adhesion and proliferation

For all adhesion and proliferation studies, cells were seeded at a density of 5×10^3 cells/cm² on plasma polymerized poly-VAA films coated on 12-well tissue culture well plates (TCPS). Untreated TCPS plates were employed as controls. After

seeding, cells were incubated for 6 hours or 3 days for adhesion or proliferation studies, respectively. The preliminary studies suggest that endothelial and fibroblast cells were mostly adhered after 6 hours of seeding (about 80-90% of cells adhered). For this reason, duration of 6 hours was selected for cell adhesion experiment and cells were allowed to grow 3 days after cell seeding for cell proliferation studies on the modified surfaces. The media were changed every 48 hours. After these predetermined periods, cells grown on the substrates were lysed with 1% Triton X-100 (MP Biomedicals, OH) for 30 minutes at 37ºC. The total cell DNA was analyzed using the Pico Green dsDNA kit (Invitrogen, CA) following the manufacturer's instructions.

4.2.5 Immnuostaining of HAECs and Fibroblasts

HAECs and 3T3 fibrobalsts were seeded at 10^4 cells/cm² on poly-VAA films coated on 35 mm polystyrene Petri dishes. Untreated Petri dishes were used as controls. After culturing for 24 hours, cells were fixed with 4% cold formaldehyde for 30 minutes and treated with 0.02% Triton X-100 for five minutes to render them permeable prior to staining. Rabbit anti-human von Willebrand Factor (vWF), IgG (Santa Cruz) and mouse anti-human tubulin IgG (DSHB, UT Iowa) were used as the primary antibodies for HAEC and fibroblasts, respectively. Bovine anti-rabbit IgG-FITC (Santa Cruz) and goat anti-mouse IgG-TR (Santa Cruz) were used as the secondary antibody. After staining, samples were placed in UltraCruz™ Mounting Medium (Santa Cruz) containing 1.5 μg/ml DAPI for DNA counterstaining. Fluorescence images were taken using a Zeiss fluorescent microscope at 20 X.

4.2.6 Statistical analysis

Analysis of the results was performed using ANOVA and t-tests with $p < 0.05$ (StatView 5.0 software, SAS Institute). For each study, the results are given as mean ± SD.

4.3 Results

4.3.1 Characterization of the plasma polymerized films

4.3.1.1 FT-IR spectroscopy

FT-IR spectra of the plasma polymerized VAA films, although relatively qualitative in nature, show progressive changes in film composition with variations in the RF duty cycles employed during the film deposition process. Figure 4.1 shows a plot of FT-IR transmission spectra of the poly-VAA films deposited at pulsed discharges at 2/30 and 10/30 on/off ratios (in ms) and under CW conditions, reading from top to bottom. These spectra reveal a progressive increase in the retention of the monomer's -COOH content with decreasing RF duty cycle (plasma on time / plasma off time) employed during the deposition. This increase can be easily noted by comparing the relative intensities of the >C=O stretching frequency for – COOH (1706 cm^{-1}) and the characteristic H-bonded – OH stretch for COOH (broad region from 3300 cm^{-1} to 2500 cm^{-1}). Additionally, there is a progressive increase in the intensity of the C-O stretching vibration (~1100 cm^{-1}) with decreasing RF duty cycle. These spectra reveal that the extent of >C=O retention is proportional to -OH retention in the film which would be consistent with the increasing presence of intact -COOH functional groups. It

can also be noted that the intensities of the C-H (~2900 cm^{-1}) absorptions, relative to the C-O containing moieties, increase with increasing RF duty cycle. This is consistent with the decreased retention of –COOH functionality, as the plasma duty cycle is increased.

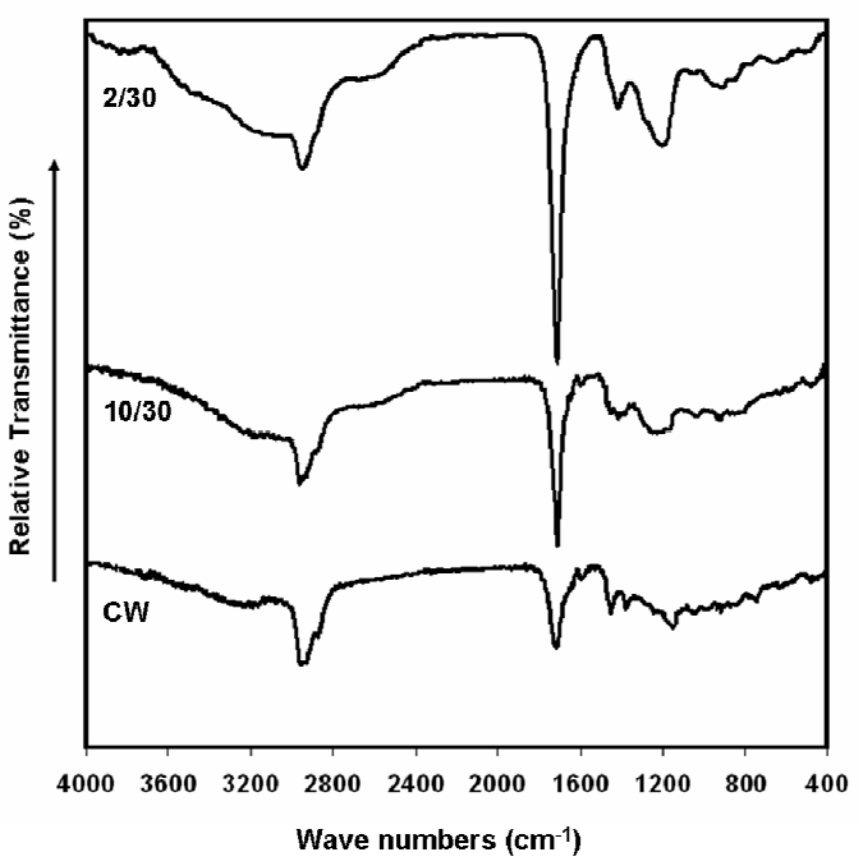

Figure 4.1 FT-IR spectra for plasma polymerized vinylacetic acid films deposited under pulsed (2/30 and 10/30) and CW plasma conditions.

4.3.1.2 High resolution X-ray photoelectron spectroscopy (XPS)

High resolution C(1s) XPS spectra are shown in Figure 4.2, along with accompanying peak assignments. The peaks centered at 284.6 eV represents C-C and C-

H groups, i.e. carbons not bonded directly to any oxygen atoms. The other peaks were fitted using the following assignments: a β-shifted carbon bonded to carboxylic acid (C-COOH) at 285.3 eV, alcohol/ether (C-OH/C-O-C) at 286.3 eV, carbonyl (C=O) at 287.5 eV and carboxylic acid (COOH) at 288.9 eV. These peak assignments are in accord with many prior analyses of this type.[149] Clearly, there is a progressive decrease in the number of carbon atoms present as -COOH as the plasma on time is increased in the order of duty cycles 2/30, 10/30 to CW mode. Table 4.1 provides a quantitative measure of the percent surface carbon functionalities obtained from integration of the deconvoluted XPS high resolution C(1s) peaks. As the data show, there is a steady decrease in the surface density of -COOH functionality from ~9% to ~3.6%, expressed as a percent of total surface carbons, as the deposition condition switched from pulsed plasma (duty cycle, 2/30) to CW plasma operating mode. The progressive increase in the peak at 284.6 eV, i.e. an increase in the C – C and C – H groups compared to other functional groups, is indicative of the increase in polymer cross-linking with increasing average power input as the plasma duty cycle is increased. Although, it was possible to obtain films containing up to 20% -COOH from the plasma polymerization of VAA monomer using even lower average power inputs[215] than those reported here, the films containing in excess of the 9% -COOH were relatively unstable in the cell culture media, no doubt reflecting the lower degree of film cross-linking as the average power is decreased. For this reason, this study was limited to films having a maximum –COOH surface density of 9%.

High resolution C(1s) XPS spectra were also obtained for a series of films ranging in thickness from 25 nm to 300 nm, all deposited using the 2ms on: 30 ms off pulsed plasma. Each of these films exhibited the same XPS spectrum as that shown in the top spectrum of Figure 4.2, thus revealing no measurable changes in the polymer composition with increasing film thickness.

Table 4.1 Percent surface functional groups of the plasma polymerized vinylacetic acid films deposited under pulsed (2/30 and 10/30) and CW plasma conditions.

Plasma condition	Avg. power input	O/C Ratio	C-C, C-H 284.6 eV	C-COOH 285.3 eV	C-OH, C-O-C 286.3 eV	C=O 287.5 eV	COOH 288.9 eV
2/30	9.4 W	0.24	70.2	9.0	8.5	3.3	9.0
10/30	37.5 W	0.22	71.2	6.2	10.8	5.6	6.2
CW	150 W	0.19	72.6	3.6	13.6	6.6	3.6

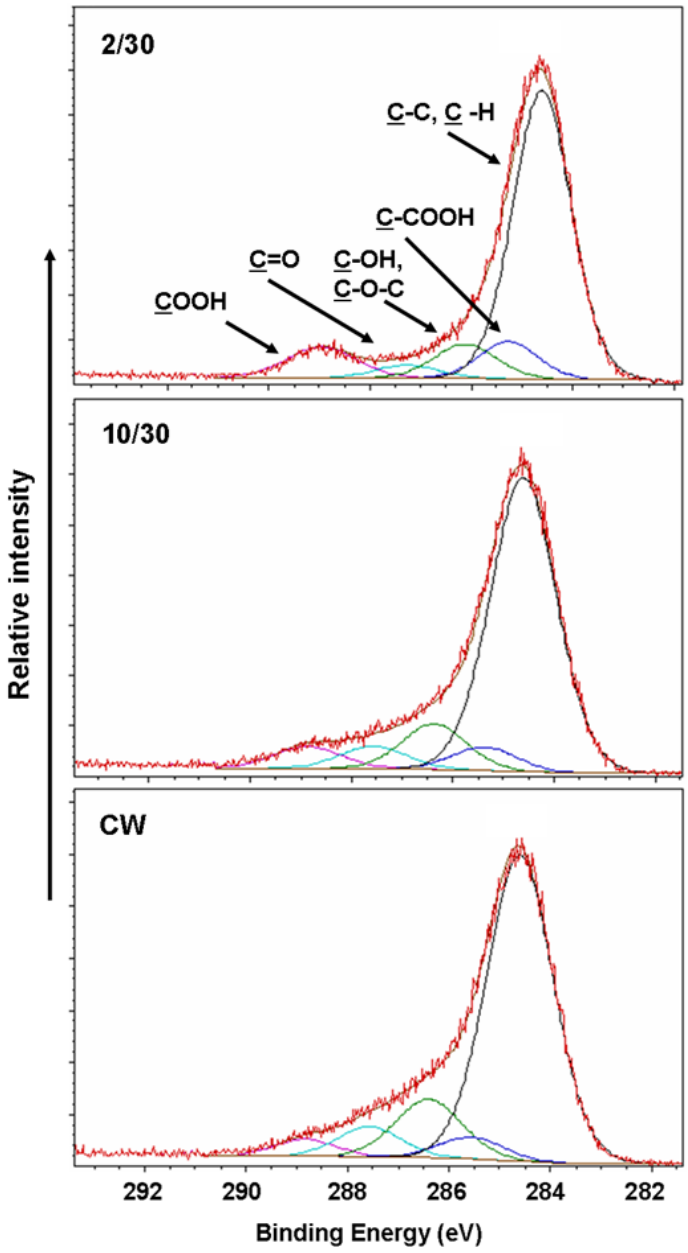

Figure 4.2 High resolution C(1s) X-ray photoelectron spectra for plasma polymerized vinylacetic acid films deposited under pulsed (2/30 and 10/30) and CW plasma conditions.

4.3.1.3 Atomic force microscopy (AFM)

Prior studies, by other workers,[216-218] have amply demonstrated that surface roughness can effect cellular behavior on surfaces. In particular, changes in the surface roughness in the micron range have been shown to effect cell attachment and morphology. For that reason, it was important to examine the surface roughness of the films employed in this experiment. The surface roughness of plasma deposited VAA films, made at 2/30 and 10/30 duty cycles and CW mode, each having film thickness of 100nm were studied. Additionally, films of different thicknesses (25 nm, 100 nm, 200 nm) deposited at the 2/30 duty cycle, were also examined by AFM. The mean roughness values (RMS) shown in Table 4.2 are an average of three different regions of 100 nm × 100 nm areas on each sample. As shown in Figure 4.3, and tabulated in Table 4.2, relatively small changes, of the order of 0.15 nm, were observed in the root mean square roughness of the surfaces employed in this study. Little change in surface roughness was noted with variation of the film thickness produced at the constant 2/30 duty cycle. Surface roughness does not vary more than ± 0.1 nm as the thickness of plasma polymerized VAA film increases from 25 nm to 200 nm, as shown in Table 4.2. Given the relative constancy of the films fabricated in this study, coupled with the fact that prior work involving morphology effects on cell growth indicate that such effects are noticeable only in the micron scale region, it was assumed that the variations in cell adhesion and proliferation observed in the current experiments were not due to any roughness variation effects of the plasma polymerized films.

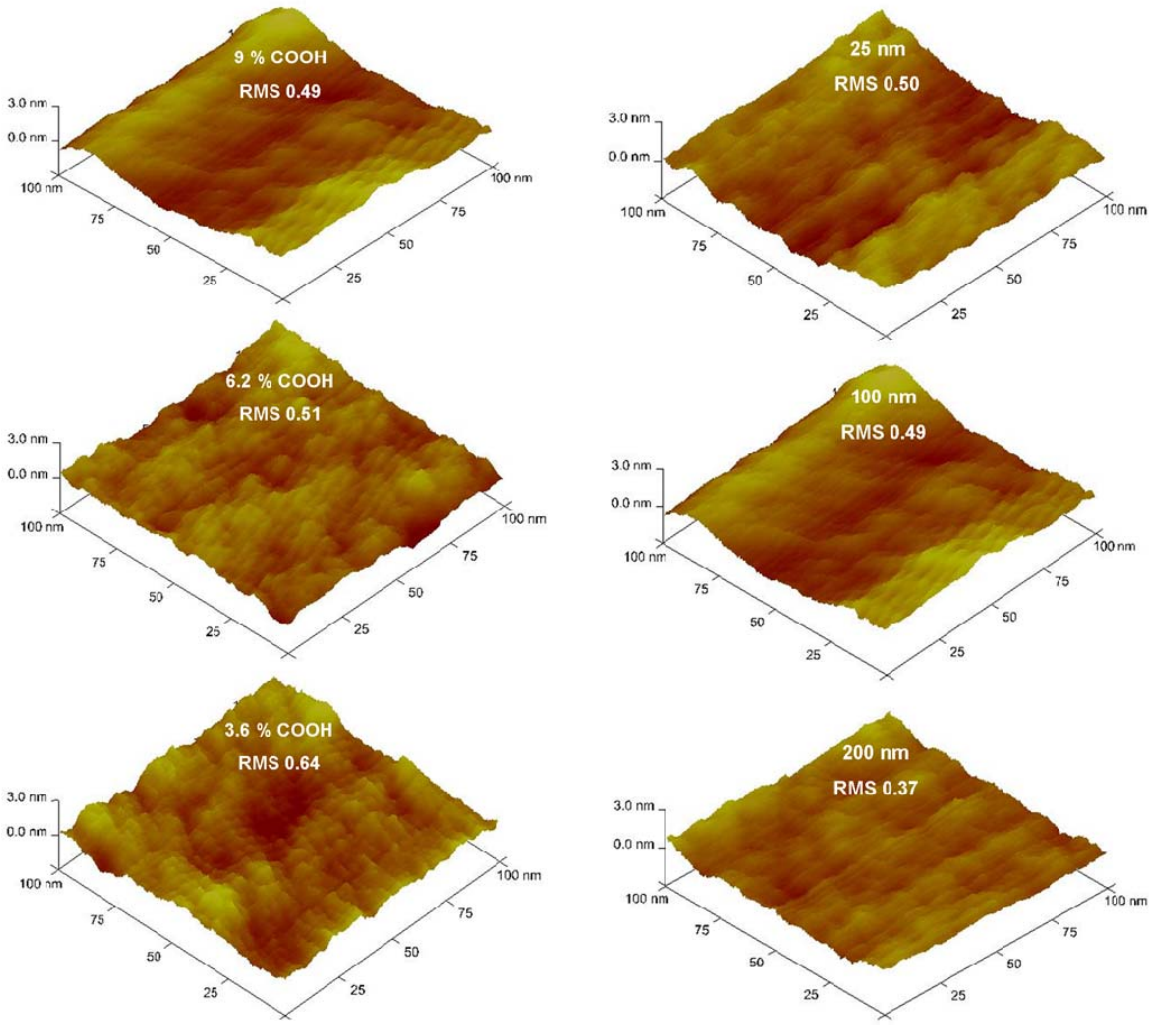

Figure 4.3 AFM images of plasma polymerized VAA surfaces for 100 nm thick films having different -COOH surface densities (left column) and different film thicknesses with constant 9% -COOH surface density (right column).

Table 4.2 AFM mean roughness values for plasma polymerized VAA films obtained for different –COOH surface densities and film thicknesses.

Plasma condition	Avg. power input (W)	% COOH retention	Roughness (RMS)
CW, 100 nm	150	3.6	0.6 ± 0.1 nm
10/30, 100 nm	37.5	6.2	0.5 ± 0.1 nm
2/30, 25 nm	9.4	8.9	0.50 ± 0.01 nm
2/30, 100 nm	9.4	9.0	0.49 ± 0.01 nm
2/30, 200 nm	9.4	8.8	0.37 ± 0.01 nm

4.3.1.4 Static water contact angle measurements

The water contact angle goniometer measurements obtained are summarized in Table 4.3. The contact angles shown represent the average of at least three measurements of each film. The measurements show a slight decrease in water contact angle with decreasing plasma on time (decreasing duty cycle). Lower contact angles clearly indicate the increased retention of polar groups, such as –COOH, on the surfaces as the plasma duty cycle is decreased, in accord with the spectroscopic data provided in Figures 4.1 and 4.2. The water contact angle measurements are significant with respect to potential variations in non-specific protein binding to these surfaces. Although the amount of surface adsorbed proteins were not quantified, it is generally accepted that protein adsorption depends on the surface wettability;[206,219] with adsorption being more pronounced on hydrophobic surfaces than on hydrophilic ones. In the current study, the water contact angle (the wettability) of the films employed varied by only ~10°,

with the one exception of the sample produced under CW conditions (Table 4.3). Furthermore, the actual wettabilities, encompassing contact angles ranging from ~40° to 60°, are in the range reported to be ideal for enhanced cell adhesion on polymer surfaces.[206,220] Given these considerations, coupled with the fact that all measurements were carried out with media containing identical serum, it is assumed that the extent of non-specific protein adsorption did not differ significantly in these experiments.

Table 4.3 Sessile drop water contact angles for plasma polymerized VAA films having different –COOH surface densities and film thicknesses.

Plasma conditions (Duty cycle, thickness)	Water contact angle after deposition (°)
2/30, 100 nm	38 ± 2
10/30, 100 nm	48 ± 3
CW, 100 nm	60 ± 1
2/30, 25 nm	39 ± 1
2/30, 50 nm	38 ± 2
2/30, 200 nm	39 ± 2
2/30, 300 nm	38 ± 1

4.3.2 Cell adhesion and proliferation as a function of –COOH surface densities on films of identical thickness

The adhesion and proliferation reported in this section pertain to growth studies on 100 nm thick films having –COOH surface densities ranging from 3.6 to 9%. After incubation for 6 hours, both HAEC and 3T3 fibroblasts had significantly higher

amounts (175-190%) of cells attached on plasma polymerized VAA films with higher (9%) –COOH surface density ($p<0.05$) compared to the 100% TCPS control. In contrast, polymers having lower –COOH (3.6 % and 6.2 %) surface densities did not increase the extent of cell attachment after 6 hours of incubation (Figure 4.4) relative to the TCPS controls.

Cell proliferation results, obtained after three days of culture, parallel the adhesion data. That is, statistically significant higher amounts of HAEC and fibroblast cells were present on the VAA plasma polymerized films with high concentration (9%) of –COOH groups ($p<0.01$), but no enhanced proliferation was shown on the polymer surfaces containing the lower densities of these groups (Figure 4.5).

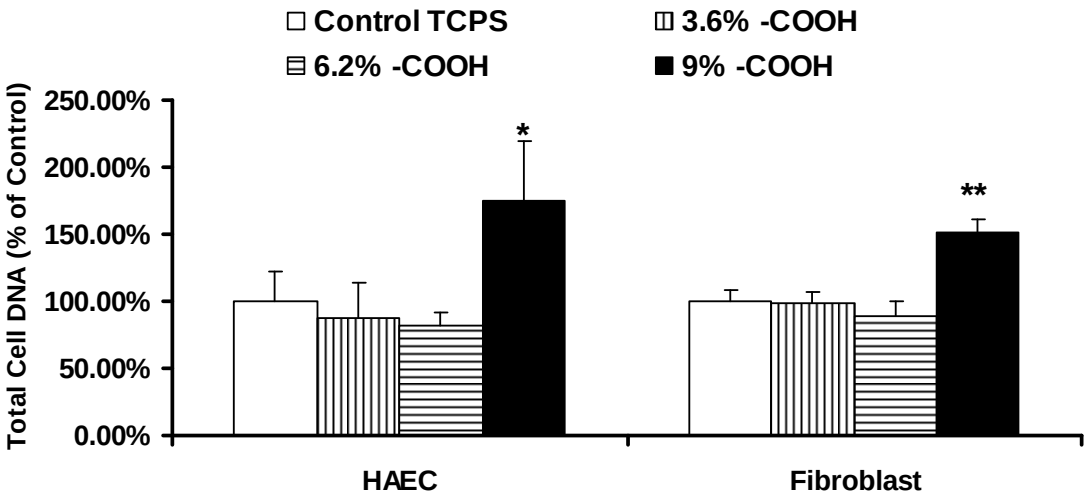

Figure 4.4 Cell adhesion data on plasma polymerized VAA films as a function of low (L), medium (M) and high (H) –COOH surface densities (n=4, *: $P<0.05$ comparing to control group of the same cell type; **: $P<0.01$ comparing to control group of the same cell type).

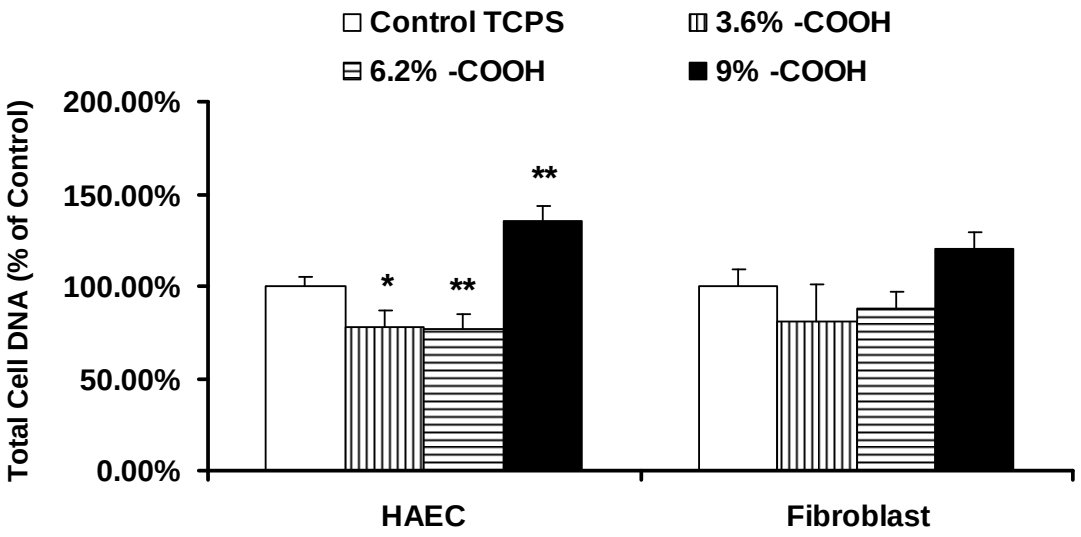

Figure 4.5 Cell proliferation plasma polymerized VAA films as a function of low (L), medium (M) and high (H) –COOH surface densities (n=4, *: P<0.05 comparing to control group of the same cell type; **: P<0.01 comparing to control group of the same cell type).

4.3.3 Cell adhesion and proliferation as a function of film thickness on polymer films having a constant surface density of –COOH groups

In these experiments, polymer films containing an identical high surface density of –COOH groups (9%), but having film thicknesses ranging from 25 to 300 nm, were examined with respect to both cell adhesion and proliferation. As shown in Figure 5, HAEC adhesion was significantly increased after 6 hours of incubation on all of these films relative to the TCPS control surfaces. Interestingly, and unexpectedly, a significant increase in cell adhesion was observed up to film thickness of 200 nm. Fibroblast adhesion was also increased on 100, 200, and 300 nm thick –COOH

containing polymer films. However, the percent increase was much less than that obtained with the HAEC cells (Figure 4.6).

The cell proliferation results, obtained after the 3-day incubation period, were quite similar with the adhesion results. Namely, HAEC still had significantly higher cell growth on VAA plasma polymerized films, with the 100 nm and 200 nm thick films exhibiting the highest cell proliferation (Figure 4.7). As also shown in Figure 4.7, proliferation of the 3T3 fibroblasts on the -COOH surfaces were only slightly higher than those on the controls. Comparing the cell morphology of HAEC and the 3T3 fibroblast grown on the untreated TCP and Poly-VAA films of 200 nm thickness, both of them showed normal morphology (Figure 4.9). vWF, used as the functional surface marker of endothelial cells, was shown well expressed by cells grown on poly-VAA, suggesting poly-VAA are biocompatible in preserving endothelial cell functions. The fibroblasts grown on poly-VAA seemed a little smaller and less spread, but with similar tubulin expression compared to control samples.

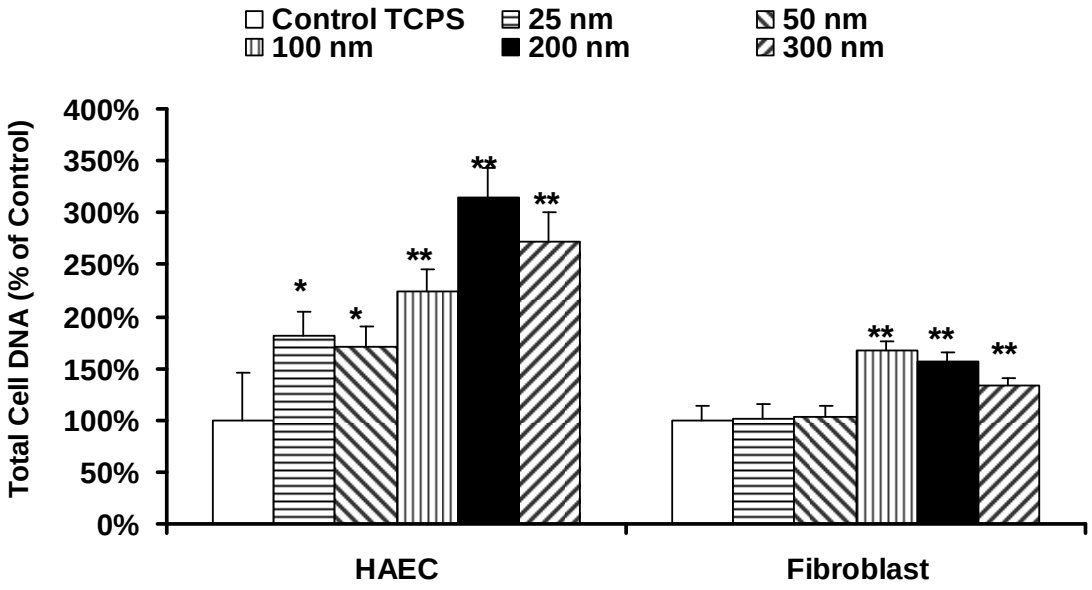

Figure 4.6 Cell adhesion data on 9% –COOH containing plasma polymerized VAA films as a function of film thickness (n=4, *: P<0.05 comparing to control group of the same cell type; **: P<0.01 comparing to control group of the same cell type).

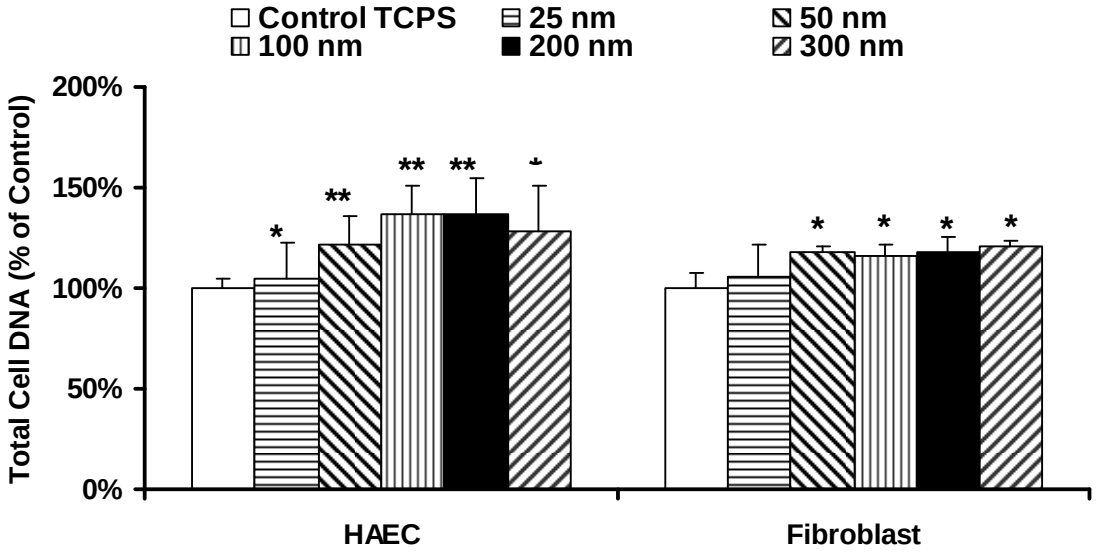

Figure 4.7 Cell proliferation data on 9% –COOH containing plasma polymerized VAA films as a function of thickness. (n=4, *: P<0.05 comparing to control group of the same cell type; **: P<0.01 comparing to control group of the same cell type).

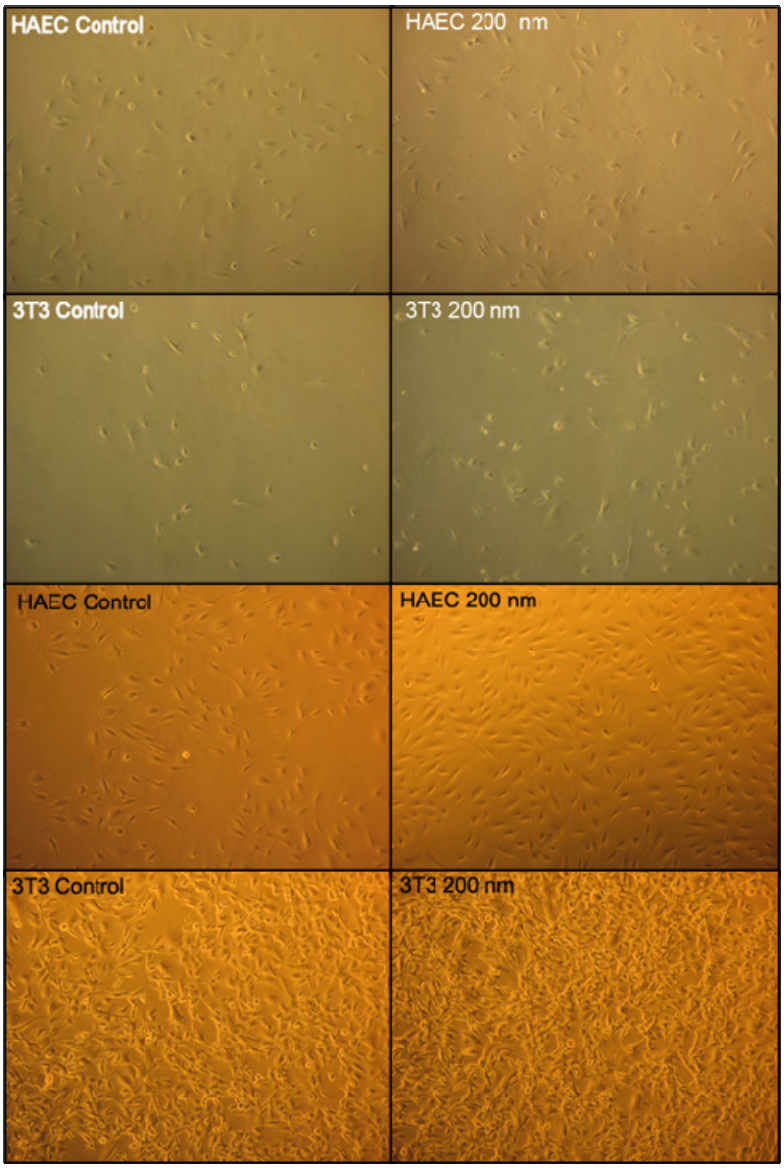

Figure 4.8 Live cell images of adhesion and proliferation of HAEC and 3T3 fibroblasts grown on bare cell culture plates (control) and on 200 nm thick 9% –COOH containing poly-VAA films. Magnification: 100×. White labeling: adhesion (8 hours after cell seeding); Black labeling: proliferation (3 days after cell seeding).

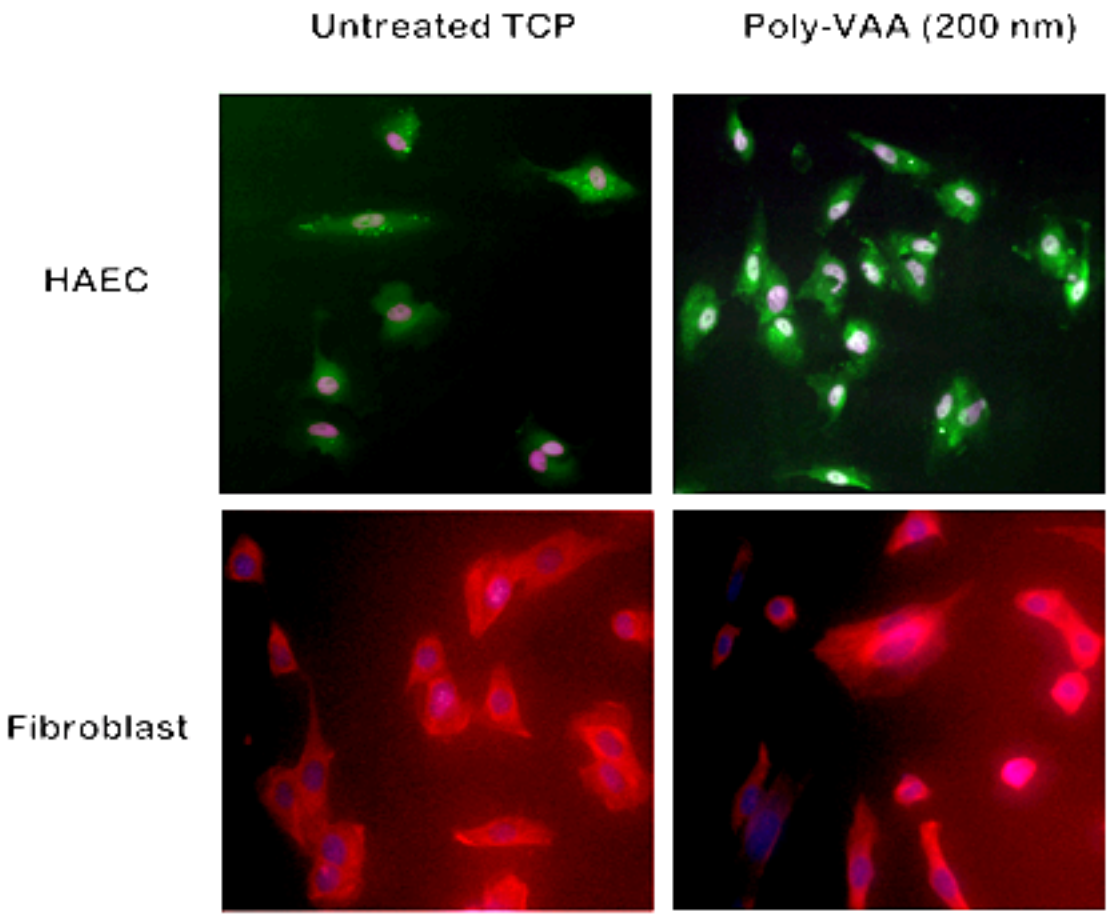

Figure 4.9 Fluorescence cell images of HAEC and 3T3 fibroblasts grown on untreated cell culture petri dishes and on 200 nm thickness 9% –COOH containing poly-VAA films. Magnification: 200×.

4.4 Discussion

Given the essential constancy of surface roughness and surface wettabilities, the results obtained permit focusing on the effects of surface functional group densities and film thickness. The goal was to employ these variables as a possible route to achieve enhanced cell adhesion and growth rates on surfaces, an important objective particularly

with respect to endothelial cells. In fact, both initial cell adhesion and cell proliferation were indeed affected by these variables, with the effects being far more significant with the HAEC cells (Figures 4.4, 4.5, 4.6 and 4.7). Dramatic increases in HAEC adhesion and growth were observed with both film composition and film thickness.

It is interesting to compare and contrast the present results with respect to prior reports involving cell cultures on –COOH functionalized surfaces. For example, Haddow et al.[203] showed there was little or no significant variation in cell attachment on surfaces having different concentrations of -COOH for keratinocytes when compared to a polyhydroxybutyrate control sample. However, an improved keratinocyte adhesion to plasma polymerized acrylic acid surfaces was reported for a surface having a low -COOH concentration (~2%); a result comparable to that observed with -COOH terminated self assembled monolayers (SAMs).[221] Both the –COOH plasma modified and the –COOH terminated self-assembled monolayer (SAM) surfaces exhibited significantly higher cell attachment and proliferation than the control TCPS surfaces employed. Cooper et al.[222] also observed an increased number of attached fibroblasts on -COOH terminated SAMs than on $-CH_3$ terminated ones but, unfortunately, did not report values for a TCPS surface. In contrast, other workers[201,202] reported a negative effect of carboxylic acid groups on smooth muscle cell attachments. Tidwell et al.[205] also reported a decreased number of endothelial cell attachments to –COOH SAM modified surfaces, than on TCPS plates. Thus, prior reports reveal both unchanged as well as either increased or decreased cell adhesion and growth on –COOH modified

surfaces dependent on the nature of the cell lines employed and the control surfaces employed.

The magnitude of enhanced cell adhesion and proliferation observed in the present study is quite significant, particularly in the case of the HAEC cells. Additionally, the strong influence of film thickness on cell growth, especially HAEC cells, was unexpected. This particular aspect of cell growth does not appear to have been considered in quantitative fashion in previous studies of this type. Possibly, the enhanced HAEC growth observed in the present work, compared to the decreased growth reported by Tidwell et al.[205] using –COOH terminated SAMs, may be rationalized in terms of this thickness effect. In the SAMs work, the actual width of the –COOH containing portion of the surface would have been much smaller than the lowest film thickness (25 nm) employed in the present study. It is also important to note that they (Tidwell et al.) used bovine aortic endothelial cells, whereas human aortic endothelial cells were employed in the present experiment. The difference in results, compared to those from prior studies, might also be due to differences in the cell source.

It is not possible to provide a molecular level explanation for the film thickness effects at this point of time. This study eliminated film compositional and morphology effects, since these variables did not change with thickness. Additionally, given the constancy of the film chemistry, it seems unlikely that these results can be attributed to differences in the concentration and distribution of initial non-specific protein adsorption. It is well-known that cell adhesion and proliferation for certain cell types

are affected by the specific adsorbed proteins such as growth factors and extracellular matrix (ECM) proteins. Thus it might be possible that cells grown on the thicker films induce an enhance secretion of specific matrix proteins and growth factors which are favorable with respect to their subsequent adherence and proliferation. Identifying of these specific factors in the future may help us to better understand the film thickness effects on cell adhesion and growth.

Perhaps more relevant considerations are recent interesting reports that cells adhere better on stiffer surfaces compared to softer substrates.[223-226] It is now well established that cells sense the mechanical stiffness of both the ECM and the neighboring cells. Integrins, the heterodimeric extracellular matrix receptors, act as the mechanosensor for the adhesion of cells on solid surfaces. Depending on the micromechanical environment of the cells, variations in the expression of cell phenotypes have also been observed.[227,228] In regard to the mechanical properties of plasma polymers, recent studies have shown that plasma polymer films become softer as the peak power input, and thus cross-link density of the films, are decreased and films are also slightly softer with an increase in the film thickness.[229,230] For example, film hardness has been shown to vary from 1.7 GPa to 3.3 GPa with increasing the plasma duty cycle.[229,230] Additionally, increased film softness has been observed for thicker films deposited at the same average power inputs, an observation attributed to increased competitive film deposition and surface ablation, leading to lower material compaction as the film thickness is increased..[229] In this study, significantly higher

numbers of cells adhered on relatively soft surfaces for both the lower duty cycle, less cross-linked (2/30) films with 9% -COOH surface density and for polymeric VAA films of film thickness >100 nm deposited for longer times at the same power input (Figure 4.6). Interestingly, it was also observed that after a certain film thickness (for example, 200 nm for HAEC and 100 nm for fibroblasts), the number of adhered cells, as well as the extent of cell proliferation appear to become either essentially independent of film thickness or decrease slightly (Figures 4.6 and 4.7). Since different cell lines have unique preferences with respect to surface stiffness;[231] it is possible that VAA films at a certain thickness exhibit an optimum surface hardness which maximizes the cell response, with this optimum softness dependent on the specific cell type. Obviously, this is an interesting question which requires further, more detailed studies. Importantly, immunostaining of both cell types (Figure 4.9) reveal that cells maintained their phenotypes and functions on poly-VAA films. Unfortunately, the stiffness of the plasma modified surfaces employed in this work could not be measured at this time. This is an important concept which should be examined further in future studies.

With respect to practical considerations, the magnitude of cell growth enhancement achieved via these surface functional group and film thickness variations should prove useful. For example, using the 9% -COOH functionalized film and the optimum thickness of 200nm, a 200% increase in initial HAEC cell adhesion was obtained and this increase translated into significantly higher cell proliferation. Furthermore, the growth comparisons were made against a TCPS control, a standard

generally acknowledged as being favorable towards cell growth. Given the acknowledged slow growth encountered in HAEC cell cultures on biomaterials, an increase of this magnitude is highly welcomed.

Finally, and equally significant, the vast majority of prior in vitro studies in this field have concentrated on a single functional group surface density and a single film thickness. However, since surface density of the monomer functional group and the thicknesses of the films employed vary significantly from laboratory to laboratory, depending on the surface modification techniques and parameters utilized, comparison of results from one group to another is not always possible or, in many cases, particularly fruitful. The importance of this fact is further illustrated in this experiment in that, as documented above, it was observed that both the –COOH functional surface density and plasma deposited film thickness exert significant influences on cell adhesion and growth. In fact, the results obtained in the present study suggest that functional group surface densities and film thicknesses should henceforth be considered when attempting to correlate or extrapolate findings from one laboratory to another. For both endothelial and fibroblast cultures, it was possible to adjust the –COOH densities and film thickness to generate surfaces that provided significantly higher cell adhesion and proliferation than observed on untreated control substrates. The present study also illustrates difficulties which will most likely be encountered in attempting to extrapolate *in vitro* acquired data on cell-surface interactions to *in vivo* studies.

4.5 Conclusion

The adherence and proliferation of endothelial and fibroblast cells were found to depend on the -COOH surface density and thickness of plasma polymerized poly(vinyl acetic acid) film deposited. The number of attached and proliferated cells for the 9% maximum attainable concentration of –COOH groups and optimum film thickness was significantly higher than that obtained in normal tissue culture polystyrene (TCPS) well plates.

CHAPTER 5

PLASMA POLYMERIZED MULTISTACKED ORGANIC BIPOLAR FILMS: A NEW APPROACH TO FLEXIBLE HIGH–*K* DIELECTRICS

5.1 Introduction

Organic based flexible dielectric films with high permittivity (ε) are desirable for future applications of organic thin film transistors, such as smartcards and radio frequency identification (RFID) tags, that might preferably be constructed on flexible substrates. With respect to development of all-organic electronic materials, advances in the development of all-polymer field-effect transistors (PFETs) have been particularly significant. Major improvements have been reported for both the semiconductor and the dielectric components of the PFETs.[232] For example, with respect to semiconductor considerations, noteworthy gains have been achieved in increasing carrier mobility and in identifying lower-cost production technology. Despite these advances, PFET operational voltages remain too high for the intended portable applications. However, voltages could be significantly lowered if a suitable flexible dielectric having high-*k* (*k*: dielectric constant), compatible with the PFET fabrication process and controllable thin film thickness, can be identified.

This chapter focuses on the organic dielectric film component of the PFETs required for all-polymer FETs. The much needed advances in this area pose difficult challenges in terms of materials science considerations. One such problem centers on the fact that organic films have inherently low-*k*, having *k* values significantly less than those of ceramic (inorganic) materials. Additionally, leakage currents through the film also pose potential problems given the generally porous nature of organic based polymeric films. On the other hand, organic films offer far more favorable prospects to satisfy flexibility requirements envisioned for the many inexpensive all-polymeric devices anticipated for the future use.

As in the case of the polymer semiconductor research, development of organic based dielectrics has received increasing attention in recent years.[233-237] A number of innovative approaches have been explored and encouraging results obtained. An example of a recent notable advance in this area is the development of σ-π molecular organosiloxane dielectric multilayers having very low threshold voltages and high-*k* (*k* ≈ 16).[238] Another frequently employed approach is to increase the *k* values of organic films by incorporation of ceramic fillers.[239,240] Although these fillers can provide a substantial increase in the dielectric constants, they simultaneously introduce undesirable complications associated with interactions in the composite inorganic-organic film, leading to increased porosity and ultimately poor adhesion between the composite and the purely organic circuit boards. More recently, an interesting report describes polymer composite films containing silver metal (Ag) nanoparticles, with the

metal loading approaching the percolation threshold.[241] The Ag particles were coated with a carbonaceous layer to prevent interparticle electrical contact and to improve compatibility between the polymeric matrix and the filler particles. Very favorable electrical properties, (*k* values, breakdown voltages, leakage current) were measured for these composite dielectric films. However, it is not clear, at this time, if these composite materials will exhibit long term stability in that particle aggregation over time would be a concern since the particles are not covalently bound to the polymer matrix molecules.

The present study involves an innovative approach to synthesis of totally organic dielectric films based on multilayered bipolar films produced by plasma enhanced chemical vapor deposition (PECVD). The layered structures were obtained by the successive polymerization of a carboxylic acid monomer followed by that of an amine containing monomer. The process involves production of alternating ultra thin layers of each monomer to create the bipolar interfaces between layers, as achieved by spontaneous proton transfer from the acid to the amine. Figure 5.1 provides a simple visualization of the nature of the bipolar interface between the two films. A radio frequency (RF) pulsed plasma reactor system was employed to provide deposition conditions that permit retention of the requisite monomer functionalities (i.e. –COOH and $–NH_2$ groups) while simultaneously providing improved film thickness control over that encountered under conventional continuous wave (CW) plasma operations.[242,243]

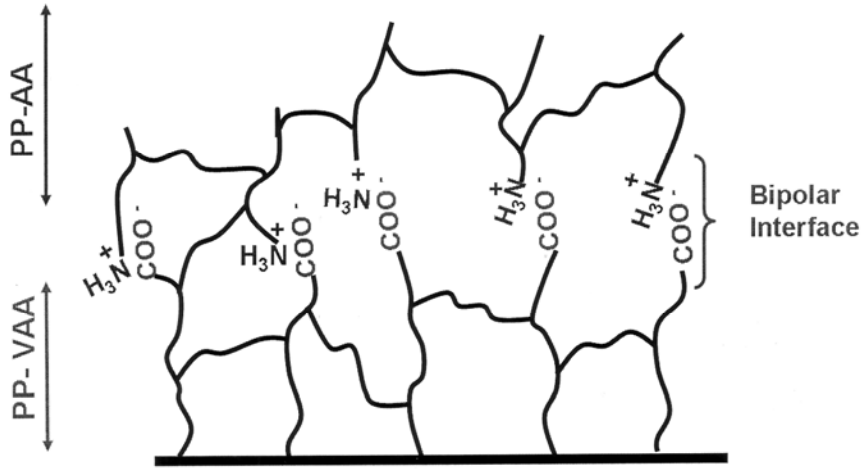

Figure 5.1 Schematic diagram of the interfacial boundary between the plasma polymerized allyl amine (PP-AA) and vinylacetic acid (PP-VAA) thin films.

5.2 Experimental

5.2.1 Pulsed plasma deposition of bipolar film

A carboxylic acid (-COOH) containing monomer, vinylacetic acid (VAA), and an amine ($-NH_2$) containing monomer, allyl amine (AA), were polymerized under pulsed plasma operational conditions. For pulsed plasma deposition of VAA, a plasma duty cycle of 2/30 (plasma on-time, ms/ plasma off-time, ms) was used at a monomer pressure of 160 mTorr and 150 W power input. Allyl amine was plasma polymerized at a duty cycle of 10/30, monomer pressure 70 mTorr and 100 W power input. The polymer films were deposited on metal-insulator-semiconductor (MIS) substrates, which were assembled and cleaned, as described below. A bell-jar shaped reactor, Figure 2.1, was employed for the plasma depositions.

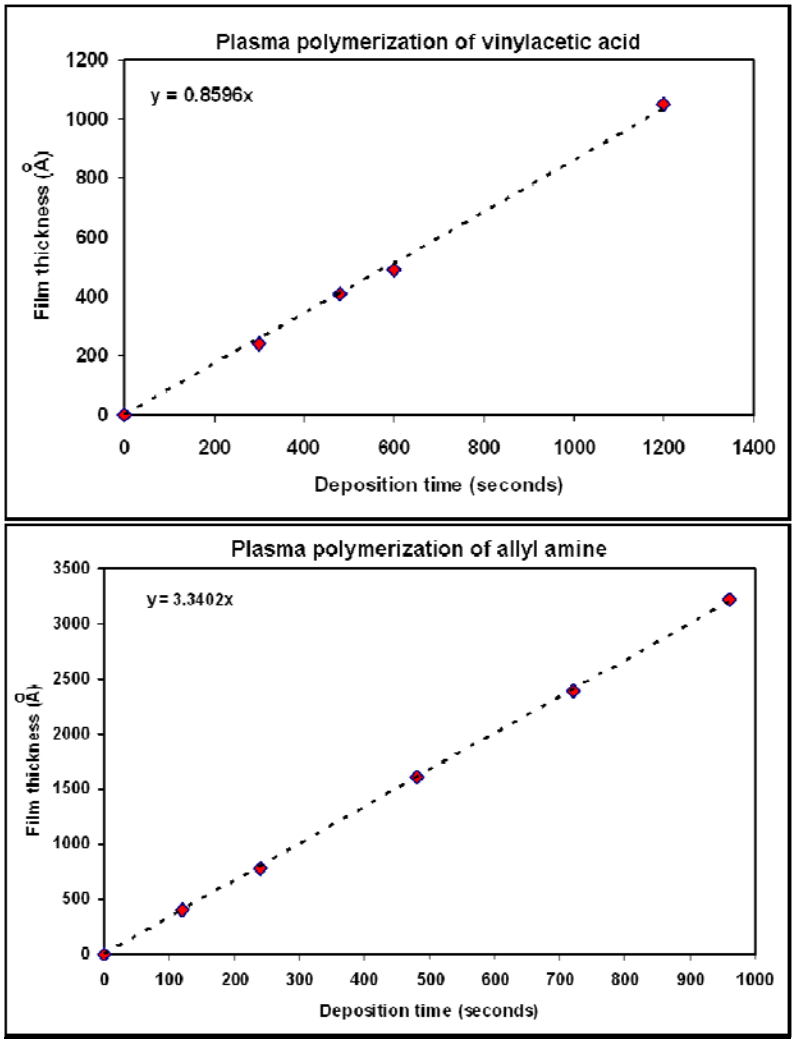

Figure 5.2 Deposition rates of plasma polymerized allyl amine (PP-AA) and vinylacetic acid (PP-VAA) thin films.

A polymeric thin film of allyl amine was first plasma deposited on the substrate which was then followed by the deposition of poly(vinylacetic acid). The sequential deposition of AA and VAA films was performed to obtain a multi-stacked layered structure containing polar groups localized at the interfaces between each consecutive layer. Plasma deposition time was varied to control the thickness of the deposited films.

Initial studies, using profilometry, revealed that deposition rates of both monomers varied linearly with deposition time under the pulsed plasma conditions employed. From the deposition rates measured, it was possible to control both the VAA and AA film thickness to desired values by use of appropriate deposition times.

5.2.2 Characterization of bipolar film

Three different sets of samples containing alternate layers of the -COOH and $-NH_2$ polymers were prepared. The number of layers and film thickness varied among the 3 sets from 4 layers to 10 layers, having nominal total thicknesses of 200, 120, and 50 nm, corresponding to individual layers of 50, 20 and 5 nm, respectively. For the 10, 6, and 4 layer thin films, the refractive index was estimated to be 1.55, 1.58 and 1.67, respectively, as measured by single wavelength ellipsometry.

5.2.3 Fabrication of a capacitor

Metal-insulator-semiconductor (MIS) capacitors were fabricated on 2" Boron-doped (100) p-type Si wafers with a resistivity of 4.2-4.4 Ω-cm. The substrates were processed through standard degreasing and RCA cleaning procedures prior to plasma polymerization. After pulsed plasma deposition of the multilayer stacks of thin films, a 100 nm Au back contact was deposited by shadow mask electron beam evaporation ($\sim 10^{-7}$ Torr) directly onto the multilayer stack surface. Thus the final MIS capacitor fabricated consisted of Au/p-Si/10-layer stack of PP-AA and PP-VAA/Au. The active area of each MIS capacitor studied was 0.283 mm^2. The final fabrication steps of the capacitors and measurement of the film dielectric properties were carried out in

Professor Paul Berger's laboratory, Department of Electrical Engineering, Ohio State University.

5.2.4 Electrical characterization

Capacitance-voltage (*C-V*) measurements were carried out with an LCR meter (Agilent 4284A) coupled with CSM/Win analysis software (Material Development Corporation, MA) at a frequency range from 1 KHz to 1 MHz at room temperature under darkness. For *C-V* measurements, the MIS capacitors were biased from –*t*/10 V to +*t*/10 V with voltage step of 0.1 V, where *t* is the total thickness (nm) of the multilayer film. The hysteresis behaviors of the MIS capacitors were recorded at a frequency of 1 MHz.

All capacitors fabricated were tested without any postdeposition annealing.

5.3 Results

5.3.1 Characterization of chemical and physical properties of bipolar films

5.3.1.1 X-ray photoelectron spectroscopy

Figure 5.3 shows a compilation of high resolution XPS data for C(1s) [panels 1A,1B,1C], N(1s) [panels 2A,2B], and O(1s)[panels 3A,3B]. Spectra of polymer films obtained from pure allyl amine and vinylacetic acid, along with the assigned chemical functionalities, are shown in panels 1A and 1B. These spectra can be contrasted with the C(1s) spectrum recorded when a thin polyallyl amine film (2 nm) was deposited on a polyvinylacetic acid film (panel 1C). As shown in 1C, the high binding energy –COOH peak (at 289 eV) has been broadened and the peak maximum shifted to a slightly lower

binding energy of 288.5 eV, a shift which is consistent with the formation of COO^- groups. The high resolution N and O atom spectra provide additional verification of the formation of polar groups. The N(1s) spectra reveal the presence of a peak at 401.7 eV in the layered film [2B] not present in the pure allyl amine film [2A]. This high binding energy peak is consistent with the presence of ammonium ion functionality. Finally, the high resolution O (1s) spectrum of the layered film reveals a low binding energy peak at 531.7 eV, which is not present in the film obtained from pure vinylacetic acid. This low binding energy peak is also consistent with the presence of COO^- groups in the layered film.

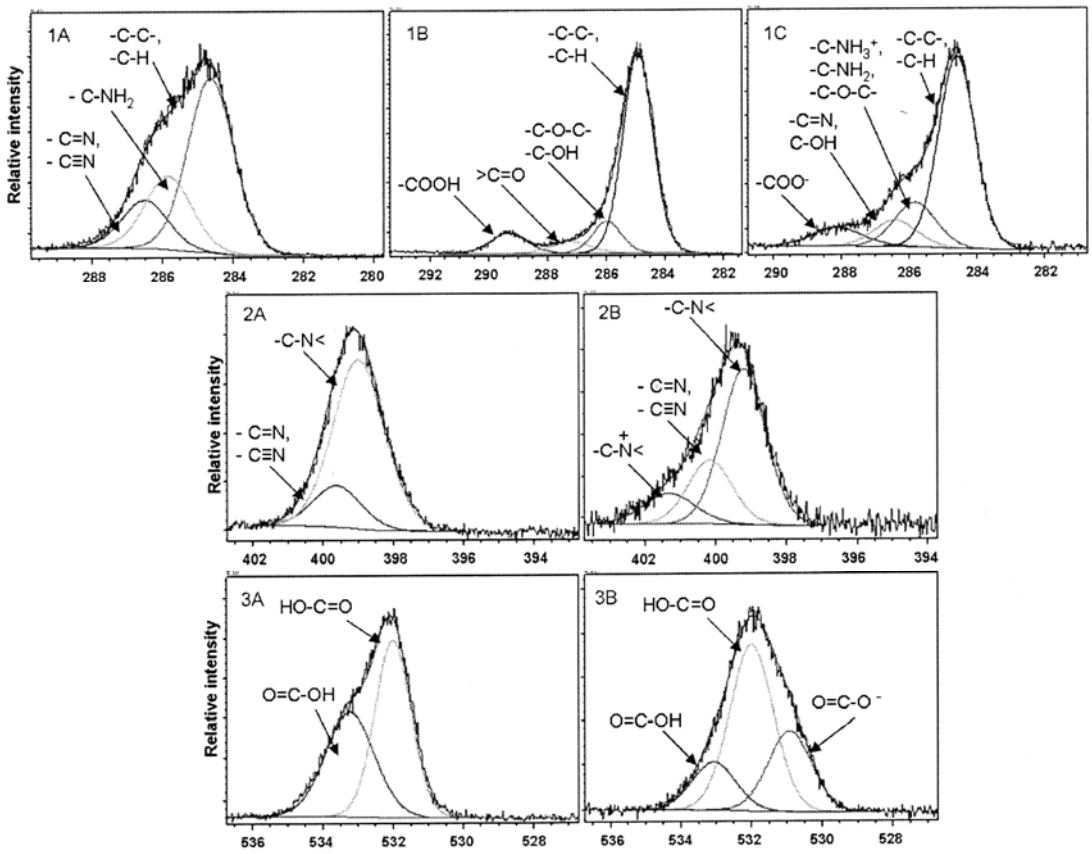

Figure 5.3 1A, 1B, 1C are high resolution C1s X-ray photoelectron spectra of plasma polymerized allyl amine (PP-AA), vinylacetic acid (PP-VAA) and the double layer bipolar film respectively. 2A and 2B are high resolution N1s for PP-AA and the double layer bipolar film respectively. 3A and 3B are high resolution O1s for PP-VAA and the double layer bipolar film respectively.

5.3.1.2 ATR FT-IR Spectroscopy

ATR FT-IR absorption spectra provide additional confirmation of the presence of a bipolar film. In these experiments, an ultrathin (2 nm) polyallyl amine film was again deposited on an equally thin 2 nm polyvinylacetic acid film, using a silicon substrate.[147] A comparison of the ATR-FT-IR spectrum of this composite sample, with

spectra of pure polyallyl amine and polyvinylacetic acid, is shown in Figure 5.4. Of special significance are the appearance of characteristic $-COO^-$ and NH_x^+ absorption bands, as indicated in Figure 5.4c, which are not present in the pure polyallyl amine (Figure 5.4a) or the pure polyvinylacetic acid films (Figure 5.4b).

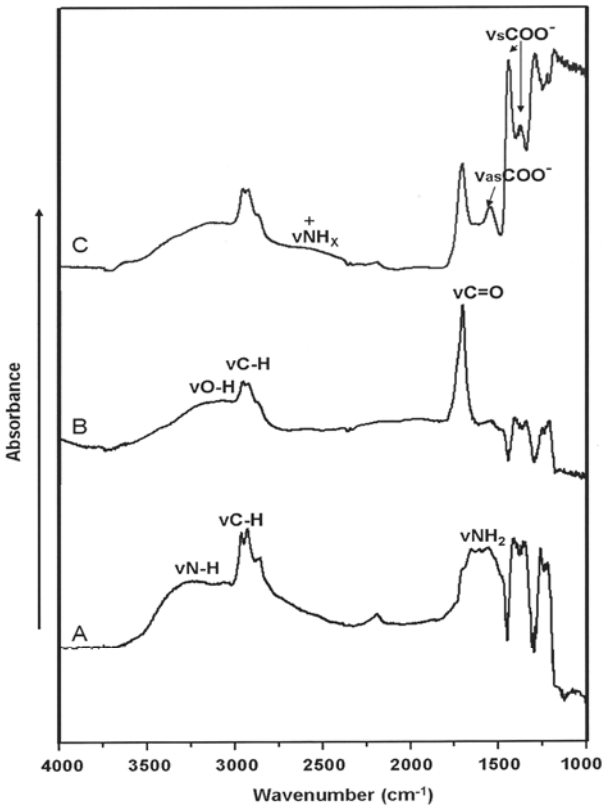

Figure 5.4 ATR-FTIR spectra of plasma polymerized (A) allyl amine (PP-AA), (B) vinylacetic acid (PP-VAA) and (C) the double layer bipolar film.

5.3.1.3 Water contact angle measurements

Static sessile water drop contact angle measurements revealed the composite film to be significantly more wettable than either pure polyallyl amine or polyvinylacetic acid single-layer films, as shown in Figure 5.5. The increased wettability of the composite film is in accord with expectations based on the polar nature of these films in light of the presence of the positive and negative ion centers.

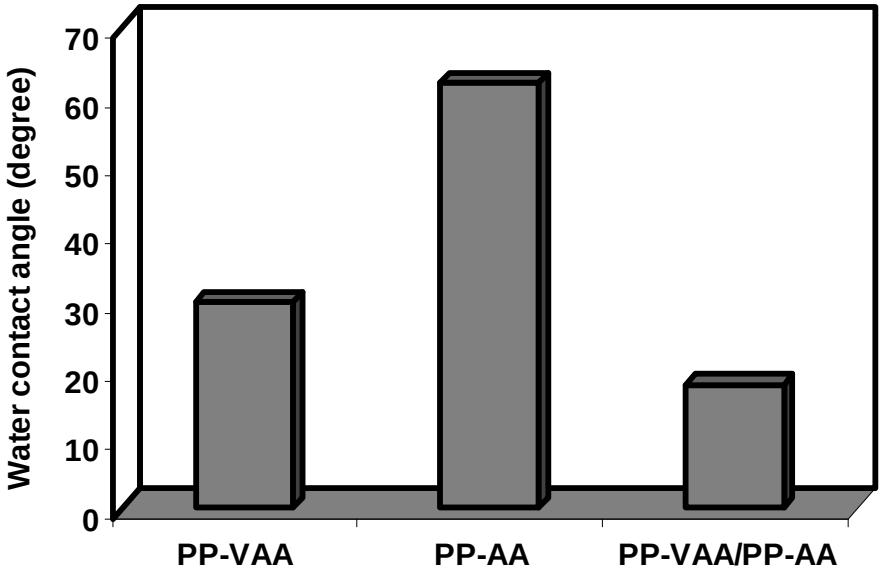

Figure 5.5 Static sessile-drop water contact angle measurements with plasma polymerized allyl amine (PP-AA), vinylacetic acid (PP-VAA) and the double layer bipolar film (PP-VAA/ PP-AA).

5.3.2.1 Capacitance-voltage (C-V) measurements

Figure 5.6a shows a typical *C-V* response of a 10-layer stack of alternating allyl amine (5 nm) and vinylacetic acid (5 nm) at 1 MHz frequency in a bias ranging from -5

V to 5 V. The high frequency response clearly shows accumulation at negative bias voltage and depletion regions at positive bias voltage. The *k* of this structure was extracted from the measured accumulation capacitance, based on the capacitance formula for a parallel capacitor,

$$\kappa = C \cdot t / \varepsilon_0 \qquad (1)$$

where *C* is the accumulation capacitance per unit area (F/cm^2), *t* is the thickness of the dielectric film and ε_0 is the permittivity of vacuum. The *k* extracted here was 6.21 at 1 MHz. The inset of Figure 5.6a shows the hysteresis behavior of the capacitor, exhibiting ~3.0 V hysteresis at 1 MHz due to uniformly distributed charges trapped in the polymer films during plasma deposition process.

The dielectric constants calculated from the capacitance measurements exhibit a dependence on the frequencies employed, with the k values decreasing with increasing frequency, as shown in Figure 5.7a. The frequency dependence of the *k* is attributed to the slow polarization of the plasma polymerized multilayer stack at higher frequencies. At lower frequencies this polarization can lead to an increase in the induced dipole.[245] The variation of *k* does not show any trend with varying the total thickness and number of multilayers, indicating that the thickness and the number of multilayers of the deposited films are not significant for controlling *k*. This phenomenon can be explained by the simulation results reported by Natori *et al*. when the ε is independent of thickness for $\varepsilon < 10$.[246] The dielectric constants of the three multilayer stacked films

studied here exhibit virtually no temperature dependence from 27°C to 147°C, indicating good thermal stability of their dielectric constants, as shown in Figure 5.7b.

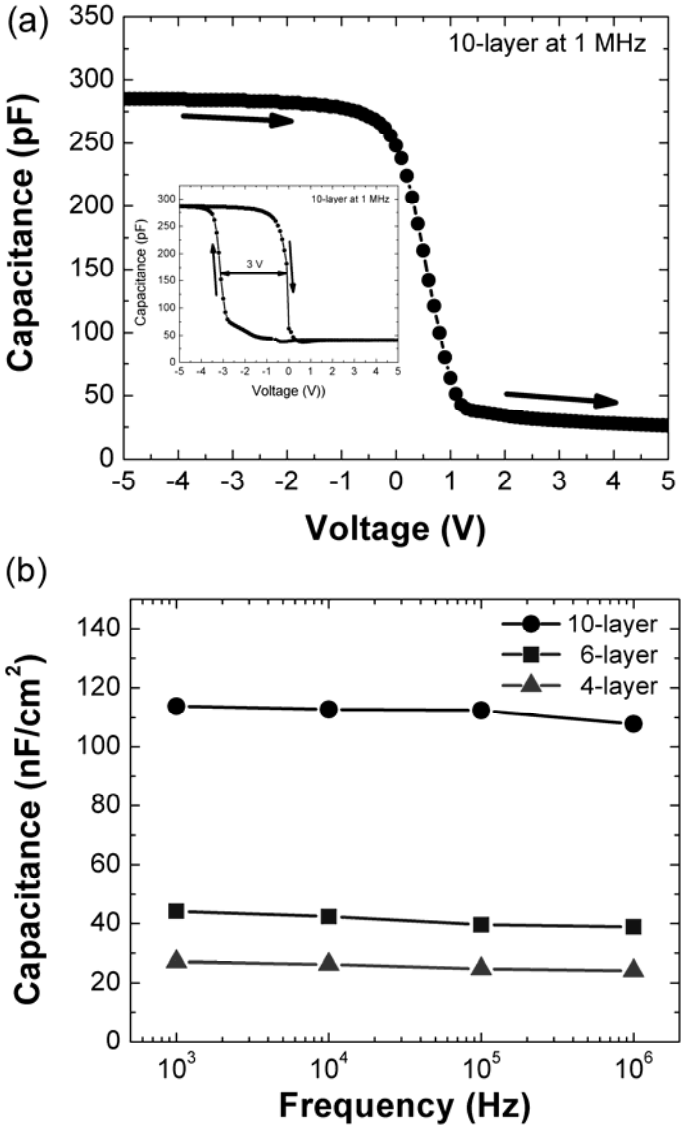

Figure 5.6 (a) *C-V* characteristics of MIS capacitor at 1 MHz for a multilayer stack of plasma polymerized allyl amine (PP-AA) and vinylacetic acid (PP-VAA) film (Au/p-Si/10-layer stack of PP-AA and PP-VAA/Au). The inset shows the hysteresis behavior of the sample. (b) Frequency dependence of the accumulation capacitance for the three different films combinations over three orders of changes in frequency.

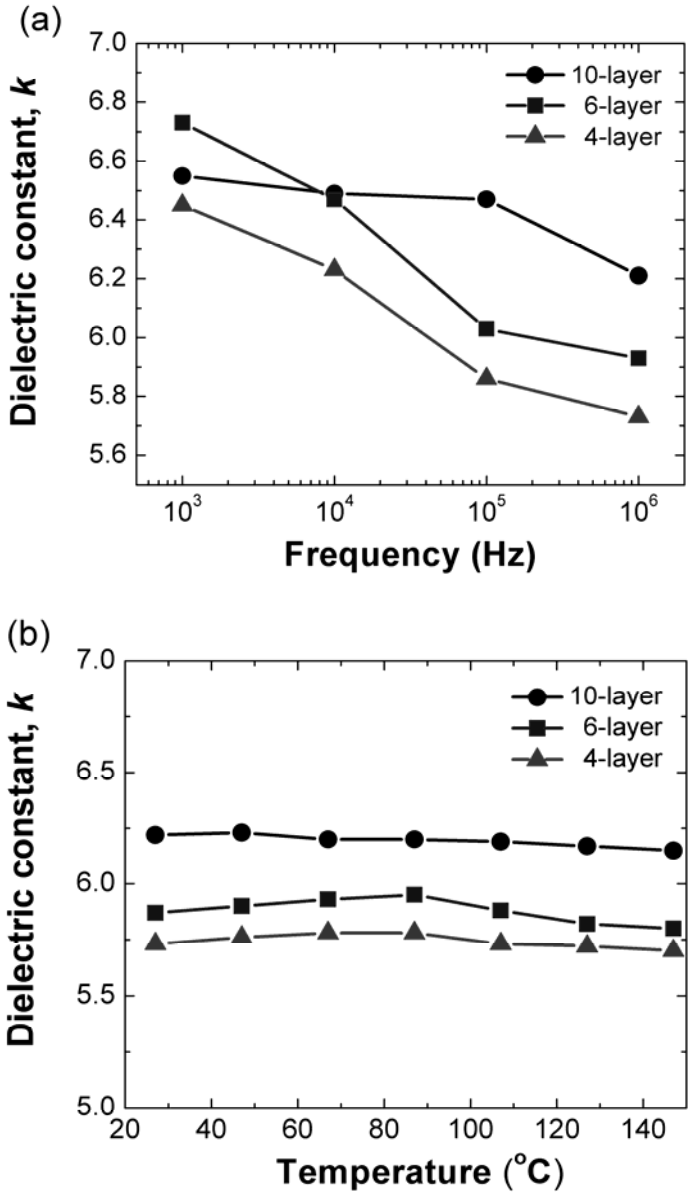

Figure 5.7 (a) The dielectric constant, *k* estimated from *C-V* measurement of a multilayer stack of plasma polymerized allyl amine (PP-AA) and vinylacetic acid (PP-VAA) film as a function of frequency. (b) The dielectric constant, *k* of three multilayer stacked films studied here as a function of temperature at 1 MHz.

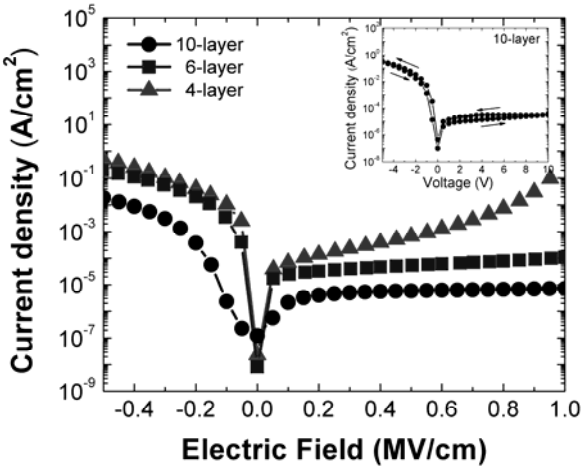

Figure 5.8 *J-V* characteristic for three different films without postdeposition annealing at room temperature. The inset shows the hysteresis behavior in the *J-V* curves for 10-layer stack film of plasma deposited allyl amine (PP AA) and vinylacetic acid (PP VAA) film.

5.3.2.2 Current density-voltage (J-V) measurements

Figure 5.8 illustrates the *J-V* characteristics of multilayer stacks. As the total thickness of a multilayer film is decreased, the leakage current density is significantly reduced. The leakage current density of a MIS capacitor with 10-layer stack was 6.5 μA/cm^2 at 1 MV/cm, which is two orders of magnitude smaller than the 6-layer stack film structure, and showed no breakdown over the voltage range shown in Figure 5.8. It should be noted that all the devices in this study were measured without any postdeposition annealing.[247] The inset of Figure 5.8 shows the hysteresis behavior of the *J-V* characteristics for a 10-layer stack of polymer films. Some hysteresis is observed in alternating forward and backward voltage sweeps. The leakage current decrease, when the total thickness of film is decreased while increasing the number of multilayers in the stack, indicates that the number of interfaces within each deposited film is a more

important factor to control the leakage current density in multilayer stacked bipolar polymer films than the aggregate thickness.

5.4 Discussion

Under pulsed RF plasma polymerization conditions, efficient retention of monomer functional groups in the polymer film has been demonstrated.[243,247] In the present work, this monomer retention capability was employed, for the first time, to create layered structures having significant concentrations of $–COO^-$ and $-NH_3^+$ polar entities. Dielectric properties of these films were studied as but one example of the potential utility of these bipolar films. An additional important new aspect of this study was demonstration that the pulsed plasma deposition technique provides sufficiently accurate film thickness controllability to construct layered structures with individual layers as thin as 2 nm. Although it was not possible to measure the thickness of individual layers, ellipsometric analysis of a ten layer stack of 5 nm altering layers confirmed a total film thickness of 50 ± 1 nm. The deposition times employed to deposit the 2 nm layers were obtained from extrapolation of deposition times employed to generate much thicker films, thus providing further confirmation of the linearity of the thickness versus deposition times under pulsed plasma conditions.

The dielectric constants of the bipolar films, ranging in value from 5.7 to 6.2 at 1 MHz, obtained without any post-deposition annealing, represent very high values for pure organic films containing only oxygen and nitrogen as heteroatoms. These high-*k* values are attributed to the unique multilayer stack of alternating layers, combined with

the significant presence of $–COO^-$ and $-NH_3^+$ polar entities that induce strong dipole orientation polarizability. The distribution of charges within a functional group with a net permanent dipole moment reorient in space in response to an external applied electric field. The relationship between ε and the total polarizability (α) is often described by the Clausius-Mossotti relationship. The α is generally additive, including electronic, atomic, and dipole orientation polarizability and, within the context of the Clausius-Mossotti relationship, can be used to estimate the contribution of each polarization group to the dielectric constant.[248] The total polarizability increases when dipole orientation polarizability increases. As a result, the *k* also increases. In this experiment, the observed small variation of the *k*, with varying total thickness and number of multilayer stacks, suggests that the *k* is mainly due to the high dipole orientation polarizability induced between alternating charged layers.

5.4 Conclusion

A multilayer stack of polymeric thin films composed of alternating amine and carboxylic acid functional groups synthesized by pulsed RF plasma polymerization produced a composite structure having a relatively high–*k* and low leakage current density, as obtained without postdeposition annealing. This high performance multilayer polymer film stack, deposited at ambient temperature and not subjected to further treatment of any kind, is promising in terms of potential use as a flexible dielectric material.

REFERENCES

1. Yakada, Y. *Biomaterials*, **1994**, *15*, 725-736.
2. Ratner, B. D. *Biosens. Bioelectron*., **1995**, *10*, 797-804.
3. Ruckenstein, E.; Li, Z. F. *Adv. Colloid. Interface. Sci*., **2005**, *113*, 43-63.
4. Falconnet, D.; Csucs, G.; Grandin, H. M.; Textor, M. *Biomaterials*, **2006**, *27*, 3044-3063.
5. Poncin-Epaillard, F.; Legacy, G. *J. Biomater. Sci. Polym. Ed.*, **2003**, *14*, 1005-1028.
6. Ozdemir, M.; Yurteri, C. U.; Sadikoglu, H. *Crit. Rev. Food Sc. Nutr.*, **1999**, *39*, 457-477.
7. Inagaki, N.; Tasaka, S.; Nakajima, T. *J. App. Polym. Sc.*, **2000**, *78*, 2389-2397.
8. Wu, Y. J.; Timmons, R. B.; Jen, J. S.; Molock, F. E. *Colloids Surf B Biointerfaces*, **2000**, *18*, 235-248.
9. Popat, K. C.; Mor, G.; Grimes, C. A.; Desai, T. A. *Langmuir*, **2004**, *20*, 8035-8041.
10. Fan, X.; Lin, L.; Dalsin, J. L.; Messersmith, P. B. *J. Am. Chem. Soc.*, **2005**, *127*, 15843-15847.
11. Salim, M.; Mishra, G.; Fowler, G. J.; O'sullivan, B.; Wright, P. C.; McArthur, S. L. *Lab Chip*, **2007**, *7*, 523-525.

12. Wu, S.; Kang, E. T.; Neoh, K. G.; Han, H. S.; Tan, K. L. *Macromolecules*, **1999**, *32*, 186 -193.

13. Haïdopoulos, M.; Turgeon, S.; Laroche, G.; Mantovani, D. *Surface and Coatings Technology*, **2005**, *197*, 278-287.

14. Yu, L.; Zhang, P.; Du, Z. *Surface and Coatings Technology*, **2000**, *130*, 110-115.

15. Mutin, P. H.; Lafond, V.; Popa, A. F.; Granier, M.; Markey, L.; Dereux, A. *Chem. Mater.*, **2004**, *16*, 5670-5675.

16. Cho, J.; Denes, F. S.; Timmons, R. B. *Chem. Mater.*, **2006**, *18*, 2989-2996.

17. Brüser, V.; Savastenko, N.; Schmuhl, A.; Junge, H.; Herrmann, I.; Bogdanoff, P.; Schröder, K. *Plasma Processes and Polymers*, **2007**, *S1*, S94-S98.

18. Ibhadon, A. O.; Greenway, G. M.; Yue, Y. *Catalysis Communications*, **2008**, *9*, 153-157.

19. Yu, Z. J.; Kang, E. T.; Neoh, K. G. *Polymer*, **2002**, *43*, 4137-4146.

20. Siau, S.; Vervaet, A.; Schacht, E.; Demeter, U.; Van Calster, A. *Thin Solid Films*, **2006**, *495*, 348-356.

21. Lintanf, A.; Mantoux, A.; Blanquet, E.; Djurado, E. *J. Phys. Chem. C*, **2007**, *111*, 5708-5714.

22. Jones, A. C.; Aspinall, H. C.; Chalker, P. R. *Surface and Coatings Technology*, **2007**, *201*, 9046-9054.

23. Cho, B.; Wang, J.; Sha, L.; Chang, J. P. *Appl. Phys. Lett.*, **2002**, *80*, 1052-1054.

24. Conley, J. F., Jr.; Ono, Y.; Solanki, R.; Stecker, G.; Zhuang, W. *Appl. Phys. Lett.*, **2003**, *82*, 3508-3510.

25. Drolet, N.; Morin, J-F.; Leclerc, N.; Wakim, S.; Tao, Y.; Leclerc, M. *Adv. Func. Mater.*, **2005**, *15*, 1671-1682.

26. Fujiwara, T.; Locklin, J.; Bao, Z. *Appl. Phys. Lett.*, **2007**, *90*, 232108/1-232108/3.

27. Källtorp, M.; Oblogina, S.; Jacobsson, S.; Karlsson, A.; Tengvall, P.; Thomsen, P. *Biomaterials*, **1999**, *20*, 2123-2137.

28. Quiñones, R.; Gawalt, E. S. *Langmuir*, **2007**, *23*, 10123-10130.

29. Killampalli, A. S.; Ma, P. F.; Engstrom, J. R. *J. Am. Chem. Soc*., **2005**, *127*, 6300-6310.

30. Campbell, G. A.; Mutharasan, R. *Anal. Chem.*, **2006**, *78*, 2328-2334.

31. Toworfe, G. K.; Composto, R. J.; Shapiro, I. M.; Ducheyne, P. *Biomaterials*, **2006**, *27*, 631-642.

32. Chen, J.; Murphy, A. R.; Esteve, J.; Ogletree, D. F.; Salmeron, M.; Fréchet, J. M. *Langmuir*, **2004**, *20*, 7703-7710.

33. Ofir, Y.; Zenou, N.; Goykhman, I.; Yitzchaik, S. *J. Phys. Chem. B*, **2006**, *110*, 8002-8009.

34. Rodrigues, S. N. ; Gonçalves, I. C. ; Martins, M. C. ; Barbosa, M. A.; Ratner, B. D. *Biomaterials*, **2006**, *27*, 5357-5367.

35. Chuang, W. H.; Lin, J. C. *J. Biomed. Mater. Res. A*, **2007**, *82*, 820-830.

36. Chaki, N. K.; Vijayamohanan, K. *Biosens. Bioelectron.*, **2002**, *17*, 1-12.

37. Senaratne, W.; Andruzzi, L.; Ober, C. K. *Biomacromolecules*, **2005**, *6*, 2427-2448.

38. Ruckenstein, E.; Li, Z. F. *Adv. Colloid. Interface Sci.*, **2005**, *113*, 43-63.

39. Flynn, N. T.; Tran, T. O. N.; Cima, M. J.; Langer, R. *Langmuir*, **2003**, *19*, 10909-10915.

40. Willey, T. M.; Vance, A. L.; van Buuren, T.; Terminello, L. J.; Fadley, C. S. *Surface Science*, **2005**, *576*, 188–196.

41. Bhattacharya, A.; B.N. Misra, B. N. *Prog. Polym. Sci*., **2004**, *29*, 767–814.

42. Gao, C.; Hu, X.; Hong, Y.; Guan, J.; Shen, J. *J Biomater Sci Polym Ed.*, **2003**, *14*, 937-950.

43. Sun, H.; Wirsén, A.; Albertsson, A. C. *Biomacromolecules*, **2004**, *5*, 2275-2280.

44. Kim, S.; Kim, E.; Kim, S.; Kim, W. *J. Colloid. Interface Sci.*, **2005**, *292*, 93-98.

45. Eckert, A. W.; Gröbe, D.; Rothe, U. *Biomaterials*, **2000**, *21*, 441-447.

46. Ulbricht, M.; Riedel, M. *Biomaterials*, **1998**, *19*, 1229-1237.

47. Ulbricht, M.; Matuschewski, H.; Oechel, A.; Hicke, H-G. *J. Membrane Sc.*, **1996**, *115*, 31-47.

48. Akiyama, Y.; Kikuchi, A.; Yamato, M.; Okano, T. *Langmuir*, **2004**, *20*, 5506-5511.

49. Hu, S.; Ren, X.; Bachman, M.; Sims, C. E.; Li, G. P.; Allbritton, N. *Anal. Chem*., **2002**, *74*, 4117-4123.

50. Yuan, J.; Chen, L.; Jiang, X.; Shen, J.; Lin, S. *Colloids Surf. B Biointerfaces*, **2004**, *39*, 87-94.

51. Dong, B.; Jiang, H.; Manolache, S.; Wong, A. C.; Denes, F. S. *Langmuir*, **2007**, *23*, 7306-7313.

52. Hsu, S. H.; Chen, W. C. *Biomaterials*, **2000**, *21*, 359-367.

53. Kim, Y. J.; Kang, I. K.; Huh, M. W.; Yoon, S. C. *Biomaterials*, **2000**, *21*, 121-130.

54. Zhou, J.; Yuan, J.; Zang, X.; Shen, J.; Lin, S. *Colloids Surf. B Biointerfaces*, **2005**, *41*, 55-62.

55. Liu, Y.; Klep, V.; Luzinov, I. *J. Am. Chem. Soc*., **2006**, *128*, 8106-8107.

56. Xu, F. J.; Zhao, J. P.; Kang, E. T.; Neoh, K. G.; Li, J. *Langmuir*, **2007**, *23*, 8585-8592.

57. Coad, B. R.; Kizhakkedathu, J. N.; Haynes, C. A.; Brooks, D. E. *Langmuir*, **2007**, *23*, 11791-11803.

58. Sun, X.; Liu, J.; Lee, M. L. *Anal. Chem*., **2008**, *80*, 856-863.

59. Apperloo, J. J.; Janssen, R. A. J.; Nielsen, M. M.; Bechgaard, K. *Adv. Mater*., **2000**, *12*, 1594-1597.

60. Arias, A. C.; Corcoran, M.; Banach, M.; Friend, R. H.; MacKenzie, J. D. *Appl. Phys. Lett.*, **2002**, *80*, 1695-1697.

61. Shi, Y.; Liu, J.; Yang, Y. *J. Appl. Phys*., **2000**, *87*, 4254-4263.

62. Chang, J-F.; Sun, B.; Breiby, D. W.; Nielsen, M. M.; Sølling, T. I.; Giles, M.; McCulloch, I.; Sirringhaus, H. *Chem. Mater*., **2004**, *16*, 4772-4776.

63. Niu, Q.; Shao, Y.; Xu, W.; Wang, L.; Han, S.; Liu, N.; Peng, J.; Cao, Y.; Wang, J. *Organic Electronics*, **2008**, *9*, 95–100.

64. Mcculloch, I.; Lu, P.; Kang, M. *J. Appl. Polym. Sci.*, **1999**, *74*, 1304–1316.

65. Wang, G.; Gan, F. *Materials Letters*, **2000**, *43*, 6–10.

66. Hoggan, E. N. Spin coating and photolithography using liquid and supercritical carbon dioxide. PhD Thesis, **2002**. UMI Number: 3076412.

67. Le Cœur, F.; Pelletier, J.; Arnal, Y.; Lacoste, A. *Surface and Coatings Technology*, **2000**, *125*, 71-78.

68. Pelletier, J. ; Anders, A. *IEEE Transactions on Plasma Sc.*, **2005**, *33*, 1944-1959.

69. Yukimura, K. *Surface and Coatings Technology*, **2001**, *136*, 1-6.

70. Yukimura, K.; Wei, R. *AIP Conference Proceedings*, **2004**, *740*, 132-147.

71. Tsyganov, I.; Maitz, M. F.; Wieser, E.; Richter, E.; Reuther, H. *Surface and Coatings Technology*, **2005**, *200*, 1041-1044.

72. Mandl, S.; Krause, D.; Thorwarth, G.; Sader, R.; Zeilhofer, F.; Horch, H. H.; Rauschenbach, B. *Surface and Coatings Technology*, **2001**, *142-144*, 1046-1050.

73. Prakash, B.; Celis, J. P. *Surface and Coatings Technology*, **2005**, *200*, 182-185.

74. Ma, Xinxin; Tang, Guangze; Sun, Mingren; Yukimura, Ken. *Surface and Coatings Technology*, **2005**, *196*, 100-103.

75. Volz, K.; Ensinger, W. *Surface and Coatings Technology*, **2002**, *156*, 237–243.

76. Liu, L.; Yamamoto, A.; Oka, Y.; Yatsuzuka, M.; Tsubakino, H. *Diamond and Related Materials*, **2005**, *14*, 1047-1050.

77. Cheng, Y.; Zheng, Y. F. *Surface and Coatings Technology*, **2006**, *200*, 4543-4548.

78. Tomita, A.; Kusuda, M.; Otsuki, S.; Oka, Y.; Nishimura, Y.; Murakami, A.; Yatsuzuka, M. *Thin Solid Films*, **2006**, *506-507*, 59-62.

79. Oka, Y.; Nishijima, M.; Hiraga, K.; Yatsuzuka, M. *Surface and Coatings Technology*, **2007**, *201*, 6647-6650.

80. Yokota, T.; Terai, T.; Kobayashi, T.; Meguro, T.; Iwaki, M. *Surface and Coatings Technology*, **2007**, *201*, 8048-8051.

81. Thornton, J. A.; Greene, J. E. *Handbook of Deposition Technologies for Films and Coatings: Science, Applications and Technology*, Bunshah, R. F. (Editor), Noyes Publications, 2nd edition, **1994**, pp 249.

82. Chinmulgund, M.; Inturi, R. B.; Barnard, J. A. *Thin Solid Films*, **1995**, *270*, 260-263.

83. Stockemer, J.; Winand, R.; Vanden Brande, P. *Surface and Coatings Technology*, **1999**, *115*, 230-233.

84. Wasielewski, R.; Domaradzki, J.; Wojcieszak, D.; Kaczmarek, D.; Borkowska, A.; Prociow, E. L.; Ciszewski, A. *Appl. Surf. Sc.*, **2008**, *254*, 4396-4400.

85. Sicha, J.; Musil, J.; Meissner, M.; Cerstvy, R. *Appl. Surf. Sc.*, **2008**, *254*, 3793-3800.

86. Ye, C.; Pan, S. S.; Teng, X. M.; Li, G. H. *J. Appl. Phys.*, **2007**, *102*, 013520/1-013520/5.

87. Lugscheider, E.; Barwulf, S.; Riester, M.; Hilgers, H. *Surface and Coatings Technology*, **1999**, *116-119*, 1172-1178.

88. Chen, W-Y; Tien, S-K; Wu, F-B; Duh, J-G. *Surface and Coatings Technology*, **2004**, *182*, 85-91.

89. Wu, F-B; Chen, Y-I.; Peng, P-J; Tsai, Y-Y; Duh, J-G. *Surface and Coatings Technology*, **2002**, *150*, 232-238.

90. Alves, V. A.; Brett, C. M. A.; Cavaleiro, A. *Surface and Coatings Technology*, **2002**, *161*, 257-266.

91. Zhang, Y.; Yang, G. H.; Kang, E. T.; Neoh, K. G.; Huang, W.; Huan, A. C. H.; Wu, S. Y. *Langmuir*, **2002**, *18*, 6373-6380.

92. Huang, F.; Wei, Q.; Liu, Y.; Gao, W.; Huang, Y. *J. Mater. Sc.*, **2007**, *4219*, 8025-8028.

93. Biederman, H.; Stelmashuk, V.; Kholodkov, I.; Choukourov, A.; Slavinska, D. *Surface and Coatings Technology*, **2003**, *174-175*, 27-32.

94. Yashuda, H. *Plasma Polymerization*, Academic Press, N.Y., **1985**.

95. Rinsch, C. L.; Chen, X.; Panchalingam, V.; Eberhart, R. C.; Wang, J-H.; Timmons, R. B. *Langmuir*, **1996**, *12*, 2995-3002.

96. Nedelmann, H.; Weigel, Th.; Hicke, H. G.; Muller, J.; Paul, D. *Surface and Coatings Technology*, **1999**, *116-119*, 973-980.

97. Srikanth, H.; Hajndl, R.; Chirinos, C.; Sanders, J.; Sampath, A.; Sudarshan, T. S. *Appl. Phys. Lett.*, **2001**, *79*, 3503-3505.

98. Deilmann, M.; Theiss, S.; Awakowicz, P. *Surface and Coatings Technology*, **2008**, *202*, 1911-1917.

99. Van Ooij, W. J.; Eufinger, S.; Guo, S. *Plasma Chemistry and Plasma Processing*, **1997**, *17*, 123-154.

100. Kravets, L.; Dmitriev, S.; Gilman, A.; Drachev, A.; Dinescu, G. *J. Membrane Sc.*, **2005**, *263*, 127-136.

101. Chen, C-H.; Yang, M-R.; Wu, S-K. *Surface and Coatings Technology*, **2008**, *202*, 2709-2714.

102. Timmons, R. B.; Griggs, A. J. Pulsed plasma polymerizations. In *Plasma Polymer Films*, Biedermann, H., Editor.; Imperial College Press: London, **2004**. pp. 217-245.

103. Pan, Y. V.; Wesley, R. A.; Luginbuhl, R.; Denton, D. D.; Ratner, B. D. *Biomacromolecules*, **2001**, *2*, 32-36.

104. Inagaki, N.; Oh-Ishi, K. *J. Polym. Sc., Polym. Chem. Ed.*, **1985**, *23*, 1445-1454.

105. Cannon, J. G.; Dillon, R. O.; Bunshah, R. F.; Crandall, P. H.; Dymond, A. M. *J. Biomed. Mater. Res.*, **1980**, *14*, 279-288.

106. Yeh, Y. S.; Iriyama, Y.; Matsuzawa, Y.; Hanson, S. R.; Yasuda, H. *J. Biomed. Mater. Res.*, **1988**, *22*, 795-818.

107. Leich, M. A.; Mackie, N. M.; Williams, K. L.; Fisher, E. R. *Macromolecules*, **1998**, *31*, 7618-7626.

108. Calderon, J. G.; Timmons, R. B. *Macromolecules*, **1998**, *31*, 3216-3224.

109. Ryan, M. E.; Hynes, A. M.; Badyal, J. P. S. *Chem. Mater.*, **1996**, *8*, 37-42.

110. Tarducci, C.; Kinmond, E. J.; Badyal, J. P. S.; Brewer, S. A.; Willis, C. *Chem. Mater.*, **2000**, *12*, 1884-1889.

111. Peppas, N. A. *Reflexive Polymers and Hydrogels: Understanding and Designing Fast Responsive Polymeric Systems*. Yui, N.; Mrsny, R. J.; Park, K., Eds.; CRC Press; Boca Raton, FL, **2004.**

112. Zhang, X. Z.; Wu, D .Q.; Chu, C. C. *Biomaterials*, **2004**, *25*, 3793-3805.

113. Zhang, X. Z.; Lewis, P. J.; Chu, C. C. *Biomaterials*, **2005**, *26*, 3299-3309.

114. Luo, Y.; Kirker, K. R.; Glenn D. Prestwich, G. D. *J Control Release*, **2000**, *69*, 169-184.

115. Linke, B.; Kernar, W.; Kiwit, M.; Pishko, M.; Heller. A. *Biosens. Bioelectronics*, **1994**, *9*, 151-158.

116. Gajovic, N.; Binyamin, G.; Warsinke, A.; Scheller, F. W.; Heller, A. *Anal. Chem.,* **2000**, *72*, 2963-2968.

117. Thoniyot, P.; Cappuccio, F. E.; Gamsey, S.; Cordes, D. B.; Wessling, R. A.; Singaram, B. *Diabetes Technology & Therapeutics*, **2006**, *8*, 279-287.

118. Schmedlen, R. H.; Masters, K. S.; West, J. L. *Biomaterials*, **2002**, *23*, 4325-4332.

119. Tana, J.; Gemeinharta, R. A.; Maa, M.; Saltzman, W. M. *Biomaterials*, **2005**, *26*, 3663-3671.

120. Canavan, H. E.; Cheng, X.; Graham, D. J.; Ratner, B. D.; Castner, D. G. *J. Biomed. Mater. Res.,* **2005**, *75A*, 1-13.

121. Alarc´on, C. D. L. H.; Twaites, B.; Cunliffe, D.; Smith, J. R.; Alexander, C. *Int. J. Pharm.,* **2005**, *295*, 77-91.

122. Gerlach, G.; Guenther, M.; Sorber, J.; Suchaneck, G. *Sensors and Actuators B*, **2005**, *111-112*, 555-561.

123. Cheng, X.; Canavan, H. E.; Stein, M. J.; Hull, J. R.; Kweskin, S. J.; Wagner, M. S.; Somorjai, G. A.; Castner, D. G.; Ratner, B. D. *Langmuir*, **2005**, *21*, 7833-7841.

124. Ito, Y.; Chen, G.; Guan, Y.; Imanishi, Y. *Langmuir*, **1997**, *3*, 2756-2759.

125. Hruby, M.; Subr, V.; Kucˇka, J.; Kozempel, J.; Lebeda, O.; Sikora, A. *Applied Radiation and Isotopes*, **2005**, *63*, 423-431.

126. Hassan, C. M.; Stewart, J. E.; Peppas, N. A. *European Journal of Pharmaceutics and Biopharmaceutics*, **2000**, *49*, 161-165.

127. Watanabe, J.; Ooya, T.; Nitta, K. H.; Park, K. D.; Kim, Y. H.; Yui, N. *Biomaterials*, **2002**, *23*, 4041-4048.

128. Hahn, M. S.; Taite, L. J.; Moon, J. J.; Rowland, M. C.; Ruffino, K. A.; West, J. L. *Biomaterials*, **2006**, *27*, 2519-2524.

129. Smith, L. E.; Rimmer, S.; MacNeil, S. *Biomaterials*, **2006**, *27*, 2806-2812.

130. Park, K. H.; Yun, K. *J. Bioscience Bioeng.*, **2004**, *97*, 374-377.

131. Schmaljohann, D.; Oswald, J.; Jørgensen, B.; Nitschke, M.; Beyerlein, D.; Werner, C. *Biomacromolecules*, **2003**, *4*, 1733-1739.

132. Gilcreest, V. P.; Carroll, W. M.; Rochev, Y. A.; Blute, I.; Dawson, K. A.; Gorelov, A. V. *Langmuir*, **2004**, *20*, 10138-10145.

133. Park, T. G.; Hoffman, A. S. *J Appl. Polym. Sc.,* **1994**, *52*, 85-89.

134. McPhee, W.; Tam, K. C.; Pelton, R. *J. Coll. Interface Sc.*, **1993**, *156*, 24-30.

135. Matsuo, E. S.; Tanaka, T. *J. Chem. Phys.*, **1988**, *89*, 1695-1703.

136. Hegewald, J.; Schmidt, T.; Eichhorn, K. J.; Kretschmer, K.; Kuckling, D.; Arndt, K. F. *Langmuir*, **2006**, *22*, 5152-5159.

137. Alexandre, E.; Schmitt, B.; Boudjema, K.; Merrill, E. W.; Lutz, P. J. *Macromol. Bioscience*, **2004**, *4*, 639-648.

138. Waber, L. M.; He, J.; Bradley, B.; Haskins, K.; Anseth, K .S. *Acta Biomaterialia*, **2006**, *2*, 1-8.

139. Liang, L.; Feng, X.; Liu, J.; Rieke, P. C.; Fryxell, G. E. *Macromolecules*, **1998**, *31*, 7845-7850.

140. Kanazawa, H.; Yamamoto, K.; Matsushima, Y. *Anal. Chem.*, **1996**, *68*, 100-105.

141. Go, H.; Sudo, Y.; Hosoya, K.; Ikegami, T.; Tanaka, N. *Anal. Chem.*, **1998**, *70*, 4086-4093.

142. Schmaljohann, D.; Beyerlein, D.; Nitschke, M.; Werner, C. *Langmuir*, **2004**, *20*, 10107-10114.

143. Tamirisa, P. A.; Koskinen, J.; Hess, D. W. *Thin Solid Films*, **2006**, *515*, 2618-2624.

144. Bullett, N.A.; Talib, R.A.; Short, R.D.; McArthur, S.L.; Shard, A.G. *Surf. Interface Anal.*, **2006,** *38*, 1109-1116.

145. Kosik, K.; Wilk, E.; Geissler, E.; Laszlo, K. *J. Phys. Chem. B*, 2008, *112*, 1065-1070.

146. Zhang, X-Z.; Chu, C-C. *J. Mater. Sc. Mater. Med.*, 2007, *18*, 1771-1779.

147. Chyan, O. M. R.; Chen, J. J.; Xu, F.; Wu, J. *Anal. Chem.*, **1997***, 69,* 2434-2437.

148. Muller, M.; Rieser, T.; Lunkwitz, K.; Meier-Haack, J. *Macromol. Rapid Comm.*, **1999**, *20*, 607-611.

149. Beamson, G.; Briggs, D. *High Resolution XPS of Organic Polymers - The Scienta ESCA300 Database*. John Wiley & Sons, **1992**.

150. Mandracchia, D.; Pitarresi, G.; Palumbo, F. S.; Carlisi, B.; Giammona, G. *Biomacromolecules*, **2004**, *5*, 1973-1982.

151. Davis, D.H.; Giannoulis, C.S.; Johnson, R.W.; Desai, T.A. *Biomaterials*, **2002**, *23,* 4019-4027.

152. Itoh, S.; Matsuda, A.; Kobyashi, H.; Ichinose, S.; Shinomiya, K.; Tanaka, J. *J. Biomed. Mater. Res. B: Appl. Biomater*., **2005**. *73,* 375-382

153. Ernsting, M.J.; Bonin, G.C.; Yang, M.; Labow, R.S.; Santerre, J.P. *Biomaterials,* **2005**, *26,* 6536-6546.

154. Johnell, M.; Larsson, R.; Siegbahn, A. *Biomaterials*, **2005**, *26,* 1731-1739.

155. Phillips, J.M.; Kao, W.J. *Tissue Eng.,* **2005**, *11,* 964-973.

156. Gao, H.; Buchapudi, K. R.; Harms-Smyth, A.; Schulte, M. K.; Xu, X.; Ji, H.-F. *Langmuir*, **2008**, *24*, 345-349.

157. Nakata,E.; Nagase, T.; Shinkai, S.; Hamachi, I. *J. Am. Chem. Soc*., **2004**, *126*, 490-495.

158. Polyak, B.; Geresh, S.; Marks, R. S. *Biomacromolecules*, **2004**, *5*, 389-396.

159. Xiao, D.; Van Le, T.; Wirth, M. J. *Anal. Chem.,* **2004**, *76*, 2055-2061.

160. Massolini, G.; Calleri, E. *J. Sep. Sci.*, **2005**, *28*, 7-21.

161. Lee, C. Y.; Nguyen, P. C. ; Grainger, D. W.; Gamble, L. J.; Castner, D. G. *Anal. Chem.*, **2007**, *79*, 4390-4400.

162. Wu, P.; Hogrebe, P.; Grainger, D. W. *Biosens. Bioelectron.*, **2006**, *21*, 1252-1263.

163. Chen, R.; Curran, S. J.; Curran, J. M.; Hunt, J. A. *Biomaterials*, **2006**, *27*, 4453-4460.

164. Liang, S.; Wang, Y.; Yu, J.; Zhang, C.; Xia, J.; Yin, D. *J. Mater. Sci. Mater. Med*., **2007**, *18*, 2297-2302.

165. Xiong, X. B.; Mahmud, A.; Uludağ, H.; Lavasanifar, A. *Biomacromolecules*, **2007**, *8*, 874-884.

166. Hu, Z.; Luo, F.; Pan, Y.; Hou, C.; Ren, L.; Chen, J.; Wang, J.; Zhang, Y. *J. Biomed. Mater. Res. A.*, **2008**, *85*, 797-807.

167. Hook, F.; Rodahl, M.; Kasemo, B.; Brzezinski, P. *PNAS*, **1998**, *95,* 12271-12276.

168. Rankl, M.; Ruckstuhl, T.; Rabe, M.; Artus, G.R.; Walser, A.; Seeger, S. *Chemphyschem*., **2006**, *7,* 837-846.

169. Kang, J.; Lambert, O.; Ausborn, M.; Schwendeman, S.P. *Int. J. Pharm*., **2008**, *357*, 235-243.

170. Desai, K.G.; Mallery, S.R.; Schwendeman, S.P. *Pharm. Res*., **2008**, *25*, 586-597.

171. Frauke Pistel, K.; Breitenbach, A.; Zange-Volland, R.; Kissel, T. *J. Control. Release*, **2001**, *73*, 7-20.

172. Chandran, S.S.; Nan, A.; Rosen, D.M.; Ghandehari, H.; Denmeade, S.R. *Mol. Cancer Ther*., **2007**, *6*, 2928-2937.

173. Pertuit, D. ; Moulari, B. ; Betz, T.; Nadaradjane, A.; Neumann, D.; Ismaïli, L.; Refouvelet, B. ; Pellequer, Y. ; Lamprecht, A. *J. Control. Release*, **2007**, *123*, 211-208.

174. Brogan, K. L.; Schoenfisch, M. H. *Langmuir*, **2005**, *21*, 3054 -3060.

175. Hersel, U.; Dahmen, C.; Kessler, H. *Biomaterials*, **2003**, *24*, 4385-4415.

176. Arai, K.; Yoshinari, K.; Matsumoto, K.; Misaki, H. *J. Immunol. Methods*, **1998**, *217*, 79-85.

177. Sung, W.C.; Chang, C. C.; Makamba, H.; Chen, S.H. *Anal. Chem*., **2008**, *80*, 1529-1535.

178. Jacobson, S.C.; Guiochon, G. *Anal. Chem*., **1992**, *64*, 1496-1498.

179. Zacharis, C.K.; Kalaitzantonakis, E. A.; Podgornik, A.; Theodoridis, G. *J Chromatogr. A*, **2007**, *1144*, 126-134.

180. Yin, J.; Wei, W.; Liu, X.; Kong, B.; Wu, L.; Gong, S. *Anal. Biochem*., **2007**, *360*, 99-104.

181. Wittman, V.P.; Woodburn, D.; Nguyen, T.; Neethling, F.A.; Wright, S.; Weidanz, J.A. *J. Immunol*., **2006**, *177*, 4187-4195.

182. Weidanz, J.A.; Piazza, P.; Hickman-Miller, H.; Woodburn, D.; Nguyen, T.; Wahl, A.; Neethling, F.; Chiriva-Internati, M.; Rinaldo, C.R.; Hildebrand, W.H. *J. Immunol. Methods*, **2007**, *318*, 47-58.

183. Walsh, M.K.; Wang, X.; Weimer, B.C. *J. Biochem. Biophys. Methods*, **2001**, *47,* 221-231.

184. Hoffman, A.S.; Hubbel, J. A. *Biomaterials Science: An Introduction to Materials in Medicine*, **2004**, Academic Press, p-226. (Table-1)

185. Socrates, G. *Infrared Characteristic Group Frequencies – Tables and Charts.* John Wiley & Sons, **1994**.

186. Wahl, A.; Weidanz, J.; Hildebrand, W. *Expert Rev. Proteomics*, **2006**, *3*, 641-652.

187. Boyan, B. D.; Hummert, T. W.; Dean, D. D.; Schwartz, Z. *Biomaterials*, **1996**, *17*, 137-146.

188. Kasemo, B. *Surface Science*, **2002**, *500*, 656-677.

189. Wernick, M.H.; Jeremias, A.; Carrozza, J.P. *Coron. Artery Dis*., **2006**, *17*, 661-665.

190. Serruys, P.W.; Daemen, J. *Circulation*, **2007**, *115*, 1433-1439.

191. Garg, P.; Mauri, L. *Curr Opin Cardiol*., **2007**, *22*, 565-571.

192. Sharifkazemi MB, Zamirian M, Aslani A. *Cardiology*, **2007**, *108*, 273-274.

193. Wan,Y.; Yang, J.; Yang, J.; Bei, J.; Wang, S. *Biomaterials*, **2003**, *24*, 3757-3764.

194. Gumpenberger, T.; Heitz, J.; Bäuerle, D.; Kahr, H.; Graz, I.; Romanin, C.; Svorcik, V.; Leisch, F. *Biomaterials*, **2003**, *24*, 5139-5144.

195. Lakard, S.; Herlem, G.; Propper, A.; Kastner, A.; Michel, G.; Valles-Villarreal, N.; Gharbi, T.; Fahys, B. *Bioelectrochemistry*, **2004**, *62*, 19-27.

196. Mitchell, S. A.; Davidson, M. R.; Emmison, N.; Bradley, R. H. *Surface Science*, **2004**, *561*, 110-120.

197. France, R. M.; Short, R. D.; Duval, E.; Jones, F. R.; Dawson, R.A.; MacNeil, S. *Chem. Mater.*, **1998**, *10*, 1176-1183.

198. Zhang, Z.; Menges, B.; Timmons, R. B.; Knoll, W.; Foerch, R. *Langmuir*, **2003**, *19*, 4765-4770.

199. El Khadali, F.; Helary, G.; Pavon-Djavid, G.; Migonney, V. *Biomacromolecules*, **2002**, *3*, 51-56.

200. Ziegelaar, B.W.; Fitton, J. H.; Clayton, A. B.; Platten, S. T.; Maley, M. A.; Chirila, T. V. *Biomaterials*, **1999**, *20*, 1979-1988.

201. Bisson, I.; Kosinski, M.; Ruault, S.; Gupta, B.; Hilborn, J.; Wurm, F.; Frey, P. *Biomaterials*, **2002**, *23*, 3149-3158.

202. Gupta, B.; Plummer, C.; Bisson, I.; Frey, P.; Hilborn, J. *Biomaterials*, **2002**, *23*, 863-871.

203. Haddow, D. B.; Steele, D. A.; Short, R. D.; Dawson, R. A.; MacNeil, S. *J. Biomed. Mater. Res.*, **2003**, *64A*, 80-87.

204. Barbosa, J. N.; Barbosa, M. A.; Aguas, A. P. *J. Biomed. Mater. Res.*, **2003**, *65A*, 429-434.

205. Tidwell, C. D.; Ertel, S. I.; Ratner, B. D. *Langmuir*, **1997**, *13*, 3404-3413.

206. Arima, Y.; Iwata, H. *Biomaterials*, **2007**, *28*, 3074-3082.

207. Elliott, J. T.; Woodward, J. T.; Umarji, A.; Mei, Y.; Tona, A. *Biomaterials*, **2007**, *28*, 576-585.

208. Faucheux, N.; Schweiss, R.; Lutzow, K.; Werner, C.; Groth, T. *Biomaterials*, **2004**, *25*, 2721–2730.

209. McClary, K. B.; Ugarova, T.; Grainger, D. W. *J. Biomed. Mater. Res.*, **2000**, *50*, 428–439.

210. Bearinger, J. P.; Castner, D. G.; Healy, K. E. *J. Biomater. Sci-Polym. Ed.*, **1998**, *9*, 629-652.

211. Tang, L.; Wu, Y.; Timmons, R. B. *J. Biomed. Mater. Res.*, **1998**, *42*, 156-163.

212. Chan, K.; Gleason, K. K. *Langmuir*, **2005**, *21*, 8930-8939.

213. Bhattacharyya, D.; Pillai, K.; Chyan, O. M. R.; Tang, L.; Timmons, R. B. *Chem. Mater.*, **2007**, *19*, 2222-2228.

214. Tarducci, C.; Schofield, W. C. E.; Badyal, J. P. S.; Brewer, S. A.; Willis, C. *Chem. Mater.*, **2002**, *14*, 2541-2545.

215. Qiu, H. Controlled chemical and morphological surface modifications via pulsed plasma polymerizations: synthesis of ultrahydrophobic surfaces. *PhD Thesis*, University of Texas at Arlington, **2001**.

216. Xu, C.; Yang, F.; Wang, S.; Ramakrishna, S. *J. Biomed. Mater. Res. A*, **2004**, *71*, 154-161.

217. Miller, D. C.; Thapa, A.; Haberstroh, K. M.; Webster, T. J. *Biomaterials*, **2004**, *25*, 53-61.

218. Kunzler, T. P.; Drobek, T.; Schuler, M.; Spencer, N. D. *Biomaterials*, **2007**, *28*, 2175-2182.

219. Scotchford, C. A.; Gilmore, C. P.; Cooper, E.; Leggett, G. J.; Downes, S. *J. Biomed. Mater. Res.*, **2002**, *59*, 84-99.

220. Lee, J. H.; Lee, J. W.; Khang, G.; Lee, H. B. *Biomaterials*, **1997**, *18*, 351-358.

221. Haddow, D. B.; France, R. M.; Short, R. D.; MacNeil, S.; Dawson, R. A.; Leggett, G. J.; Cooper, E. *J. Biomed. Mater. Res.*, **1999**, *47*, 379-387.

222. Cooper, E.; Wiggs, R.; Hutt, D. A.; Parker, L.; Leggett, G. J.; Parker, T. L. *J. Mater. Chem.*, **1997**, *7*, 435–441.

223. Pelham, R. J., Jr.; Wang, Y. L. *PNAS*, **1997**, 94, 13661-13665.

224. Guo, W. H.; Frey, M. T.; Burnham, N. A.; Wang, Y. L. *Biophys. J.*, **2006**, *90*, 2213-2220.

225. Lo, C. M.; Wang, H. B.; Dembo, M.; Wang, Y. L. *Biophys. J.*, **2000**, 79, 144-152.

226. Discher, D. E.; Janmey, P.; Wang, Y. L. *Science*, **2005**, *310*, 1139-1143.

227. Wells, R. G. *Hepatology*, **2008**, *47,* 1394-1400.

228. Rehfeldt, F.; Engler, A. J.; Eckhardt, A.; Ahmed, F.; Discher, D. E. *Adv. Drug Delivery Rev.*, **2007**, *59,* 1329-1339.

229. Cech, V.; Vanek, J.; Goruppa, A. A.; Jones, F. R. *J. Mater. Sc.*, **2005**, *40*, 5099-5102.

230. Cech, V.; Inagaki, N.; Vanek, J.; Prikryl, R.; Grycova, A.; Zemek, J. *Thin Solid Films*, **2006**, *502*, 181-187.

231. Levental, I.; Georges, P. C.; Janmey, P. A. *Soft Matter*, **2007**, *3*, 299-306.

232. Facchetti,A.; Yoon, M. H.; Marks, T. J. *Adv. Mater*., **2005**, *17*, 1705-1725.

233. Veres, J.; Ogier, S. D.; Leeming, S. W.; Cupertino, D. C.; Khaffat, S. M. *Adv. Func. Mater*., **2003**, *13*, 199-204.

234. Parashkov, R.; Becker, E.; Ginev, G.; Riedl, T.; Johannes, H. H.; Kowalsky, W. *J. Appl. Phys*., **2004**, *95*, 1594-1596.

235. Park, J.; Park, S. Y.; Shim, S.; Kang, H.; Lee, H. H. *Appl. Phys. Lett*., **2004**, *85*, 3283-3285.

236. Sandberg, H. G. O.; Bäcklund, T. G.; Österbacka, R.; Stubb, H. *Adv. Mater*., **2004**, *16*, 1112-1115.

237. Singh, T. B.; Meghdadi, F.; Günes, S.; Marjanovic, N.; Horowitz, G.; Lang, P.; Bauer, S.; Sariciftci, N. S. *Adv. Mater*., **2005**, *17*, 2315-2320.

238. Yoon, M-H.; Facchetti, A.; Marks, T. J. *PNAS*, **2005**, *102*, 4678-4682.

239. Bai, Y.; Cheng, Z. Y.; Bharti, V.; Xu, H. S.; Zhang, Q. M. *Appl. Phys. Lett*., **2000**, *76*, 3804-3806.

240. Dang, Z. M.; Shen, Y.; Nan, C. W. *Appl. Phys. Lett*., **2002**, *81*, 4814-4816.

241. Shen, Y.; Lin, Y.; Lin, M.; Nan, C. W. *Adv. Mater*., **2007**, *19*, 1418-1422.

242. Hu, J.; Yin, C.; Mao, H.-Q.; Tamada, K.; Knoll, W. *Adv. Func. Mater*., **2003**, *13*, 692-697.

243. Zhang, J.; Feng, X.; Xie, H.; Shi, Y.; Pu, T. ; Guo, Y. *Thin Solid Films*, **2003**, *435*, 108-115.

244. Klemberg-Sapieha, J. E.; Sapieha, S.; Wertheimer, M. R.; Yelon, A. *Appl.*

Phys. Lett., **1980**, *37*, 104-106.

245. Brown, P. J.; Sirringhaus, H.; Harrison, M.; Shkunov, M.; Friend, R. H. *Phys. Rev. B*., **2001**, *63*, 125204/1-125204/11.

246. Natori, K.; Otani, D.; Sano, N. *Appl. Phys. Lett*., **1998**, *73*, 632-634.

247. Xu, Y.; Berger, P. R.; Cho, J.; Timmons, R. B. *J. Elec. Mater*., **2004**, *33*, 1240-1247.

248. Hougham, G.; Tesoro, G.; Viehbeck, A.; Chapple-Sokol, J. D. *Macromolecules*, **1994**, *27*, 5964-5971.

BIOGRAPHICAL INFORMATION

Dhiman Bhattacharyya was born in Calcutta, India. He grew up in a liberal, open minded Hindu family. He received his junior and high school degrees from Ballygunge Government High School. He attended New Alipore College, an affiliated college to the University of Calcutta, for his Bachelor of Science (B.Sc.) degree with Chemistry Honors. He decided to continue his study in Applied Chemistry at the University of Calcutta and entered into the Bachelor of Technology (B.Tech.) program in Polymer Science & Technology in the year 1998. During this program, he experienced two months industrial practical training at Phillips Carbon Black Ltd., Durgapur, India. He continued his studies in polymer in the same department and earned Master of Technology (M.Tech.) in 2003. He joined the Chemistry & Biochemistry Department at the University of Texas at Arlington in the year of 2003. Dhiman started working on applications of plasma surface modification in Dr. Timmons' Plasma Chemistry Research Laboratory in 2004 and successfully finished his PhD in 2008.